

Award Number: W81XWH-05-1-0617

TITLE: Closed-loop Noninvasive Ultrasound Glucose Sensing and Insulin Delivery

PRINCIPAL INVESTIGATOR: Nadine Smith, Ph.D.
Michael Pishko, Ph.D.
Robert Gabbay, M.D., Ph.D.
Jacob Werner, D.V.M.

CONTRACTING ORGANIZATION: Pennsylvania State University
University Park, PA 16802

REPORT DATE: September 2007

TYPE OF REPORT: Annual

PREPARED FOR: U.S. Army Medical Research and Materiel Command
Fort Detrick, Maryland 21702-5012

DISTRIBUTION STATEMENT: Approved for Public Release;
Distribution Unlimited

The views, opinions and/or findings contained in this report are those of the author(s) and should not be construed as an official Department of the Army position, policy or decision unless so designated by other documentation.

REPORT DOCUMENTATION PAGE

Form Approved
OMB No. 0704-0188

Public reporting burden for this collection of information is estimated to average 1 hour per response, including the time for reviewing instructions, searching existing data sources, gathering and maintaining the data needed, and completing and reviewing this collection of information. Send comments regarding this burden estimate or any other aspect of this collection of information, including suggestions for reducing this burden to Department of Defense, Washington Headquarters Services, Directorate for Information Operations and Reports (0704-0188), 1215 Jefferson Davis Highway, Suite 1204, Arlington, VA 22202-4302. Respondents should be aware that notwithstanding any other provision of law, no person shall be subject to any penalty for failing to comply with a collection of information if it does not display a currently valid OMB control number. **PLEASE DO NOT RETURN YOUR FORM TO THE ABOVE ADDRESS.**

1. REPORT DATE 01-09-2007		2. REPORT TYPE Annual		3. DATES COVERED 19 Sep 2006 – 18 Sep 2007		
4. TITLE AND SUBTITLE Closed-loop Noninvasive Ultrasound Glucose Sensing and Insulin Delivery				5a. CONTRACT NUMBER		
				5b. GRANT NUMBER W81XWH-05-1-0617		
				5c. PROGRAM ELEMENT NUMBER		
6. AUTHOR(S) Nadine Smith, Ph.D. Michael Pishko, Ph.D. Robert Gabbay, M.D., Ph.D. Jacob Werner, D.V.M.				5d. PROJECT NUMBER		
				5e. TASK NUMBER		
				5f. WORK UNIT NUMBER		
7. PERFORMING ORGANIZATION NAME(S) AND ADDRESS(ES) Pennsylvania State University University Park, PA 16802				8. PERFORMING ORGANIZATION REPORT NUMBER		
9. SPONSORING / MONITORING AGENCY NAME(S) AND ADDRESS(ES) U.S. Army Medical Research and Materiel Command Fort Detrick, Maryland 21702-5012				10. SPONSOR/MONITOR'S ACRONYM(S)		
				11. SPONSOR/MONITOR'S REPORT NUMBER(S)		
12. DISTRIBUTION / AVAILABILITY STATEMENT Approved for Public Release; Distribution Unlimited						
13. SUPPLEMENTARY NOTES Original contains colored plates: ALL DTIC reproductions will be in black and white.						
14. ABSTRACT Numerous studies have shown that ultrasound can successfully be used for noninvasive blood glucose monitoring and transdermal insulin delivery. To facilitate the ability of a diabetic patient to avoid repeated needle sticks to monitor blood glucose level and painful daily injections of insulin, this basic research proposal will study the feasibility of safe and portable ultrasonic system to do both. Specifically using the low profile and light weight "cymbal" transducer, a potentially portable ultrasound array of will be designed. Moreover the feasibility of a "smart" diabetes management system will be developed to control both the glucose monitoring and insulin delivery system. The report herein describes the year one progress for this award and there are no deviations from the original research plan and this research is progressing on schedule.						
15. SUBJECT TERMS ultrasound, transdermal, diabetes, insulin, glucose, noninvasive						
16. SECURITY CLASSIFICATION OF:				UU	18. NUMBER OF PAGES 70	19a. NAME OF RESPONSIBLE PERSON USAMRMC
a. REPORT U	b. ABSTRACT U	c. THIS PAGE U	19b. TELEPHONE NUMBER (include area code)			

Table of Contents

Introduction.....	4
Body.....	5
Key Research Accomplishments.....	7
Reportable Outcomes.....	8
Conclusions.....	9
References.....	10
Appendices.....	11

I. INTRODUCTION

Medical devices are an \$82.4 billion annual business, and the U.S. currently holds a competitive advantage in this industry. The U.S. medical and dental equipment industries are known worldwide for producing high quality devices using advanced technology. The U.S. is expected to remain competitive globally because of its lead in innovative technology. The demand for advanced medical devices is growing due to the aging U.S. population, growing obesity rates, longer life expectancy and greater prevalence of disability [1]. As the demand for advanced medical technologies grows, there is an increasing need for engineers to develop innovative technologies.

Approximately 16 million people in the United States suffer from diabetes [2]. Diabetes is a risk factor for heart disease, stroke, and birth defects and shortens average life expectancy by up to 15 years. It costs the nation in excess of \$100 billion per year and accounts for about 25% of Medicare expenditures. Until a cure can be found, management of diabetes often requires painful repetitive blood glucose tests and insulin injections up to three or four times each day.

In this research effort today, we are determining the feasibility of a safe and portable ultrasonic system with a built-in, real-time electronic feedback loop (i.e. "smart") between the glucose monitoring and insulin delivery functions; control of blood sugar will be made automatic and continuous, in a noninvasive way. Using the thin cymbal transducer design, an ultrasound array (or "ultrasound patch") has demonstrated noninvasive insulin delivery for pronounced glucose reduction in animals (rats and rabbits) [3-7] and has been featured in several public medical sites such as WebMD (WebMD "Needle-Free Insulin Delivery on the Way"). Both the interstitial fluid glucose monitoring and ultrasonic insulin delivery techniques have been proven effective by others but the cymbal technology provides the opportunity to reduce the size of the required hardware dramatically, making possible a patch-sized system that can be conveniently worn by the patient continuously. In addition, limited research has attempted to combine the technologies into a self-controlled, feedback driven smart system for automatic blood sugar control. Such a system would be far less dependent on the compliance of the patient.

Based on this fundamental research, a feasible and practical ultrasound insulin delivery device is being developed, a device which will alleviate the painful daily injections experienced by diabetic patients and lead to an "artificial pancreas". Our collaborating team is multidisciplinary in nature combining strength in clinical medicine (Dr. Gabbay), veterinary medicine (Dr. Werner), basic science and engineering (Dr. Smith).

II. BODY

The over goal of this research is to develop a practicable (i.e. safe, portable, low-cost, efficient) ultrasound device to noninvasively transport insulin across the skin. To accomplish this task, this research will explore the use of novel, low profile transducers for drug delivery in addition to determining the optimal frequency and exposure conditions. Based on initial prototype designs, acoustic field characteristics of the transducers and arrays will be further optimized based on experimental results and complementary simulations. Once several prototypes are constructed, the acoustic field will be evaluated using exposimetry and dosimetry techniques along with quantifying cavitation events and thermal effects. The efficacy for transdermal delivery will be accessed by determining the permeability of insulin with *in vitro* skin. *In vivo* evaluation of the ultrasound devices will test insulin delivery using a diabetic animal model by monitoring the blood glucose levels with the cymbal. Mechanism for enhanced permeability due to ultrasound will be determined also be studied. Damage to the *in vitro* / *in vivo* skin along with underlying tissue from the ultrasound will be evaluated from histological microscopy studies. Using a cymbal glucose sensor system, the feasibility of controlled insulin delivery will be tested. Summarizing from the original grant application, the overall specific tasks for this project are:

- Task 1. Ergonomic cymbal transducer design for glucose monitoring and insulin delivery (Mo. 1-12)
- Task 2. Accurate characterization of the acoustic field (Months 1-24)
- Task 3. Closed-loop, feedback controlled for a "synthetic pancreas" (Months 1-12)
- Task 4. In vivo evaluation using a diabetic pig models (Months 12-24)
- Task 5. Dissemination of Results (Months 6-24)

For the second year, we have focused on Tasks 1, 2, 4 and 5. Work on Task 3 was reported last year in our Annual Report 2006 and will be reported again in the Final Report for 2008. Since this report allows "that publications and/or presentations may be substituted for detailed descriptions of methodology but must be referenced in the body of the report" we would like to utilize the appendix for details and summarize the accomplishments of the tasks in the following subsections.

Ila. Task 1 Transducer design for insulin delivery and Task 2. Accurate characterization of the acoustic field [8]

Previous use of laboratory sonicators for transdermal drug delivery has led to the development of portable solutions. Novel lightweight and compact cymbal technology has key attributes for the development of a portable device. Arrays of cymbal transducers have been shown to be effective in delivering therapeutic levels of insulin to decrease hyperglycemic glucose levels in rats, rabbits and pigs. The potential mechanism suggests that ultrasound interacts with the structured lipids within the intracellular channels of the stratum corneum to permeabilize the structure for diffusion of the insulin. To improve delivery efficiency of the cymbal arrays, an increase in the spatial intensity field without increasing the size of the device or I_{sptp} was desired. A 3 x 1 rectangular cymbal array was designed for this purpose. Rectangular cymbals maximized packing density and allowed the flexural cap resonance and the ceramic length mode resonance frequencies to be designed closer in frequency. Bringing the cap and ceramic resonances closer together increased the transmitting power and improved the electrical efficiency. In addition, by using higher order modes excited in the cap while operating at the first ceramic resonance frequency, the intensity spatial area was increased compared to the circular array. With a similar intensity ($I_{sptp} \approx 50 \text{ mW/cm}^2$), our goal was to determine if the 3 x 1 rectangular cymbal array could perform significantly better than the 3 x 3 circular array for blood glucose reduction in

hyperglycemic rabbits. Nine New Zealand White rabbit (3.2–4.7 kg) experiments were performed in three groups: control ($n = 3$) and ultrasound exposure with the 3 x 3 circular cymbal array ($n = 3$) or 3 x 1 rectangular cymbal array ($n = 3$). The rabbits were anesthetized and their thigh area was shaved for the exposure. While lying in the lateral recumbent position, a 1 mm thick, water tight standoff (reservoir) which held the insulin was fastened between the rabbit's thigh and the ultrasound arrays. At the beginning of the experiment and every 15 minutes for 90 minutes, 0.3 ml of blood was collected from the ear vein to determine the blood glucose level (mg/dl) using a glucose monitoring system. For comparison between individual rabbits, the change in the blood glucose level was normalized to their initial baseline value. For the control group, the glucose level increased (i.e. more hyperglycemic) to maximum of $+80.0 \pm 28.8$ mg/dl over the 90 minute experiment. Using the 3 x 3 circular array, the blood glucose level decreased to -146.7 ± 17.8 mg/dl at 90 minutes. However, in comparison using the 3 x 1 rectangular cymbal array, the blood glucose decreased faster and to level of -200.8 ± 5.9 mg/dl after 90 minutes. These results indicated the feasibility of the rectangular cymbal array as an improved device for portable drug delivery by decreasing the power consumed and increasing the insulin delivery rate. This research was performed by the Graduate Students (Mr. J Luis, engineering and Ms. EJ Park, animals) under the guidance and in the laboratory of the Principal Investigator (Dr. NB Smith) of this research. The methodology and other details of these results are in:

Appendix I: Luis J, Smith NB, Meyer RJ. "Rectangular cymbal arrays for ultrasonic transdermal insulin delivery. *Journal of the Acoustical Society of America*" 122 (4), October 2007.

IIb. Task 4. In vivo evaluation using a diabetic pig models [9;10]

In previous studies, ultrasound mediated transdermal drug delivery has shown a promising potential as a method for noninvasive drug administration. For prospective future human application, this study was designed to determine the feasibility of lightweight cymbal transducer array as a practical device for noninvasive transdermal insulin delivery in large pigs.

Six Yorkshire pigs (100 - 140 lbs) were divided into two groups. As the control ($n = 3$), the first group did not receive any ultrasound exposure with the insulin. The second group ($n = 3$) was treated with ultrasound and insulin at 20 kHz with an $I_{sptp} = 100$ mW/cm² at a 20% duty cycle for 60 minutes. With the pigs in lateral recumbency after anesthesia, the ultrasound transducer with insulin was placed on the axillary area of the pig. At the beginning and every 15 minutes up to 90 minutes, the blood glucose level was determined using a glucose monitoring system. To compare the results of individual animals, the change of blood glucose level was normalized to each animal's initial glucose value at the start of the experiment.

Although each animal had a different initial glucose level, the mean and standard error for the six animals was 146 ± 13 mg/dl. For the control group, the blood glucose level increased to 31 ± 21 mg/dl compared to the initial baseline over the 90 minute experiment. However for the ultrasound with insulin treated group, the glucose level decreased to -72 ± 5 mg/dl at 60 minutes ($p < 0.05$) and continued to decreased to -91 ± 23 mg/dl in 90 minutes ($p < 0.05$).

The results indicate the feasibility of ultrasound mediated transdermal insulin delivery using the cymbal transducer array in animal with a similar size and weight to a human. Based on these result, the cymbal array has potential as a practical ultrasound system for noninvasive transdermal insulin delivery for diabetes management. Again,

this research was performed by a Graduate Student (Ms. EJ Park) under the direct guidance and in the laboratory of the Principal Investigator (Dr. NB Smith). Dr. Jacob Werner (Penn State Large Animal Veterinarian) was integral to the success of this work. The methodology and other details of these results are in:

Appendix II: E. J. Park, J. Werner, and N. B. Smith, "Ultrasound mediated transdermal insulin delivery in pigs using a lightweight transducer," *Pharm. Res.*, vol. 24, no. 7, pp. 1396-1401, July 2007.

Additionally this research received a special comment from the Editor of *Pharmaceutical Research* regarding the novel nature of this work. The yellow highlighted section (near the end) of the Editorial from *Pharmaceutical Research* is included in:

Appendix III: A. K. Banga, "Theme section: transdermal delivery of proteins," *Pharm. Res.*, vol. 24, no. 7, pp. 1357-1359, July 2007.

IIc. Task 5. Dissemination of results (Months 6-24)

From this research we have published and presented (at conferences) the following:

J. Luis, N. B. Smith, and R. J. Meyer, "Rectangular cymbal arrays for improved ultrasonic transdermal insulin delivery," *Journal of the Acoustical Society of America*, vol. 122, no. 4 2007.

E. J. Park, J. Werner, and N. B. Smith, "Ultrasound mediated transdermal insulin delivery in pigs using a lightweight transducer," *Pharm. Res.*, vol. 24, no. 7, pp. 1396-1401, July 2007.

Luis, J. Park, E.J., Meyer, R.J., Smith, N.B., "Rectangular cymbal arrays for improved ultrasonic transdermal insulin delivery", *Proceedings of the IEEE 2007 Ultrasonics Symposium, Medical Applications: Therapy & Diagnosis*, New York, NY, 29-31 October 2007.

Park, E.J., Werner, J. and Smith, N.B., " Noninvasive Insulin Delivery in Large Pigs (> 100 lbs) Using the Lightweight Cymbal Array " *Proceedings of the IEEE 2007 Ultrasonics Symposium, Medical Applications: Therapy & Diagnosis*, New York, NY, 29-31 October 2007.

Luis, J. E.J. Park*, R.J. Meyer, and N.B. Smith. 2007. Rectangular cymbal arrays for improved ultrasonic transdermal insulin delivery. *Diabetes Research Conference*, University Park, PA, April 13.

Park, E.J., J. Werner, and N.B. Smith. 2007. Noninvasive ultrasound transdermal insulin delivery using large pigs. *Diabetes Research Conference*, University Park, PA, April 13.

Smith, N. and R. Newnham. 2006. Noninvasive ultrasound insulin delivery and glucose sensing using the low-profile cymbal. *Center of Excellence in Piezoelectric Materials and Devices*, Penn Stater Conference Center Hotel, University Park, PA, October 30 – 31.

III. KEY RESEARCH ACCOMPLISHMENTS:

- The 3 x 1 rectangular array delivered twice the amount of insulin as our original 3 x 3 circular array design without any increase to the intensity. This translates into a both safe and effective device.
- Using pigs which had a similar weight to a young adult (100 - 140 lbs) we have demonstrated noninvasive delivery of a clinically significant insulin dose.

- In addition to the goals of work for insulin delivery, we have use the device for ultrasound with liposomes as a potentially valuable treatment option for melanoma patients. (in Appendix IV)

IV. REPORTABLE OUTCOMES

Appendix I: Luis J, Smith NB, Meyer RJ. "Rectangular cymbal arrays for **improved** ultrasonic transdermal insulin delivery". Journal of the Acoustical Society of America" 122 (4), October 2007.

Appendix II: E. J. Park, J. Werner, and N. B. Smith, "Ultrasound mediated transdermal insulin delivery in pigs using a lightweight transducer," Pharm. Res., vol. 24, no. 7, pp. 1396-1401, July 2007.

Beyond just insulin, our ultrasound device has the potential to treat melanoma through delivery of drugs to the cell. Melanoma is the most deadly form of skin cancer. Currently early surgical removal is the best treatment option for melanoma patients with little hope of successful treatment of late stage melanoma. Clearly new treatment options must be explored. Topical administration of drugs provides the advantage of being able to apply large quantities of drug in close proximity to the tumor without the issue of systemic side effects. However, the natural barrier formed by the skin must first be overcome for topical treatment to become a viable option. With this in mind we have sought to use low-frequency ultrasound to transiently permeabilize the stratum corneum and successfully deliver liposomal siRNA to melanoma cells residing at the basement membrane. B-Raf is one of the most frequently activated genes in melanoma, making it an ideal candidate for targeting via siRNA. By targeting directly the most common activating mutation, V600E, off target effects associated with inhibiting B-Raf in normal cells can be avoided. The novel liposomes used in this study load siRNA, protect it from the outside environment and lead to knockdown of target message. Combining ultrasound with liposomal siRNA we show that siRNA can be delivered into melanoma cells in artificial reconstructed skin. Additionally, we show that siRNA to mutant B-Raf can effectively inhibit melanoma growth in reconstructs and in mice by 60% and 30% respectively. Therefore, ultrasound with liposomal siMutB-Raf is a potentially valuable treatment option for melanoma patients.

Appendix IV: M. A. Tran, G. Raghavendra, E. J. Park, J. Adair, N. B. Smith, M. Kester, and G. P. Robertson, "Targeting Cutaneous Melanoma Using Ultrasound and Liposomes Containing siRNA Against Mutant (V600E) B-Raf," Cancer Research, (submitted) 2007.

Table 1. Student research supported or work sponsored by this award

Student Name	Department	Obtained
EJ Park	Bioengineering	PhD 2007 (pending, comprehensive exam passed)
Ravi Patel	Bioengineering (Pre-Medicine Track)	B.S. degree in 2009
Nicholas Charles Rubert	Physics	B.S. degree in May 2008

V. CONCLUSION

Herein, a "smart" diabetes management system will be developed to control the glucose monitoring and insulin delivery system and possibly lead the way to the dream of an "artificial pancreas". The human body strives to maintain baseline conditions (e.g. 37°C temperature, blood pressure 120/80) and yet is highly adaptive within boundaries. When exercising, the body sweats to remove heat and the heart rate increases to transport oxygenated blood to the necessary organs [11]. Additionally, physiological responses are also dependant on individual conditions as age, weight, sex and metabolism. Therefore, medical devices should also be adaptive to best work *with* a physiological system. To approach this problem, the devices should act and react in a similar manner to return us to healthy biological baseline. Devices should *sense* their environment, determine the *controlled* response and *act* to implement that response. The engineering approach to copy the body's natural response is to design devices that are adaptive in their methodology.

For example, to develop the for diabetes care, novel, low profile and light weight transducers are being developed. Specifically using the "cymbal" transducer, a portable ultrasound array of cymbals will be designed and constructed for noninvasive glucose monitoring and insulin delivery. This system consists of three parts: the noninvasive ultrasound glucose sensor, an adaptive closed-loop feedback-controller and the transdermal ultrasound delivery device (i.e. artificial pancreas). For the ultrasound insulin delivery device, an intensity-dose curve will be determined (current work) and the controller will be used to vary the intensity for the proper dose to reduce the glucose. The controller consists of a simple, single-input, single-output, proportional-plus-integrator-plus-derivative (PID) controller. Conceptually, the glucose monitor will screen for increases in blood glucose levels. When the monitor detects an increase in glucose above a critical level, the controller activates the transducer. Therefore, an "adaptive" diabetes management system can be developed to control the glucose monitoring and insulin delivery system. Yet beyond diabetes, ultrasound mediated drug deliver has additional applications for cancer [12] and other therapeutic treatments [13].

VI. REFERENCES

- [1] A. Hussain, B. Claussen, A. Ramachandran, and R. Williams, "Prevention of type 2 diabetes: a review," *Diabetes Res. Clin. Pract.*, vol. 76, no. 3, pp. 317-326, June 2007.
- [2] Congressionally Established Diabetes Research Working Group, "Conquering Diabetes: A Strategic Plan for the 21st Century," NIH Publication No. 99-4398, 1999.
- [3] S. Lee, B. Snyder, R. E. Newnham, and N. B. Smith, "Noninvasive ultrasonic transdermal insulin delivery in rabbits using the light-weight cymbal array," *Diabetes Technol. Ther.*, vol. 6, no. 6, pp. 808-815, Dec. 2004.
- [4] S. Lee, V. Nayak, J. Dodds, M. Pishko, and N. B. Smith, "Ultrasonic mediated glucose measurements *in vivo* using the cymbal array," *Ultrasound Med. Biol.*, vol. 31, no. 7, pp. 971-977, 2005.
- [5] S. Lee, V. Nayak, J. Dodds, M. Pishko, and N. B. Smith, "Glucose measurements with sensors and ultrasound," *Ultrasound Med. Biol.*, vol. 31, no. 7, pp. 971-977, July 2005.
- [6] S. Lee, B. Snyder, R. E. Newnham, and N. B. Smith, "Noninvasive ultrasonic transdermal insulin delivery in rabbits using the light-weight cymbal array," *Diabetes Technol. Ther.*, vol. 6, no. 6, pp. 808-815, Dec. 2004.
- [7] S. Lee, R. E. Newnham, and N. B. Smith, "Short ultrasound exposure times for noninvasive insulin delivery in rats using the lightweight cymbal array," *IEEE Trans. Ultrason. Ferroelectr. Freq. Control*, vol. 51, no. 2, pp. 176-180, Feb. 2004.
- [8] J. Luis, N. B. Smith, and R. J. Meyer, "Rectangular cymbal arrays for improved ultrasonic transdermal insulin delivery," *Journal of the Acoustical Society of America*, vol. 122, no. 4 2007.
- [9] E. J. Park, J. Werner, and N. B. Smith, "Ultrasound mediated transdermal insulin delivery in pigs using a lightweight transducer," *Pharm. Res.*, vol. 24, no. 7, pp. 1396-1401, July 2007.
- [10] A. K. Banga, "Theme section: transdermal delivery of proteins," *Pharm. Res.*, vol. 24, no. 7, pp. 1357-1359, July 2007.
- [11] J. Enderle, S. Blanchard, and J. Bronzino, *Introduction to Biomedical Engineering*. New York, NY: Academic Press, 2005.
- [12] M. A. Tran, G. Raghavendra, E. J. Park, J. Adair, N. B. Smith, M. Kester, and G. P. Robertson, "Targeting Cutaneous Melanoma Using Ultrasound and Liposomes Containing siRNA Against Mutant (V600E) B-Raf," *Cancer Research*, vol. (submitted) 2007.

- [13] N. B. Smith, "Perspectives on Transdermal Ultrasound Mediated Drug Delivery," 2 ed 2007.

VII. APPENDICES

Appendix I: Luis J, Smith NB, Meyer RJ. "Rectangular cymbal arrays for **improved** ultrasonic transdermal insulin delivery". Journal of the Acoustical Society of America" 122 (4), October 2007.

Appendix II: E. J. Park, J. Werner, and N. B. Smith, "Ultrasound mediated transdermal insulin delivery in pigs using a lightweight transducer," Pharm. Res., vol. 24, no. 7, pp. 1396-1401, July 2007.

Appendix III: A. K. Banga, "Theme section: transdermal delivery of proteins," Pharm. Res., vol. 24, no. 7, pp. 1357-1359, July 2007.

Appendix IV: M. A. Tran, G. Raghavendra, E. J. Park, J. Adair, N. B. Smith, M. Kester, and G. P. Robertson, "Targeting Cutaneous Melanoma Using Ultrasound and Liposomes Containing siRNA Against Mutant (V600E) B-Raf," Cancer Research, (submitted) 2007.

1 Rectangular cymbal arrays for improved ultrasonic transdermal 2 insulin delivery

Appendix I

3 Joseph Luis

4 *Graduate Program in Acoustics, The Pennsylvania State University, University Park, Pennsylvania 16802*

5 Eun Joo Park

6 *Department of Bioengineering, The Pennsylvania State University, University Park, Pennsylvania 16802*

7 Richard J. Meyer, Jr.

8 *Applied Research Laboratory, The Pennsylvania State University, University Park, Pennsylvania 16802*9 Nadine Barrie Smith^{a)}10 *Graduate Program in Acoustics, The Pennsylvania State University, University Park, Pennsylvania 16802*

11 (Received 5 April 2007; revised 13 July 2007; accepted 16 July 2007)

12 Circular cymbal ultrasound arrays have been shown to be effective in delivering therapeutic levels
13 of insulin in rats, rabbits, and pigs. To improve delivery efficiency, a rectangular cymbal design was
14 desired in order to achieve a broader spatial intensity field without increasing the size of the device
15 or the spatial-peak temporal-peak intensity (I_{SPTP}). With a similar intensity (50 mW/cm^2), the goal
16 was to determine if the 3×1 rectangular cymbal array could perform significantly better than the
17 3×3 circular array for glucose reduction in hyperglycemic rabbits. Rabbit experiments were
18 performed using three groups: nonsonicated control ($n=3$), ultrasound exposure using a circular
19 cymbal array ($n=3$), and ultrasound exposure using a rectangular cymbal array ($n=3$). Rabbits were
20 anesthetized and a water tight reservoir that held the insulin was fastened on the rabbit's thigh. At
21 the beginning of the experiment and every 15 min for 90 min, the blood glucose level was
22 determined. For comparison between individual rabbits, the absolute level is normalized by
23 subtracting out the baseline in order to arrive at the change in glucose level. For the control group,
24 the normalized glucose level increased (more hyperglycemic) to $+80.0 \pm 28.8 \text{ mg/dl}$ (mean \pm SEM).
25 Using the circular array, the glucose level decreased to $-146.7 \pm 17.8 \text{ mg/dl}$ at 90 min. However,
26 using the rectangular cymbal array, the glucose decreased faster and to a level of $-200.8 \pm 5.9 \text{ mg/dl}$
27 after 90 min. These results indicated the feasibility of the rectangular cymbal array as an improved
28 device for drug delivery. © 2007 Acoustical Society of America. [DOI: 10.1121/1.2769980]

29 PACS number(s): 43.38.Fx, 43.80.Sh [TDM]

Pages: 1–XXXX

30

31 **I. INTRODUCTION**

32 Noninvasive methods of drug delivery have been studied
33 for some time to eliminate the pain induced by methods such
34 as injections.^{1–5} In particular, a large number of type I and
35 type II diabetics require blood glucose level regulation by
36 injections. Studies have shown that ultrasound mediated
37 transdermal drug delivery offers promising potential for non-
38 invasive drug administration.^{6–9} Ultrasound accomplishes
39 this by making the skin permeable, which allows drugs to
40 more readily diffuse. The working principle, although not
41 completely understood, has been suggested to be the result of
42 cavitation.^{10–13} Low frequency ultrasound in the vicinity of
43 20 kHz is capable of generating microbubbles in the water
44 and tissue layers. These bubbles allow water channels to be
45 produced within the cellular lipid bilayers. The resulting dis-
46 order created in the *stratum corneum* facilitates the crossing
47 of a hydrophilic drug or molecule. To this end, the number of

48 drugs and compounds that have been shown to transdermally
49 cross skin via ultrasound is ever increasing.⁹ This work fur-
50 ther explores the use of ultrasonic treatments as a promising
51 method for delivering therapeutic levels of drugs to patients.

52 In addition to having a system to sonicate and deliver
53 drugs transdermally, it would be useful to have a portable
54 delivery device.⁷ A transducer array has been developed that
55 can produce the necessary intensity levels to increase skin
56 permeability and maintain a low profile.¹⁴ The low-profile
57 “ultrasound patch” uses the cymbal, which is a flextensional
58 transducer made of a circular piezoelectric ceramic sand-
59 wичed between two metal end caps.^{14–17} The small radial
60 displacement of the ceramic is mechanically transformed
61 into larger displacements by the metal caps. Cymbal trans-
62 ducers can be arranged into arrays of any size and maintain a
63 low profile, be lightweight, and be conformable.

64 Various animal tests using rats, rabbits, and pigs have
65 been performed to demonstrate the feasibility of the 2×2
66 and 3×3 circular cymbal arrays in transdermal insulin de-
67 livery systems.^{18–20} These circular cymbal array designs
68 were able to produce significant reductions in glucose levels.
69 Specifically, in previous rat experiments, the 2×2 array was
70 used to deliver 20 kHz ultrasound operating at a spatial-peak

^{a)}Author to whom correspondence should be addressed at College of Engi-
neering, Department of Bioengineering, The Pennsylvania State Univer-
sity, 218 Hallowell Building, University Park, PA 16802. Electronic mail:
nbs@enr.psu.edu

71 temporal-peak intensity (I_{SPTP}) of 100 mW/cm² for 90 min.
 72 Xylazine was used as a general anesthetic as well as to cause
 73 temporary hyperglycemia.^{21,22} Results indicated a blood glu-
 74 cose decrease (mean±standard deviation) of
 75 297.7±52.8 mg/dl after 90 min.¹⁸ Since therapeutic levels of
 76 insulin would need to be delivered to larger animals, a 3
 77 ×3 circular array configuration was built. Experiments on
 78 rabbits were performed under the same intensity and pulse
 79 conditions using the slightly larger 3×3 array. For rabbits,
 80 the blood glucose decrease was 136.1±26.1 mg/dl after
 81 90 min.¹⁹

82 Although the cymbal transducer allows for a thin device,
 83 its circular geometry is not optimal for array packaging. For
 84 a portable insulin delivery device, we would also prefer a
 85 cymbal transducer that is electrically more efficient at the
 86 operating frequency in order to minimize battery drain. One
 87 improvement can be made by bringing the ceramic and cap
 88 resonances closer together. Doing so increases the displace-
 89 ment of the caps and increases the electrical efficiency.

90 In an ultrasound device for transdermal drug delivery, a
 91 larger spatial average intensity can offer higher drug diffu-
 92 sion rates with a larger permeabilized skin area. Previous 2
 93 ×2 and 3×3 cymbal arrays have shown spatial intensity
 94 distributions with high intensities at the center of the device
 95 and a rapid intensity decrease away from the spatial
 96 peak.^{19,23} This type of spatial intensity distribution results in
 97 larger arrays that are not able to adequately improve the in-
 98 sulin delivery rate. By exciting higher order modes in the
 99 cymbal cap, we can broaden the spatial extent of the inten-
 100 sity field. To achieve a greater electrical efficiency and obtain
 101 a broader spatial intensity field at a 1 mm distance from the
 102 transducer, a rectangular cymbal was designed and
 103 evaluated.²⁴ The rectangular array was no larger than the 3
 104 ×3 circular array previously tested and *in vivo* rabbit experi-
 105 ments were performed herein to verify the effectiveness of
 106 the device.

107 II. MATERIAL AND METHODS

108 A. Transducer development

109 Details regarding the development of the cymbal trans-
 110 ducer have been described elsewhere.^{14,24,25} The cymbal
 111 transducer is a novel flextensional transducer capable of pro-
 112 ducing very low frequencies. The cymbal transducer has a
 113 compact, lightweight structure with an adjustable resonance
 114 frequency. In the cymbal transducer design, the caps on the
 115 lead zirconate-titanate (PZT) ceramic contained a shallow
 116 cavity beneath its inner surface. The fundamental mode of
 117 vibration is the flexing of the end caps caused by the radial
 118 motion of the ceramic. Therefore, the overall displacement of
 119 the device is a combination of the axial motion of the disk
 120 plus the radial motion amplified by the end caps.

121 The circular cymbal arrays use the first resonance fre-
 122 quency of the caps for acoustic radiation.^{15,16,25–27} In order to
 123 be near a low frequency, it was necessary to increase the cap
 124 size such that the close operation frequency excites higher
 125 order modes in the cap. Higher order modes will create a
 126 more desirable spatial intensity profile. Yet, increasing the

overall size of a circular ceramic decreases the first ceramic
 resonance frequency. Radial modes are governed by

$$J_1(\eta) = 1 - \sigma^p, \quad \text{Appendix I} \quad (1) \quad 129$$

where J_1 is the Bessel function of the first kind of first order,
 η is an argument proportional to the frequency, and σ^p is a
 planar Poisson's ratio. Here σ^p is defined by $-\frac{s_{12}^E}{s_{11}^E}$, where
 s^E is the compliance under zero electric field.^{28–30} The first
 root of Eq. (1) places the ceramic resonance of the circular
 cymbal near 100 kHz, which is far from the 20 kHz first
 resonance of the cap. A larger cap with a rectangular ceramic
 geometry resolves this issue. The rectangular cymbal oper-
 ates in the 3-1 ceramic mode³¹ where the longitudinal strain
 is given by

$$S_s(x) = d_{31}E_0 \left[\cos(kx) + \tan\left(\frac{kl}{2}\right) \sin(kx) \right], \quad (2) \quad 140$$

where d is the piezoelectric strain constant (C/N), E_0 is the
 electric field applied (V), $k = \omega/c$, c is the speed of sound in
 the long bar (m/s), and l is the length of the bar (m). The
 expression for the admittance of the 3-1 bar is shown as

$$Y = \frac{j\omega w d_{31}^2}{s_{11}^E k t} \sin(kl) \left[1 + \tan^2\left(\frac{kl}{2}\right) \right] + \frac{j\omega w l}{t} \left[\varepsilon_{33}^T - \frac{d_{31}^2}{s_{11}^E} \right], \quad (3) \quad 145$$

where w is the width of the bar (m) and t is the bar thickness
 (m), and ε^P is the permittivity under zero stress. From Eqs.
 (2) and (3) the ceramic resonances now occur when kl
 $= (2n-1)\pi$, giving a first ceramic resonance of $f_r = c/2l$. A
 bar length of 50 mm, similar to 3×3 circular array dimen-
 sions, results in a first resonance of 32 kHz. The system can
 now be operated at the ceramic resonance instead of the cap
 resonance giving maximum longitudinal strain of the bar. It
 was desired to design the rectangular array to have the same
 area as the 3×3 circular array. In order to have a rectangular
 array of the same size, a 3×1 array was made with element
 dimensions of 50×13×3 mm³.

B. Transducer modeling

A finite element model of a single element rectangular
 transducer was developed to predict the cap displacement
 and electrical impedance. The finite element analysis code
 ATILA (ISEN, Lille, France, Hamonic) was used. ATILA is a
 particularly useful tool for piezoelectric and magnetostrictive
 systems³² and has been previously used for the simulation of
 these flextensional transducers. Figure 1(a) shows a 1/8th
 model of a single rectangular transducer element and the
 predicted cap displacement when operated at the first ce-
 ramic resonance. Modeled at 32 kHz, Fig. 1(b) is a contour
 plot showing the axial displacement of the rectangular cym-
 bal caps at the first resonance frequency. The color bar rep-
 resents the displacement in meters.

C. Rectangular array construction

Construction of the rectangular cymbal transducers was
 done by hand. It is important to maintain symmetry when
 fabricating the transducers. Rectangular Navy Type I 402

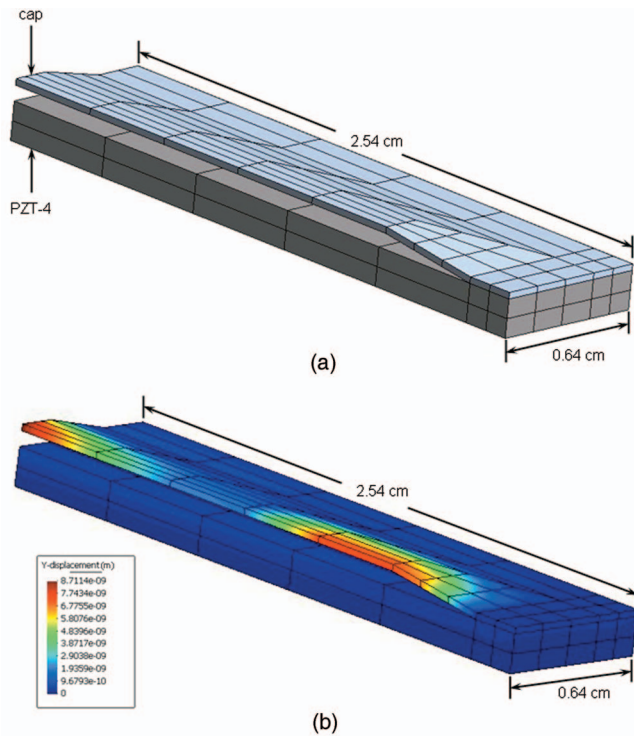


FIG. 1. (a) ATILA finite element analysis software was used to establish a 1/8th model of a single element rectangular cymbal transducer. (b) Using ATILA, the predicted cap displacement when operated at the first ceramic resonance was modeled. The axial displacement of the rectangular cymbal caps is indicated with the color bar and the displacement is in meters.



(a)



(b)

FIG. 2. (Color online) (a) A single element rectangular cymbal transducer was constructed from titanium cap molded from a shaping die. Caps were bonded to the ceramics using epoxy. (b) Multielement arrays were made by electrically connecting the transducers and potting them in polyurethane. The 3×1 rectangular array (right) was designed to be comparable in size to the 3×3 circular array (left).

176 ceramics (Piezokinetics, Inc., Bellefonte, PA) were poled in
 177 the thickness direction to use in the 3-1 bar configuration.
 178 The titanium caps were punched from 0.25-mm-thick sheets
 179 (Item 10385, Alfa Aesar, Ward Hill, MA). Initially, titanium
 180 was cut into strips the same width and length as the rectan-
 181 gular ceramic. The cap was shaped by pressing the cap using
 182 a specially machined shaping die. One cap at a time was
 183 placed in the shaping die and pressed (Model 3012, Carver,
 184 Inc., Wabash, IN) at 60 kpsi. Cap heights were measured at
 185 the center of the cap using a precise dial gauge (Model
 186 254MZ-300, L. S. Starrett Co., Athol, MA); for symmetry,
 187 caps with the closest cap heights were paired together. Caps
 188 were bonded to the ceramics using Eccobond® epoxy (Em-
 189 erson & Cuming, Billerica, MA) base and 15 LV catalyst in
 190 a 3:1 ratio. After a rectangular cymbal transducer was con-
 191 structed [Fig. 2(a)], the admittance (magnitude and phase)
 192 was measured in air using a network analyzer (Agilent
 193 E5100A, Santa Clara, CA) for comparison to the ATILA
 194 model as a function of frequency.

195 Multielement arrays were made by electrically connect-
 196 ing the rectangular transducers and potting the elements in
 197 polyurethane (URALITE® polymer, FH 3550, H.B. Fuller,
 198 St. Paul, MN). The two part polyurethane with a 90A shore
 199 hardness was mixed, degassed, and poured on the array,
 200 which was set in a mold. To compare the delivery efficiency
 201 of the 3×3 circular design to the new 3×1 rectangular de-
 202 sign, a previously constructed circular array was used.¹⁹ Fig-
 203 ure 2(b) shows a 3×3 array (left) with nine circular cymbal
 204 transducers compared to a 3×1 array using three rectangular
 205 cymbal transducers (right).

To drive the rectangular and cymbal arrays, a (rf) signal 206
 was generated by a frequency pulse/function generator (Agi- 207
 lent 32250A, Palo Alto, CA) and amplified by a rf amplifier 208
 (Model 40A12, Amplifier Research, Souderton, PA). The 209
 electrical impedance of both the rectangular and circular ar- 210
 ray was tuned to the output impedance of the amplifier using 211
 an external inductive-capacitive (LC) π network. Pulse pe- 212
 riod, duty cycle, and on-time of the rf signal from the fre- 213
 quency generator was monitored using an oscilloscope (Tek- 214
 tronix 2213A, Beaverton, OR). For the experiments, the 215
 signal generator operated at approximately 32 kHz with 216
 pulse durations of 200 ms and pulse repetition period of 1 s 217
 (i.e., 20% duty cycle); the amplifier gain was set to 50 dB. 218
 Pulsed ultrasound was used to avoid damaging heat build-up 219
 to either the array's piezoceramic or the animal's skin. 220

D. Far field measurements 221

As a method of comparing the transducer efficiency, far 222
 field measurements in water were acquired at the anechoic 223

224 acoustic test facilities in the Applied Research Laboratory
 225 (State College, PA). Transmitting voltage response (TVR),
 226 complex impedance, and directivity patterns were measured.
 227 Transmit system performance in terms of volt-amperes per
 228 acoustic watt was calculated. TVR is a ratio of the sound
 229 pressure at a distance of 1 m in a specified direction to the
 230 voltage applied. The reference voltage is 1 V and the ratio is
 231 expressed in dB re $1 \mu\text{Pa m/V}$. In an ideal case, all the elec-
 232 trical power is converted to acoustic power. However, in this
 233 particular system, the transducer behaves like a capacitor and
 234 the conversion of electrical to acoustic power is not ideal.
 235 The volt-ampere per acoustic watt ratio ($V A/P_{acs}$) accounts
 236 for both real and reactive electrical power and a ratio of one
 237 would imply 100% efficiency. For the cymbal transducers
 238 used in previous arrays, a typical untuned value of $V A/P_{acs}$
 239 is on the order of 100.

240 E. Near field exposimetry

241 Of interest is the intensity profile close to the arrays for
 242 potential bioeffects. For possible practical clinical use, the
 243 transducer face will be approximately 1 mm away from the
 244 skin. At that distance it is necessary to know how the acous-
 245 tic intensity field is distributed spatially. The intensity was
 246 determined according to exposimetry guidelines previously
 247 established.^{33,34} For the acoustic field at a plane 1 mm from
 248 the transducer face, the ultrasonic intensities from the arrays
 249 were determined with a calibrated miniature (4 mm diam-
 250 eter) omnidirectional reference hydrophone (Model TC4013,
 251 S/N: 5199093, RESON, Inc., Goleta, CA). The arrays were
 252 submerged in a water tank ($51 \times 54 \times 122 \text{ cm}^3$), which was
 253 made almost anechoic by placing 1.27-cm-thick rubber
 254 sound absorbing material around its wall. To minimize cavi-
 255 tation effects, a custom made degasser reduced the dissolved
 256 oxygen content of the distilled water to 1 to 2 ppm. Pulse
 257 period, duty cycle, and on-time of the signal from the fre-
 258 quency generator and hydrophone were acquired using an
 259 Agilent 54622A 100 MHz digitizing oscilloscope (Agilent,
 260 Palo Alto, CA).

261 Precise, computer controlled positioning of the hydro-
 262 phone was performed by a Velmex Positioning System
 263 (Velmex Inc., East Bloomfield, NY). Pressure waves de-
 264 tected by the hydrophone were recorded by a digitizing os-
 265 cilloscope. A computer-controlled exposimetry positioning
 266 system was used for automated scanning. The scanning step
 267 size for each device was 1 mm and the scanning area was
 268 $90 \times 90 \text{ mm}^2$. Spatial peak-temporal peak intensities (I_{sptp})
 269 were determined over a plane 1 mm from the array face us-
 270 ing the hydrophone based on three to five scannings of the
 271 array for a mean and standard error of the intensity results.
 272 Exposimetry field maps were normalized and plotted in deci-
 273 bels with respect to the highest intensity (I_{sptp}) in order to
 274 show the spatial distribution of intensity from the maximum
 275 radiation point.

276 F. Animal experiments

277 Ultrasonic assisted transdermal insulin delivery tests on
 278 animals were performed to determine the effectiveness of the
 279 two exposure array designs. Experimental protocol for the

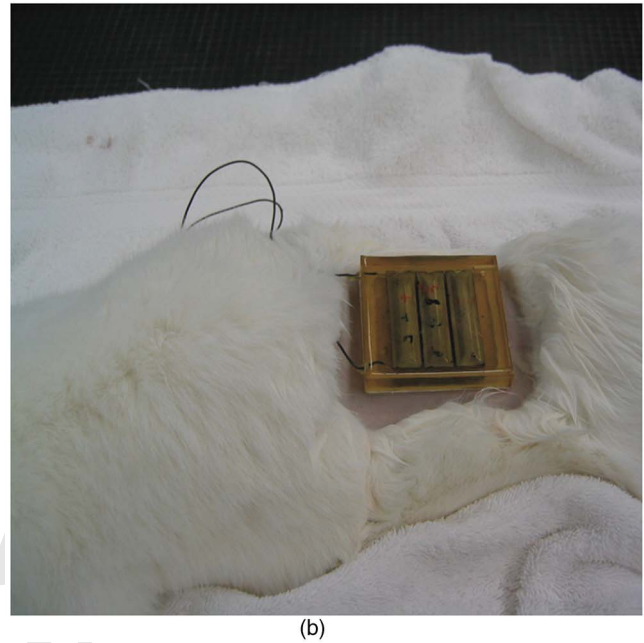
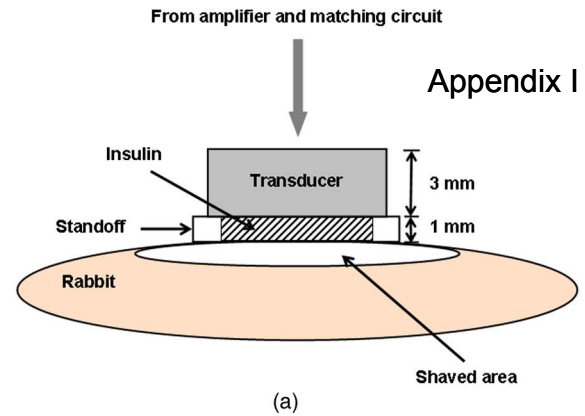


FIG. 3. (Color online) (a) Illustration and (b) photograph of the animal setup for the transdermal insulin transport experiments. With the rabbit placed in a lateral recumbent position, a 1-mm-thick, water-tight standoff filled with insulin was arranged between the thigh and the array.

use of rabbits was reviewed and approved by the Institutional
 Animal Care and Use Committee at the Pennsylvania State
 University. New Zealand White rabbits (3.2–4.7 kg) were
 divided into the three groups (control, 3×3 circular array,
 and 3×1 rectangular array) and nine experiments were per-
 formed with $n=3$ animals in each group. Each animal was
 anesthetized with a combination of ketamine hydrochloride (
 40 mg/kg intramuscularly, Ketaject®, Phoenix, St. Joseph,
 MO) and sodium xylazine (10 mg/kg intramuscularly, Xyla-
 Ject®, Phoenix, St. Joseph, MO). The hair of the thigh area
 was shaved; a depilatory agent was very briefly applied to
 the skin to remove any remaining hair and thoroughly
 cleaned.

In addition to its use as a general anesthetic, xylazine
 was used to cause temporary but sustained hyperglycemia
 (up to 12 h) in rabbits.^{21,22} With a rabbit placed in the lateral
 recumbent position [Fig. 3(a) diagram and Fig. 3(b) photo], a
 1-mm-thick, water-tight, standoff was fixed between the
 thigh and the array (both circular and rectangular design)
 using double-sided tape (3M, St. Paul, MN). Through small

300 holes in the back of the arrays, the reservoir inside of the
 301 standoff was filled with 4 ml of insulin (Humulin® R, rDNA
 302 U-100, Eli Lilly Co., Indianapolis, IN). The insulin was di-
 303 luted with a saline solution to prepare 50 units/ml of insulin.
 304 Previous experiments have shown that this dilution does not
 305 affect the overall results.³⁵ Care was taken to remove all
 306 bubbles from the solution in the reservoir between the thigh
 307 and the arrays.

308 Prior to beginning the experiment, 0.3 ml of blood was
 309 collected from the ear vein of each rabbit for a baseline
 310 blood glucose analysis. The glucose level (mg/dl) in the rab-
 311 bit blood was determined using an ACCU-CHEK™ Instant®
 312 (Roche Diagnostics Co., Indianapolis, IN) blood glucose
 313 monitoring system. Multiple samples (three to six each time)
 314 were taken from each rabbit for the baseline and at every
 315 subsequent 15 min interval for a total of 90 min. The time
 316 from the initial injection of the ketamine-xylazine until the
 317 baseline glucose measurement was no greater than 20 min.
 318 For comparison between individual rabbits, the absolute
 319 level is normalized by subtracting out the baseline in order to
 320 arrive at the change in glucose level.

321 For each rabbit, the entire experiment lasted a total of
 322 90 min. The control group ($n=3$) used insulin in the reser-
 323 voir without any ultrasound operating (designated the
 324 “control—insulin without ultrasound”). For the exposure
 325 groups, the second group ($n=3$) used insulin in the standoff
 326 with ultrasound exposure using the 3×3 circular array
 327 ($I_{sptp}=50.1 \pm 1.3 \text{ mW/cm}^2$), whereas the last group ($n=3$)
 328 used insulin with ultrasound exposure using the 3×1 rectan-
 329 gular array operated at a comparable intensity (I_{sptp}
 330 $=50.8 \pm 0.6 \text{ mW/cm}^2$). For all three groups, the standoff res-
 331 ervoir with the insulin was removed at 60 min, although glu-
 332 cose measurements continued until 90 min from the start.
 333 After the experiments, the rabbits were carefully observed
 334 until recovery from the anesthesia.

335 Statistical analysis was performed using Microsoft EX-
 336 CEL® (Microsoft Corp., Redmond, WA). The blood glucose
 337 versus time data for each group was analyzed as mean and
 338 standard error ($x \pm \text{SEM}$). An analysis of variance (ANOVA)
 339 was used to analyze the statistical significance of the differ-
 340 ences among the means of groups. The p value was used to
 341 determine if the between-group differences are significantly
 342 greater than those attributable to chance. For the data, a
 343 single was used if the p value was less than the 0.05 level of
 344 significance.

345 III. RESULTS

346 A. Exosimetry

347 After bonding the cap to the piezoceramic, each rectan-
 348 gular transducer’s admittance in air was measured and com-
 349 pared to the ATILA predicted admittance. Figure 4(a) shows a
 350 typical measured and calculated admittance (magnitude and
 351 phase) for a single element rectangular transducer in air prior
 352 to potting in polyurethane. TVR and a volt-ampere per
 353 acoustic watt ratio ($V A/P_{acs}$) were determined for the 3
 354 $\times 1$ rectangular arrays and the 3×3 circular arrays. Figure
 355 4(b) shows the measured TVR for the 3×3 circular and the

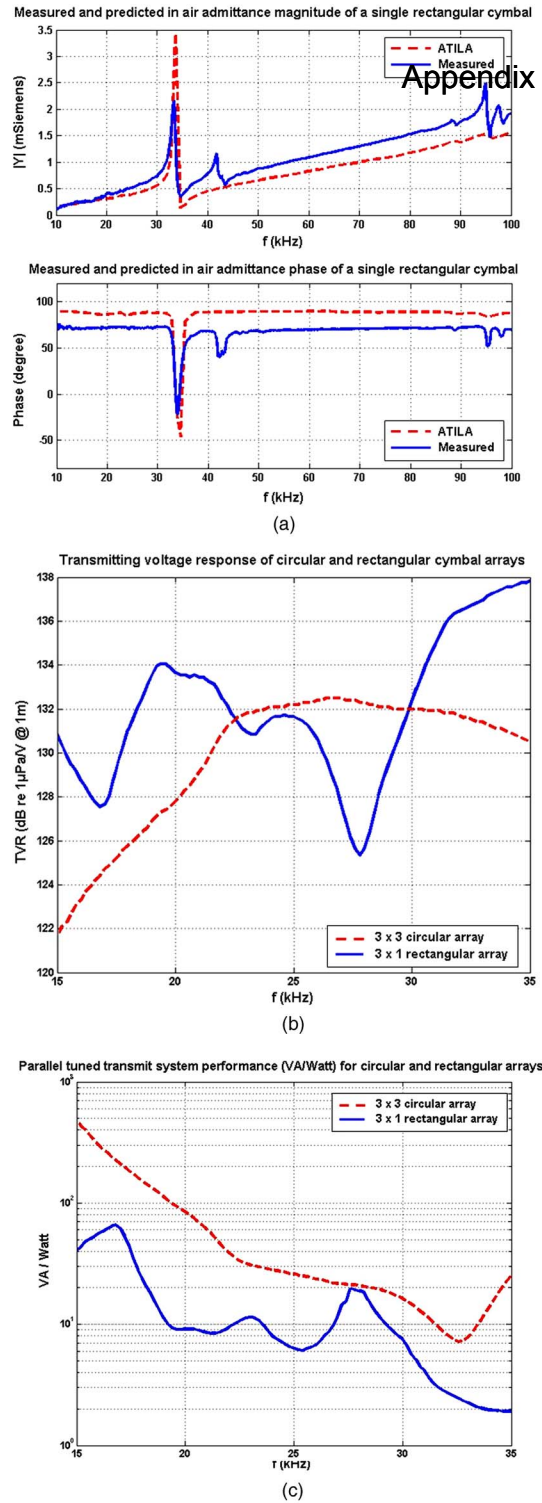


FIG. 4. (Color online) (a) Measured and ATILA predicted admittance (magnitude and phase) of a rectangular cymbal transducer in air. (b) Transmitting voltage response (TVR) comparison of a 3×1 rectangular and 3×3 circular array. Except for the dips, the rectangular array has a greater TVR than the circular array. The dips in the TVR for the rectangular array were due to asymmetrical modes in the device possibly caused by uneven bonding. (c) Parallel tuned $V A/P_{acs}$ ratios for both arrays, which indicates an improved efficiency for the rectangular array over the circular array.

3×1 rectangular arrays with dips near 17, 23, and 29 kHz in the TVR for the rectangular array, which are due to asymmetrical modes in the device.

359 Over the frequency range of interest including the reso-
 360 nance of the arrays (circular, 20 kHz; rectangular, 32 kHz),
 361 the $V A/P_{acs}$ ratio was compared between the 3×3 circular
 362 and the 3×1 rectangular arrays. For single frequency opera-
 363 tion the arrays can be tuned to obtain a high efficiency at the
 364 operating frequency. For this particular work, the arrays were
 365 parallel tuned. An inductor was placed in parallel with the
 366 device and was designed to resonate at a user-specified fre-
 367 quency with the known clamped capacitance of the array.
 368 Figure 4(c) shows the measured tuned $V A/P_{acs}$ ratios for the
 369 3×3 circular and the 3×1 rectangular arrays. Manifested as
 370 dips in the TVR in Fig. 4(b), there are peaks in Fig. 4(c) that
 371 correspond to asymmetrical modes in the transducer due to
 372 small asymmetries in the device introduced during the con-
 373 struction process. Moreover the $V A/P_{acs}$ ratios for the 3
 374 $\times 3$ circular is lower than the ratio for 3×1 rectangular ar-
 375 rays indicating an improved efficiency for the rectangular
 376 array compared to the circular array.

377 To compare drug delivery efficiency of the rectangular
 378 and the circular designs, both arrays were driven such that
 379 the I_{sptp} would be similar. From multiple exposimetry scans,
 380 the intensity of the 3×1 rectangular array was I_{sptp}
 381 $= 50.8 \pm 0.6 \text{ mW/cm}^2$ while the intensity of the 3×3 circular
 382 array was $I_{sptp} = 50.1 \pm 1.3 \text{ mW/cm}^2$. Exposimetry field maps
 383 were plotted in decibels with respect to the highest intensity
 384 (I_{sptp}) in order to show spatial distribution of the intensity
 385 field from the maximum radiation point. Using similar I_{sptp}
 386 driving conditions, the intensity field was determined in a
 387 plane 1 mm from the array face for both the rectangular and
 388 the circular designs. Figure 5(a) shows a typical two-
 389 dimensional scanning plot of the temporal peak intensity for
 390 the 3×3 circular cymbal transducer over a $90 \times 90 \text{ mm}^2$
 391 area with 1 mm steps. The grayscale bar on the side of the
 392 graph illustrates the normalized temporal peak intensity
 393 change in decibels. Under similar driving conditions, a 90
 394 $\times 90 \text{ mm}^2$ two-dimensional plot of the temporal peak inten-
 395 sity was acquired for the rectangular array [Fig. 5(b)]. As
 396 seen in Fig. 5, even though two arrays have similar I_{sptp}
 397 values, the intensity distributions were different with the 3
 398 $\times 1$ rectangular array having a larger area of high intensity.

AQ:
 #1

399 **B. Animal experiment results**

400 Results of the ultrasonic transdermal insulin delivery in
 401 rabbits for the three groups are graphed (Fig. 6) as the
 402 change in the blood glucose level during the 90 min experi-
 403 ment. After the rabbits were anesthetized, the average initial
 404 glucose level of the nine rabbits was $241.0 \pm 1.9 \text{ mg/dl}$. Gen-
 405 erally for normal rabbits, the blood glucose level is approxi-
 406 mately $100\text{--}135 \text{ mg/dl}$.^{21,22} For comparison between the
 407 rabbits, the change in the blood glucose level was normal-
 408 ized to a baseline, which was the initial glucose level for
 409 each rabbit.

410 Data were graphed as the mean \pm standard error
 411 ($x \pm \text{SEM}$) of each group. For the control group (Fig. 6, dia-
 412 monds, “insulin without ultrasound”), the glucose level in-
 413 creased to $63.7 \pm 22.8 \text{ mg/dl}$ after 30 min compared to the
 414 initial baseline. Over the 90 min experiment the slope of this
 415 blood glucose increase was $+45.7 \text{ mg/dl/h}$ ($r^2=0.7$) to a

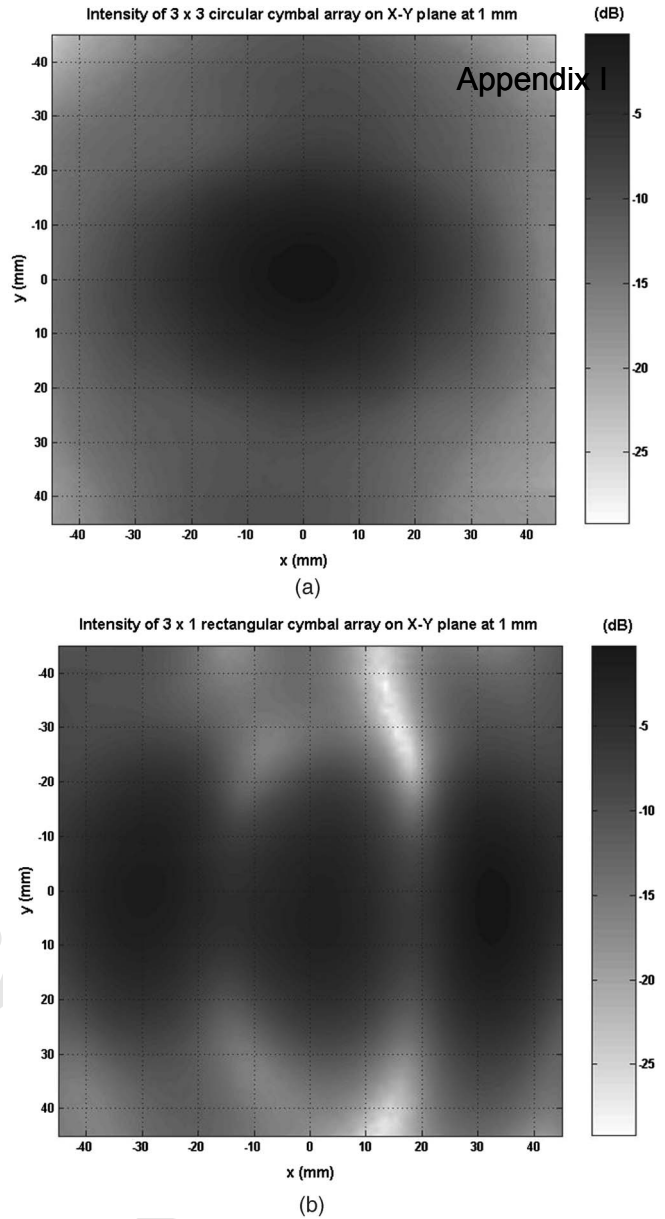


FIG. 5. Temporal peak intensity profiles of a (a) 3×3 circular and (b) 3×1 rectangular array at a plane 1 mm from the array face. With a similar spatial peak temporal peak intensity for both arrays ($\approx 50 \text{ mW/cm}^2$), it is evident that the rectangular array produces a broader spatial intensity field pattern than the circular array. The grayscale bar in decibels indicates the intensity field normalized to the peak intensity.

maximum of $+80.0 \pm 28.8 \text{ mg/dl}$. For the ultrasound and in-
 416 sulin exposure group using the 3×3 circular array (Fig. 6,
 417 squares), the glucose level decreased to $-26.7 \pm 20.7 \text{ mg/dl}$
 418 in 30 min and $-100.8 \pm 25.1 \text{ mg/dl}$ in 60 min from the initial
 419 baseline level. After the 3×3 circular array and the insulin
 420 reservoir were removed at 60 min, the glucose level contin-
 421 ued to decrease to $-146.7 \pm 17.8 \text{ mg/dl}$ at 90 min. Use of the
 422 3×1 rectangular array shows a shows a similar trend but
 423 larger magnitude in the decrease in blood glucose levels in
 424 the rabbits (Fig. 6, triangles). In comparison to the circular
 425 array results at 30 min, use of the 3×1 rectangular array
 426 showed a decrease in the blood glucose to
 427 $-64.3 \pm 15.1 \text{ mg/dl}$ and to $-157.2 \pm 9.7 \text{ mg/dl}$ at 60 min. For
 428

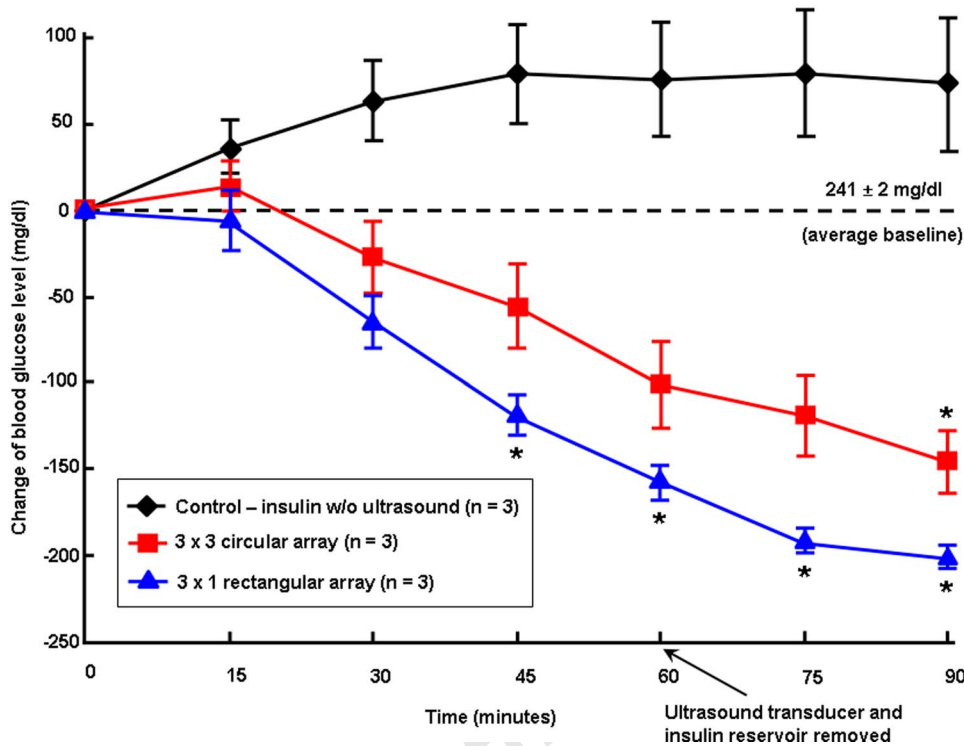


FIG. 6. (Color online) Over a period of 90 min for the control group, the average glucose level increased (i.e., more hyperglycemic) to a maximum of +80.0 mg/dl. While the blood glucose level of the rabbits decreased from the insulin with ultrasound exposure ($I_{\text{sptp}}=50 \text{ mW/cm}^2$) using both arrays, the decrease was greater using the 3×1 rectangular array. Statistically significant differences (p values < 0.5 , indicated by asterisks) were observed using the rectangular array at 45, 60, 75, and 90 min, while the only statistically significant difference observed using the circular array occurred at 90 min.

429 the final reading at 90 min the blood glucose level was
430 $-200.8 \pm 5.9 \text{ mg/dl}$ using the rectangular array.

431 To determine the statistical significance between the
432 control and ultrasound exposure groups using either the cir-
433 cular or rectangular array results in Fig. 6 an ANOVA was
434 used to analyze these data. Asterisks adjacent to a blood
435 glucose-time data point were used if there existed statisti-
436 cally significant difference between the control and exposure
437 data. Comparison of the control with the 3×3 circular array
438 data indicated that there was a statistically significant differ-
439 ence between the groups at 90 min ($p=0.04^*$). However,
440 comparison between control and the 3×1 rectangular array
441 groups indicated that a statistically significant difference ex-
442 isted between these data at 45, 60, 75, and 90 min with p
443 values of 0.02^* , 0.02^* , 0.01^* , and 0.01^* , respectively.

444 An examination of the rabbit's skin was performed after
445 ultrasound exposure to check for discoloration or visible le-
446 sions on the skin surface. The skin did not indicate any no-
447 ticeable damage or change immediately after the stand-off
448 was removed and for a period of two weeks after the experi-
449 ments.

450 IV. DISCUSSION

451 Cymbal designs have been shown to be effective at de-
452 livering therapeutic levels of insulin based on the decrease in
453 blood glucose level after ultrasound exposure *in vivo*. A new
454 cymbal transducer design with a rectangular shape was mod-
455 eled, constructed, and tested as an improvement over the
456 circular design currently under investigation.

457 Several methods were used to initially evaluate the de-
458 sign. Using the ATILA finite element analysis software, the
459 in-air admittance agreed well between the model and the
460 measured magnitude and phase result [Fig. 4(a)]. Individual
461 transducers were connected in an array pattern and encased

in polyurethane for in-water electrical efficiency evaluation. 462
For potential future application as a portable system, an un- 463
tuned device would drain a battery quickly. At single fre- 464
quency operation, the arrays can be tuned to obtain a high 465
efficiency at the operating frequency. For this particular 466
work, both arrays were parallel tuned. An inductor was 467
placed in parallel with the device and was designed to reso- 468
nate at a specified frequency with the known clamped ca- 469
pacitance of the array. By doing so, the efficiency was in- 470
creased in the operating band for both arrays [Fig. 4(c)] 471
compared to an untuned array (graph not shown). Addition- 472
ally, the TVR for the 3×3 circular array was compared to 473
that of the 3×1 rectangular array [Fig. 4(b)]. From Fig. 4, 474
there are dips in the TVR for the rectangular array that are 475
due to asymmetrical modes in the device. These are due to 476
asymmetries in the device caused by assembling the trans- 477
ducers by hand. Over the rest of the band the rectangular 478
arrays outperform the previous circular cymbals. Yet more- 479
over, the rectangular array generally appears to be more ef- 480
ficient than the circular array except where the $V A/P_{\text{acs}}$ plot 481
has peaks due to the asymmetries. For this delivery system, 482
the arrays are intended to operate at a single frequency and 483
the asymmetrical modes are of minimal consequence. In or- 484
der to use a large frequency band, the manufacturing process 485
needs to be improved to eliminate asymmetries that occur. 486

Beyond electrically evaluating the arrays for potential 487
use as a drug delivery device, the arrays needed to be char- 488
acterized in terms of the spatial and temporal intensity. For 489
comparison, both arrays were driven such that the I_{sptp} would 490
be similar ($\approx 50 \text{ mW/cm}^2$). Although the I_{sptp} values were 491
similar, the spatial distribution of the temporal peak intensity 492
for the rectangular array [Fig. 5(b)] was much larger than the 493
circular [Fig. 5(a)] array. For the 3×3 circular array, the nine 494
individual transducers appear to be operating as a large 495

496 plane-piston transducer with a new effective aperture instead
497 of nine circular transducers. In contrast, the rectangular array
498 shows three peaks giving rise to an intensity field more
499 widely distributed. This larger field can be used to permeabi-
500 lize a larger area for increased drug delivery.

501 To evaluate this speculation, experiments were per-
502 formed using hyperglycemic rabbits. Comparable to previous
503 experiments using the cymbal array and rabbits,^{19,23} the 3
504 \times 3 circular array decreased the blood glucose level to a
505 statistically significant level (-146.7^* mg/dl at 90 min) com-
506 pared to the control group (Fig. 6). However, using the 3
507 \times 1 rectangular array, the blood glucose level decreased
508 faster and to a lower level than the circular design (
509 -200.8^* mg/dl at 90 min). Based on these results, there ap-
510 pears to be a relationship between the spatial extent of the
511 intensity field and the efficiency of insulin delivery. While
512 increasing the spatial-peak intensity may delivery more insu-
513 lin into the body, this approach also has potential hazardous
514 bioeffects.³⁶ As with diagnostic ultrasound, the bioeffects
515 and safety of each device needs to be carefully monitored
516 since it will not matter how much of any drug can be trans-
517 ported if the skin is burned, damaged, or the procedure is
518 painful. Therefore increasing the spatial extent of the inten-
519 sity field may be a better approach than increasing the peak
520 intensity.

521 In terms of human diabetes, a person is considered dia-
522 betic if their blood sugar level is above 140 mg/dl after 8 h
523 of fasting. People without diabetes have fasting sugar levels
524 that generally run between 70 and 110 mg/dl. A glucose of
525 110–126 mg/dl is classified as impaired fasting glucose,
526 140–200 mg/dl is impaired glucose tolerance, and greater
527 than 200 mg/dl is considered diabetic.^{37–39} In this last situa-
528 tion a diabetic person would need to inject enough insulin to
529 reduce their blood glucose by about 100 mg/dl. Intensities
530 used herein ($I_{\text{sp}} \approx 50 \text{ mW/cm}^2$) are about one-half of what
531 we have used in previous studies.^{19,23,35,40} Compared to our
532 previous circular array results, the rectangular design pro-
533 duced a similar blood glucose decrease but with less peak
534 intensity.

535 Use of transdermal drug delivery techniques has practi-
536 cal clinical application to medications that need to be in-
537 jected multiple times either daily or weekly. A recent com-
538 prehensive review on ultrasound drug delivery states that
539 “small-sized low-frequency transducers need to be developed
540 so that patients can wear them.”⁷ We feel that the cymbal
541 meets this need, and the design has a significant amount of
542 trade space for optimization. As with diagnostic ultrasound
543 imaging, drug delivery using therapeutic ultrasound requires
544 a delicate balance between safety and efficacy and requires
545 careful scientific study. The bioeffects and safety of each
546 device need to be carefully monitored since it will not matter
547 how much of any drug can be transported if the skin is
548 burned, damaged, or the procedure is painful.

549 ACKNOWLEDGMENT

550 This work was supported by the Department of Defense
551 Technologies for Metabolic Monitoring Award No.
552 W81XWH-05-1-0617.

- 553
554
555
556
557
558
559
560
561
562
563
564
565
566
567
568
569
570
571
572
573
574
575
576
577
578
579
580
581
582
583
584
585
586
587
588
589
590
591
592
593
594
595
596
597
598
599
600
601
602
603
604
605
606
607
608
609
610
611
612
613
614
615
616
617
618
619
620
621
622
623
624
625
626
- 1 M. R. Prausnitz, “Reversible skin permeabilization for transdermal deliv-
ery of macromolecules,” *Crit. Rev. Ther. Drug Carrier Syst.* **14**, 455–483
(1997).
- 2 M. R. Prausnitz, “A practical assessment of transdermal drug delivery by
skin electroporation,” *Adv. Drug Delivery Rev.* **35**, 61–76 (1999).
- 3 F. Montorsi *et al.*, “Transdermal electromotive multi-drug administration
for Peyronie’s disease: Preliminary results,” *J. Androl* **21**, 85–90 (2000).
- 4 Y. Wang, R. Thakur, Q. Fan, and B. Michniak, “Transdermal iontophore-
sis: Combination strategies to improve transdermal iontophoretic drug deliv-
ery,” *Eur. J. Pharm. Biopharm.* **60**, 179–191 (2005).
- 5 A. Nanda, S. Nanda, and N. M. Ghilzai, “Current developments using
emerging transdermal technologies in physical enhancement methods,”
Curr. Drug Deliv. **3**, 233–242 (2006).
- 6 S. Mitragotri and J. Kost, “Low-frequency sonophoresis: A review,” *Adv.
Drug Delivery Rev.* **56**, 589–601 (2004).
- 7 W. G. Pitt, G. A. Hussein, and B. J. Staples, “Ultrasonic drug delivery—a
general review,” *Expert. Opin. Drug Deliv.* **1**, 37–56 (2004).
- 8 M. B. Brown, G. P. Martin, S. A. Jones, and F. K. Akomeah, “Dermal and
transdermal drug delivery systems: Current and future prospects,” *Drug
Deliv.* **13**, 175–187 (2006).
- 9 N. B. Smith, “Perspectives on transdermal ultrasound mediated drug deliv-
ery,” *International Journal of Nanomedicine* **2**, (2007).
- 10 S. Mitragotri, D. A. Edwards, D. Blankschtein, and R. Langer, “A mecha-
nistic study of ultrasonically-enhanced transdermal drug delivery,” *J.
Pharm. Sci.* **84**, 697–706 (1995).
- 11 S. Mitragotri, D. Blankschtein, and R. Langer, “An explanation for the
variation of the sonophoretic transdermal transport enhancement from
drug to drug,” *J. Pharm. Sci.* **86**, 1190–1192 (1997).
- 12 H. R. Guzman, A. J. McNamara, D. X. Nguyen, and M. R. Prausnitz,
“Bioeffects caused by changes in acoustic cavitation bubble density and
cell concentration: A unified explanation based on cell-to-bubble ratio and
blast radius,” *Ultrasound Med. Biol.* **29**, 1211–1222 (2003).
- 13 R. K. Schlicher, H. Radhakrishna, T. P. Tolentino, R. P. Apkarian, V.
Zarnitsyn, and M. R. Prausnitz, “Mechanism of intracellular delivery by
acoustic cavitation,” *Ultrasound Med. Biol.* **32**, 915–924 (2006).
- 14 E. Maione, K. K. Shung, R. J. Meyer, J. W. Hughes, R. E. Newnham, and
N. B. Smith, “Transducer design for a portable ultrasound enhanced trans-
dermal drug delivery system,” *IEEE Trans. Ultrason. Ferroelectr. Freq.
Control* **49**, 1430–1436 (2002).
- 15 J. F. Tressler, W. Cao, K. Uchino, and R. E. Newnham, “Finite element
analysis of the cymbal-type flextensional transducer,” *IEEE Trans. Ultra-
son. Ferroelectr. Freq. Control* **45**, 1363–1369 (1998).
- 16 J. Zhang, J. W. Hughes, R. J. Meyer, K. Uchino, and R. E. Newnham,
“Cymbal array: A broad band sound projector,” *Ultrasonics* **37**, 523–529
(2001).
- 17 R. J. Meyer, A. Dogan, C. Yoon, S. M. Pilgrim, and R. E. Newnham,
“Displacement amplification of electroactive materials using the cymbal
flextensional transducer,” *Sens. Actuators, A* **87**, 157–162 (2001).
- 18 N. B. Smith, S. Lee, and K. K. Shung, “Ultrasound-mediated transdermal
in vivo transport of insulin with low-profile cymbal arrays,” *Ultrasound
Med. Biol.* **29**, 1205–1210 (2003).
- 19 B. Snyder, S. Lee, R. E. Newnham, and N. B. Smith, “Ferroelectric trans-
ducer arrays for transdermal insulin delivery,” *J. Mater. Sci.* **41**, 211–216
(2006).
- 20 E. J. Park, J. Werner, and N. B. Smith, “Ultrasound mediated transdermal
insulin delivery in pigs using a lightweight transducer,” *Pharmacol. Res.*
24, 1396–1401 (2007).
- 21 M. Pavlovic, K. Wroblewski, Y. Manevich, S. Kim, and J. E. Biaglow,
“The importance of choice of anaesthetics in studying radiation effects in
the 9L rat glioma,” *Br. J. Cancer Suppl.* **27**, S222–S225 (1996).
- 22 N. Kawai, R. F. Keep, and A. L. Betz, “Hyperglycemia and the vascular
effects of cerebral ischemia,” *Stroke* **28**, 149–154 (1997).
- 23 S. Lee, B. Snyder, R. E. Newnham, and N. B. Smith, “Noninvasive ultra-
sonic transdermal insulin delivery in rabbits using the light-weight cymbal
array,” *Diabetes Technol. Ther.* **6**, 808–815 (2004).
- 24 R. E. Newnham, Q. C. Xu, and S. Yoshikawa, “Transformed stress direc-
tional acoustic transducer,” 4,999,819, 12 March 1991.
- 25 R. E. Newnham, Q. C. Xu, and S. Yoshikawa, “Metal-electroactive ce-
ramic composite actuators,” 5,276,657, 4 January 1994.
- 26 A. Dogan, K. Uchino, and R. E. Newnham, “Composite piezoelectric
transducer with truncated conical endcaps cymbal,” *IEEE Trans. Ultrason.
Ferroelectr. Freq. Control* **44**, 597–605 (1997).
- 27 R. E. Newnham and A. Dogan, “Metal-electroactive ceramic composite
transducer,” 5,729,077, 17 March 1998.

Appendix I

AQ:
#2

AQ:
#3

AQ:
#4

AQ:
#5

- 627 ²⁸W. P. Mason, "Electrostrictive effect in barium titanate ceramics," *Phys. Rev.* **74**, 1134–1147 (1948). 646
- 628 ²⁹A. H. Meitzler, H. M. Obryan, and H. F. Tiersten, "Definition and measurement of radial mode-coupling factors in piezoelectric ceramic materials with large variations in poissons ratio," *SU20*, 233–239 (1973). 647
- 629 ³⁰IEEE Standards Board, *IEEE Standard on Piezoelectricity* (Ferroelectrics and Frequency Control Society Standards Committee of the IEEE Ultrasonics, New York, 1988). 648
- 630 ³¹N. Setter, *Piezoelectric Materials in Devices* (EPFL Swiss Federal Institute of Technology, Lausanne, Switzerland, 2002). 649
- 631 ³²B. Hamonic, J. C. Debus, J. N. Decarpigny, D. Boucher, and B. Tocquet, "Analysis of a radiating thin-shell sonar transducer using the finite element method," *J. Acoust. Soc. Am.* **86**, 1245–1253 (1989). 650
- 632 ³³*IEEE Guide for Medical Ultrasound Field Parameter Measurements* (IEEE, New York, 1990). 651
- 633 ³⁴AIUM, *Acoustic Output Labeling Standard for Diagnostic Ultrasound Equipment* (American Institute of Ultrasound in Medicine, Laurel, MD, 1998). 652
- 634 ³⁵N. B. Smith, S. Lee, E. Maione, R. B. Roy, S. McElligott, and K. K. Shung, "Ultrasound-mediated transdermal transport of insulin *in vitro* through human skin using novel transducer designs," *Ultrasound Med. Biol.* **29**, 311–317 (2003). 653
- 635 ³⁶S. Lee, V. Nayak, J. Dodds, M. Pishko, and N. B. Smith, "Glucose measurements with sensors and ultrasound," *Ultrasound Med. Biol.* **31**, 971–977 (2005). 654
- 636 ³⁷H. Rifkin and D. Porte, *Ellenberg and Rifkin's Diabetes* (Elsevier Science, New York, 1990). 655
- 637 ³⁸J. E. Shaw *et al.*, "Impaired fasting glucose or impaired glucose tolerance. What best predicts future diabetes in Mauritius?," *Diabetes Care* **22**, 399–402 (1999). 656
- 638 ³⁹G. P. Carnevale Schianca, A. Rossi, P. P. Sainaghi, E. Maduli, and E. Bartoli, "The significance of impaired fasting glucose versus impaired glucose tolerance: Importance of insulin secretion and resistance," *Diabetes Care* **26**, 1333–1337 (2003). 657
- 639 ⁴⁰S. Lee, R. E. Newnham, and N. B. Smith, "Short ultrasound exposure times for noninvasive insulin delivery in rats using the lightweight cymbal array," *IEEE Trans. Ultrason. Ferroelectr. Freq. Control* **51**, 176–180 (2004). 658
- 640 659
- 641 660
- 642 661
- 643 662
- 644 663
- 645 664

Appendix I

Research Paper

Ultrasound Mediated Transdermal Insulin Delivery in Pigs Using a Lightweight Transducer

E. J. Park,¹ Jacob Werner,² and Nadine Barrie Smith^{3,4}

Received February 14, 2007; accepted March 26, 2007

Purpose. In previous studies, ultrasound mediated transdermal drug delivery has shown a promising potential as a method for noninvasive drug administration. For prospective future human application, this study was designed to determine the feasibility of lightweight cymbal transducer array as a practical device for noninvasive transdermal insulin delivery in large pigs.

Materials and Methods. Six Yorkshire pigs (100–140 lbs) were divided into two groups. As the control ($n=3$), the first group did not receive any ultrasound exposure with the insulin. The second group ($n=3$) was treated with ultrasound and insulin at 20 kHz with an $I_{\text{sptp}}=100 \text{ mW/cm}^2$ at a 20% duty cycle for 60 min. With the pigs in lateral recumbency after anesthesia, the ultrasound transducer with insulin was placed on the axillary area of the pig. At the beginning and every 15 min up to 90 min, the blood glucose level was determined using a glucose monitoring system. To compare the results of individual animals, the change of blood glucose level was normalized to each animal's initial glucose value at the start of the experiment.

Results. Although each animal had a different initial glucose level, the mean and standard error for the six animals was $146 \pm 13 \text{ mg/dl}$. For the control group, the blood glucose level increased to $31 \pm 21 \text{ mg/dl}$ compared to the initial baseline over the 90 min experiment. However for the ultrasound with insulin treated group, the glucose level decreased to $-72 \pm 5 \text{ mg/dl}$ at 60 min ($p < 0.05$) and continued to decrease to $-91 \pm 23 \text{ mg/dl}$ in 90 min ($p < 0.05$).

Conclusion. The results indicate the feasibility of ultrasound mediated transdermal insulin delivery using the cymbal transducer array in animal with a similar size and weight to a human. Based on these result, the cymbal array has potential as a practical ultrasound system for noninvasive transdermal insulin delivery for diabetes management.

KEY WORDS: diabetes; drug delivery; insulin; transducer; ultrasound.

INTRODUCTION

Use of needles for multiple injection of drugs, such as insulin for diabetes, can be painful. As a result, prescribed drug noncompliance can result in severe medical complications. Several noninvasive methods exist for transdermal drug delivery. These include chemical mediation using liposomes and chemical enhancers or physical mechanisms such as microneedles, iontophoresis, electroporation, and ultrasound (1–5). Ultrasound enhanced transdermal drug delivery presents advantages over traditional injection drug delivery methods which are invasive and painful. Currently only a small amount of drugs have been successfully administered transdermally for clinical applications because of the low skin

permeability to these relatively large molecules. This low permeability is mainly attributed to the outermost skin layer, *stratum corneum*, which consists of a condensed and ordered structure of cells, keratinocytes, compassed by lipid bilayers. Once the drug crosses *stratum corneum*, the next epidermal layer is less problematic to traverse, and consequently the drug can reach the capillary bed to be absorbed (6,7).

Recent reviews have shown that ultrasound mediated transdermal drug delivery offers promising potential for noninvasive drug administration (8–10). The working principle of sonophoresis, although not completely understood, has been suggested to be the result of cavitation (11–14). Low frequency ultrasound is capable of generating microbubbles in the water and tissue. These bubbles allow water channels to be produced within the lipid bilayers. The resulting disorder created in the *stratum corneum* facilitates the crossing of a hydrophilic drug or molecule. To this end, the number of drugs and compounds which have been shown to transdermally cross skin via ultrasound is ever increasing (15).

Noninvasive methods for transdermal delivery of insulin have particular public interest due to the increasing problem of diabetes. Approximately 16 million people suffer from

¹Department of Bioengineering, Pennsylvania State University, University Park, Pennsylvania, USA.

²Animal Resource Program, Pennsylvania State University, University Park, Pennsylvania, USA.

³Graduate Program in Acoustics, Pennsylvania State University, University Park, Pennsylvania, USA.

⁴To whom correspondence should be addressed. (e-mail: nbs@enr.psu.edu)

diabetes mellitus in the United State alone. From a human and economic perspective, it is one of the most costly diseases and management of diabetes often requires painful repetitive insulin injections up to three to four times each day (16,17). Thus the research for safe and convenient noninvasive insulin delivery is increasing every year. Over a frequency range of 20–105 kHz, enhanced transport in the presence of ultrasound has been shown in both *in vitro* and *in vivo* experiments (6,18–23). Many early experiments were performed using either an ultrasound sonicator, ultrasonic bath or commercial transducer. For example investigators have demonstrated effective *in vivo* transport of insulin at 48 kHz using an ultrasonic bath (24) and 105 kHz (18) using a commercially obtained transducer. The major drawback so far in exploiting ultrasound for noninvasive drug delivery is the large size and poor mobility of the ultrasound device. Commercial sonicators are large, heavy, table-top devices specifically designed for lysis of cells, catalyzing reactions, creating emulsions or cleaning.

A recent comprehensive review on ultrasound drug delivery states that “small-sized low-frequency transducers need to be developed so that patients can wear them” (9). There are several possible low frequency transducer designs that can be used in a drug delivery application, such as the low frequency flextensional resonators (25), tonpilz transducers (26), or “thickness”-type resonators (27). One other inexpensive candidate is the low-profile, light weight cymbal transducer for a portable device. This flextensional transducer has a thickness of less than 2 mm, weighs less than 3 g and resonates between 1 and 100 kHz depending on geometry (28–30). Multiple cymbals can be patterned side-by-side into 2×2 and 3×3 arrays for increased spatial intensity fields for drug transport. Consequently the use of the low-profile, light weight cymbal ultrasound array has previously demonstrated transport enhancement of insulin across *in vitro* human skin (23), *in vivo* rats (31,32) and rabbits (33,34). Additionally the cymbal design has also been used for noninvasive glucose sensing (35).

Yet for prospective human application, a milestone to a practical clinical device of this research requires that the efficacy of the cymbal array be demonstrated on animals larger than rats and rabbits. Larger and possessing a blood volume similar to humans, pigs are an appropriate animal models for further experimentation in evaluating the practicability of this ultrasound device. Based on the positive results from our previous research, the purpose of this study was to determine the feasibility of ultrasound mediated transdermal delivery of insulin *in vivo* using pigs to mimic possible future applications in humans.

MATERIALS AND METHODS

Ultrasound Transducer Array

Details regarding the design and construction of the cymbal transducer and the multi-element array have been described elsewhere (28–30). Briefly, the cymbal transducer is a novel flextensional transducer capable of producing very low frequencies (Fig. 1a). The cymbal transducer has a compact, lightweight structure with an adjustable resonance

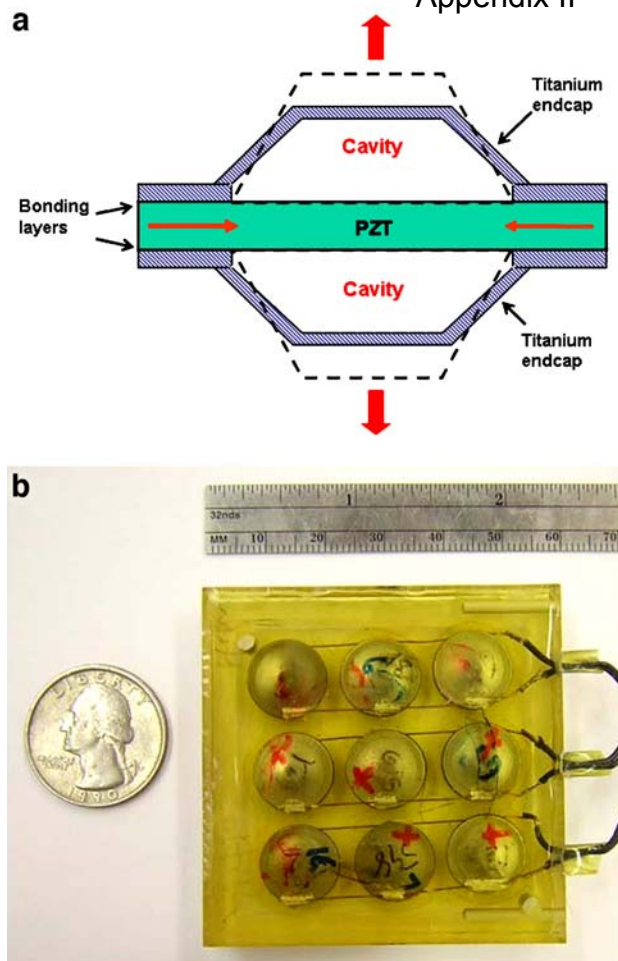


Fig. 1. **a** The cymbal transducer operated at a frequency of 20 kHz. Placed between two titanium caps with air cavities beneath, the motion of the cymbal disk moves the caps which to give rise to radial oscillations. *Dashed lines* represent the flexing of the caps and the *arrows* indicate the motion. **b** A light weight, low-profile array was constructed using nine cymbal transducers which were connected in parallel and encased in a polymer.

frequency. In the cymbal transducer design, the caps on the lead zirconate-titanate (PZT) ceramic contained a shallow cavity beneath its inner surface. The fundamental mode of vibration is the flexing of the end caps caused by the radial motion of the ceramic represented by the dashed lines in Fig. 1a. Therefore, the overall displacement of the device is a combination of the axial motion of the disk plus the radial motion amplified by the end caps. Amplification factors can be as high as 40 times that of the ceramic by itself (36). Specifically, the piezoelectric disc was made from PZT-4 (Piezokinetics, Inc., Bellefonte, PA), had a diameter of 12.7 mm, and was 1 mm thick. PZT-4 was chosen because this material has a high failure voltage threshold compared to ceramics with similar efficiency. Caps were made of 0.25-mm thick titanium while the thin glue layer between the caps and the ceramic disk was made of Eccobond[®] (Emerson & Cuming, Billerica, MA) epoxy. For the array, four transducers were connected in parallel and encased in URALITE[®] polymer (FH 3550, H.B. Fuller, St. Paul, MN, USA) to produce a transducer array arrangement. A three-by-three

Ultrasound Transdermal Insulin Delivery in Pigs

(3×3) elemental pattern was used for the array and was in a 56×56×8 mm³ block (Fig. 1b).

To drive the array, a radio frequency (RF) signal was generated by a frequency pulse/function generator (Agilent 32250A, Palo Alto, CA) and amplified by an RF amplifier (Model 40A12, Amplifier Research, Souderton, PA). The electrical impedance of the array was tuned to the output impedance of the amplifier by an external inductor-capacitor tuning network. Pulse period, duty cycle and exposure time of the RF signal from the frequency generator was monitored using an oscilloscope (Tektronix 2213A, Beaverton, OR). For the experiments, the signal generator operated at 20 kHz with pulse duration of 200 ms and pulse repetition period of 1 s (i.e. 20% duty cycle); the amplifier gain was set to 50 dB. Pulsed ultrasound was used to avoid damaging heat build-up to either the array or animal's skin.

Ultrasound Exosimetry

The intensity was determined according to exosimetry guidelines established by the American Institute of Ultrasound in Medicine (37,38). For the acoustic field at a plane 1 mm from the transducer face, the ultrasonic intensities from the array were measured with a calibrated miniature (4 mm diameter) omnidirectional reference hydrophone (Model TC4013, S/N: 5199093, RESON, Inc., Goleta, CA). The cymbal array was submerged in a water tank (51×54×122 cm³) which was made almost anechoic by placing 1.27 cm thick rubber sound absorbing material around its wall. A custom made degasser, built in-house, reduced the dissolved oxygen content of the distilled water to 1–2 ppm to reduce cavitation effects. Pulse period, duty cycle and exposure time of the signal from the frequency generator and hydrophone was acquired using an Agilent 54622A 100 MHz digitizing oscilloscope (Agilent, Palo Alto, CA).

Precise, computer controlled positioning of the hydrophone was performed by a Velmex Positioning System (Velmex Inc., East Bloomfield, NY). Pressure waves detected by the hydrophone were recorded by a digitizing oscilloscope. A computer-controlled exosimetry positioning system was used for automated scanning. The scanning step size for each device was 1 mm and the scanning area was 80×80 mm². Spatial peak-temporal peak (I_{sptp}) and spatial average-temporal peak (I_{satp}) intensities were determined over a plane 1 mm from the array face using the hydrophone based on 3–5 scanning of the array for a mean and standard deviation of the intensity results. The intensity of cymbal transducer array was $I_{\text{sptp}}=100.8\pm 0.6$ mW/cm² and $I_{\text{satp}}=30.7\pm 0.6$ mW/cm².

Animal Experiments

The pigs were anesthetized and euthanized by procedures approved by the Institutional Animal Care and Use Committee (IACUC) at the Pennsylvania State University. Six Yorkshire pigs (100–140 lbs) obtained from the Penn State Swine Center were divided into two experimental groups. As the control ($n=3$), the first group did not receive any ultrasound exposure with the insulin while second group ($n=3$) was treated with ultrasound and insulin. Each animal was pre-anesthetized for intubation with a combination of ketamine hydrochloride (10–12 mg/kg intramuscularly,

Appendix II

Ketaject[®], Phoenix, St. Joseph, MO) and sodium xylazine (1–2 mg/kg intramuscularly, Xyla-Ject[®], Phoenix, St. Joseph, MO). Pigs were fitted with an intravenous (IV) catheter in the auricular vein and an endotracheal tube (size 6–7) was inserted into the airway. Anesthesia throughout the remaining experiment was maintained to surgical depth via inhalant isoflurane (Isothesia[™], Abbott Laboratories, North Chicago, IL) using an inhalational anesthesia unit (Narkovet Deluxe, North American Drager, Telford, PA).

The axillary area of the pigs were shaved using an electric shaver, and a depilatory agent was applied to the skin of both groups, control and exposure, to eliminate any remaining hair. With the pig in the lateral recumbency (Fig. 2a), a 1 mm thick, water-tight standoff was attached (Fig. 2b) between the skin and the array using tissue glue (Vetbond[®], 3M, St. Paul, MN). The reservoir within standoff was filled with insulin (Humulin[®] R, rDNA U-100, Eli Lilly and Co., Indianapolis, IN) through a small hole in the back of the array for both the control and exposure experiments. To prevent disruption of ultrasound transmission, care was taken to remove all bubbles from the solution in the reservoir (standoff) between the axillary area and the array.

At the beginning of the experiment, blood sample (0.3 ml) was collected from the ear vein of each pig for a baseline glucose level analysis. The glucose level (mg/dl) in the blood was determined using ACCU-CHEK[™] blood glucose monitoring system (Roche Diagnostics Co., Indianapolis, IN, USA). Multiple blood samples (2–4 each time) were taken

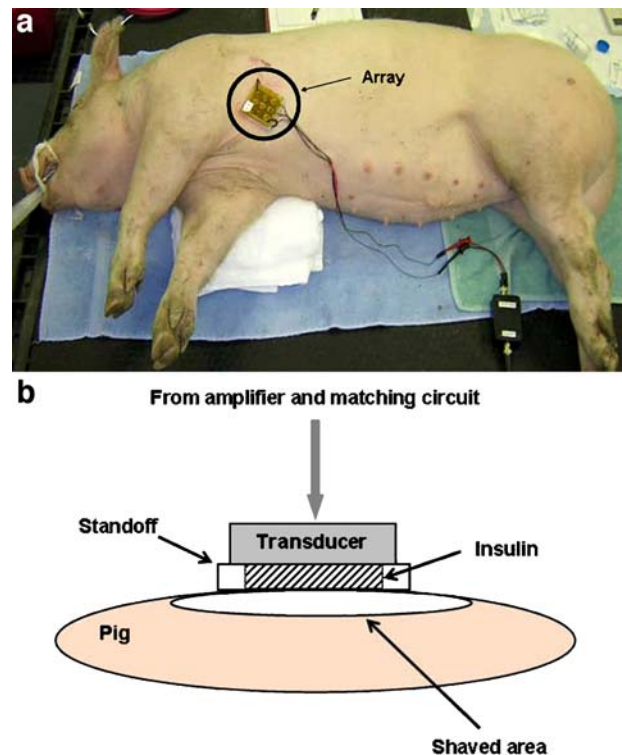


Fig. 2. a Photograph of a transdermal insulin delivery experiment with pig placed in a lateral recumbent position with the array attached. b Illustration of the experiment with a 1 mm thick water tight standoff arranged between the axillary area and the array. The reservoir within the standoff was filled with insulin through a small hole in the back of the array.

every 15 min for 90 min. Elapsed time from the initial injection of the ketamine-xylazine until the first glucose measurement was no greater than 15 min. For comparison between the pigs, the change in the blood glucose level was normalized to a baseline with respect to each animal's initial blood glucose recording at 0 min.

For comparison between the results of each pig, the change of blood glucose level was normalized with respect to the initial blood glucose level of each pig. The control group (three pigs) used insulin inside the reservoir without ultrasound exposure while the second group (three pigs) was treated with ultrasound and insulin at 20 kHz with an $I_{\text{sptp}} = 100 \text{ mW/cm}^2$ for 60 min. For both groups, the standoff reservoir with the insulin or saline was removed at 60 min although glucose determination continued until 90 min from the start. At the end of the experiments, the pig was euthanized (Pentobarbital, Fatal Plus[®], 130 mg/kg IV, Vortech Pharmaceuticals, Ltd., Dearborn MI) under anesthesia.

Statistical analysis was performed using Microsoft Excel[®] (Microsoft Corp., Redmond, WA). The blood glucose verses time data were pooled for each group and analyzed as its mean and standard error ($\bar{x} \pm \text{s.e.}$). An ANOVA was used to analyze the statistical significance of the differences among the means of groups. The p-value was used to determine if the between-group differences are significantly greater than chance. For all the data, a single or double asterisk was used if the p-value is less than the 0.05 or 0.01 level of significance, respectively.

RESULTS

Results of the ultrasonic transdermal insulin delivery in large pigs for the two groups are graphed (Fig. 3) as the change in the blood glucose level during the 90 min experiment in terms of the mean and standard error. After the pigs were anesthetized, the average initial glucose level of the six pigs was $146 \pm 13 \text{ mg/dl}$. Generally for pigs, the blood glucose level is approximately 100–110 mg/dl (39,40). As mentioned, for comparison between the pigs the change in the blood glucose level was normalized to a baseline which was the initial glucose level for each pig.

For the control group (insulin without ultrasound), the glucose level increased to $31 \pm 21 \text{ mg/dl}$ compared to the initial baseline over the 90 min experiment. The slope of this increase was $+20 \text{ mg/dl/h}$ ($r^2 = 0.9$). In contrast with the ultrasound exposure group (insulin with ultrasound), the glucose level decreased to $-74 \pm 5 \text{ mg/dl}$ at 60 min and continued to decrease to $-91 \pm 9 \text{ mg/dl}$ at 90 min after the stand off was removed. Additionally, a gross examination of the pig's skin was performed after exposure to look for visible lesions on the skin surface. Visual examination of the post ultrasound exposed skin did not indicate any noticeable damage or significant change to the skin.

To determine the statistical significance between the results in Fig. 3 of the two groups at the 15 min increment time points of experiment, an ANOVA was used to analyze this data. Asterisks above a glucose-time data point were used if there existed statistical difference between the control and exposure. At 15 min the analysis showed no statistical difference between the groups. However comparison of the control against the ultrasound exposure groups at 30 min and

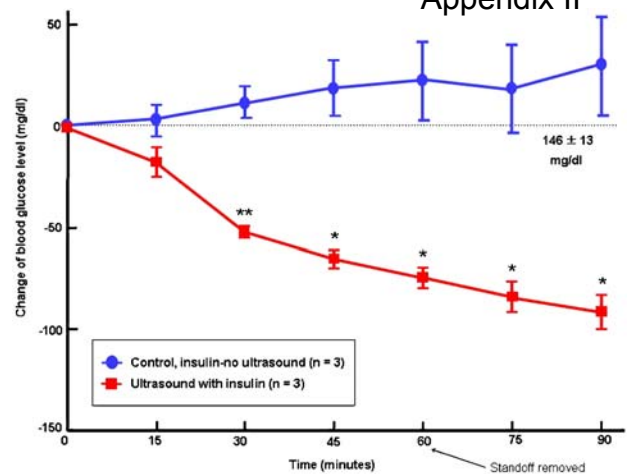


Fig. 3. Over a period of 90 min, the blood glucose level of pig decreased to $-91 \pm 9 \text{ mg/dl}$ at 90 min for ultrasound mediated transdermal insulin delivery. An ANOVA analysis of the control and ultrasound exposed groups at 30 min and greater indicated that the results were statistically significant at p values of 0.05 or better.

greater indicated that the results were statistically significant at a p value of 0.05 or better.

DISCUSSION

The goal of this research was to determine if a light-weight, low-profile ultrasound device based cymbal transducer device could be used for *in vivo* transdermal insulin in animals which approximate the size and weight of a human. Although commercial sonicators have been admirable devices for demonstrating drug delivery, the ultrasonic probe or converter from a sonicators can weigh almost a kilogram or more while the cymbal array weighs less than 38 g. Individual cymbals (Fig. 1a) can be arranged into multi-element array designs (Fig. 1b) since this can increase the effective aperture of ultrasound area with respect to skin area and some research indicates that the delivery dose increases with ultrasound exposure area (23). Interestingly the cymbal design originates from underwater research for Navel applications and current research is underway to incorporate existing battery technology in the miniaturization of portable power (41).

Generally xylazine causes hyperglycemia in rats and rabbits (42–45). Specifically for pigs, xylazine suppresses insulin release (46) which resulted in the higher initial average blood glucose level of 146 mg/dl pigs. The mean value for normal blood glucose levels for pigs is approximately 108.5 mg/dl (40) yet the use of the xylazine appears to have the continual effect of increasing the glucose level at a rate of 20 mg/dl/h even after the experiment started. This may indicate either the lack of passive permeability of the pig's skin to the insulin or the sustained consequence of the xylazine. Yet the useful effect of using these insulin suppressed pigs was to demonstrate the feasibility of reducing a high glucose level ($\approx 150 \text{ mg/dl}$) to a normal glucose level (below 100) albeit for a pig model. In contrast to the control group, the ultrasound with insulin group showed a blood glucose level decrease of -91 mg/dl at 90 min compared to the baseline. Moreover compared to the control at 90 min, the

difference between the two groups was approximately 120 mg/dl and the ANOVA analysis indicated there was a statistical difference ($p>0.05$) between the two groups at the time points of 30 min and greater.

To examine these results in terms of human diabetes, a person is considered diabetic if their blood sugar level is above 140 mg/dl after fasting. People without diabetes have fasting sugar levels that generally run between 70–110 mg/dl. When fasting, glucose of 110–126 mg/dl is classified as impaired fasting glucose, 140–200 mg/dl is impaired glucose tolerance and greater than 200 mg/dl is considered diabetic (47–49). In this case a diabetic person would need to inject enough insulin to reduce their blood glucose by about 100 mg/dl. Summarizing our previous ultrasound exposure results using hyperglycemic animals at 90 min, the glucose level continued to decrease to -296.7 ± 52.8 mg/dl in rats and -208.1 ± 29 mg/dl in rabbits (23,33). Although the decrease in blood glucose in this pig research was not as large in the rats and rabbits, this may be due to the fact that the blood volume and body mass is far greater for pigs. Nevertheless the results indicate that the array was capable of safely reducing a diabetic glucose level to a normal range. In conclusion, results herein demonstrate a promising pre-clinical outcome for the low profile cymbal array to be used for ultrasound enhanced *in vivo* insulin transport using an animal model which mimics human use.

ACKNOWLEDGEMENTS

This work was supported by the Department of Defense Technologies for Metabolic Monitoring Award Number W81XWH-05-1-0617.

REFERENCES

1. M. R. Prausnitz. Reversible skin permeabilization for transdermal delivery of macromolecules. *Crit. Rev. Ther. Drug Carrier Syst.* **14**:455–483 (1997).
2. M. R. Prausnitz. A practical assessment of transdermal drug delivery by skin electroporation. *Adv. Drug Deliv. Rev.* **35**:61–76 (1999).
3. F. Montorsi, A. Salonia, G. Guazzoni, L. Barbieri, R. Colombo, M. Brausi, V. Scattoni, P. Rigatti, and G. Pizzini. Transdermal electromotive multi-drug administration for Peyronie’s disease: preliminary results. *J. Androl.* **21**:85–90 (2000).
4. Y. Wang, R. Thakur, Q. Fan, and B. Michniak. Transdermal iontophoresis: combination strategies to improve transdermal iontophoretic drug delivery. *Eur. J. Pharm. Biopharm.* **60**:179–191 (2005).
5. A. Nanda, S. Nanda, and N. M. Ghilzai. Current developments using emerging transdermal technologies in physical enhancement methods. *Curr. Drug Deliv.* **3**:233–242 (2006).
6. J. Kost. Ultrasound-assisted insulin delivery and noninvasive glucose sensing. *Diabetes Technol. Ther.* **4**:489–497 (2002).
7. M. J. King, I. Badea, J. Solomon, P. Kumar, K. J. Gaspar, and M. Foldvari. Transdermal delivery of insulin from a novel biphasic lipid system in diabetic rats. *Diabetes Technol. Ther.* **4**:479–488 (2002).
8. K. Tachibana and S. Tachibana. The use of ultrasound for drug delivery. *Echocardiography* **18**:323–328 (2001).
9. W. G. Pitt, G. A. Hussein, and B. J. Staples. Ultrasonic drug delivery—a general review. *Expert Opin Drug Deliv.* **1**:37–56 (2004).

10. S. Mitragotri. Healing sound: the use of ultrasound in drug delivery and other therapeutic applications. *Nat. Rev. Drug Discov.* **4**:255–260 (2005).
11. S. Mitragotri, D. A. Edwards, D. Blankschtein, and R. Langer. A mechanistic study of ultrasonically-enhanced transdermal drug delivery. *J. Pharm. Sci.* **84**:697–706 (1995).
12. S. Mitragotri, D. Blankschtein, and R. Langer. An explanation for the variation of the sonophoretic transdermal transport enhancement from drug to drug. *J. Pharm. Sci.* **86**:1190–1192 (1997).
13. H. R. Guzman, A. J. McNamara, D. X. Nguyen, and M. R. Prausnitz. Bioeffects caused by changes in acoustic cavitation bubble density and cell concentration: a unified explanation based on cell-to-bubble ratio and blast radius. *Ultrasound Med. Biol.* **29**:1211–1222 (2003).
14. R. K. Schlicher, H. Radhakrishna, T. P. Tolentino, R. P. Apkarian, V. Zarnitsyn, and M. R. Prausnitz. Mechanism of intracellular delivery by acoustic cavitation. *Ultrasound Med. Biol.* **32**:915–924 (2006).
15. N. B. Smith. Perspectives on transdermal ultrasound mediated drug delivery. *International Journal of Nanomedicine* **2**(2). (2007). (in press).
16. Congressionally established diabetes research working group. Conquering diabetes: a strategic plan for the 21st century. NIH Publication No. 99-4398. 1999.
17. The Whitaker Foundation. *Biomedical engineering and the fight against diabetes, 2003 Annual Report*. The Whitaker Foundation, Arlington, VA, 2004.
18. K. Tachibana. Transdermal delivery of insulin to alloxan-diabetic rabbits by ultrasound exposure. *Pharm. Res.* **9**:952–954 (1992).
19. S. Mitragotri, D. Blankschtein, and R. Langer. Ultrasound-mediated transdermal protein delivery. *Science* **269**:850–853 (1995).
20. I. Zhang, K. K. Shung, and D. A. Edwards. Hydrogels with enhanced mass transfer for transdermal drug delivery. *J. Pharm. Sci.* **85**:1312–1316 (1996).
21. A. Boucaud, L. Tessier, L. Machet, L. Vaillant, and F. Patat. Transdermal delivery of insulin using low frequency ultrasound. In *Proceedings of the IEEE 2000 Ultrasonics Symposium, San Juan Porto Rico*, 2000, pp. 1453–1456.
22. A. Boucaud, M. A. Garrigue, L. Machet, L. Vaillant, and F. Patat. Effect of sonication parameters on transdermal delivery of insulin to hairless rats. *J. Control. Release* **81**:113–119 (2002).
23. N. B. Smith, S. Lee, E. Maione, R. B. Roy, S. McElligott, and K. K. Shung. Ultrasound mediated transdermal transport of insulin through *in vitro* human skin using novel transducer designs. *Ultrasound Med. Biol.* **29**:311–317 (2003).
24. K. Tachibana and S. Tachibana. Transdermal delivery of insulin by ultrasonic vibration. *J. Pharm. Pharmacol.* **43**:270–271 (1991).
25. D. Stansfield. *Underwater electroacoustic transducers*. Bath University Press, Bath, UK, 1990.
26. O. B. Wilson. *An introduction to the theory and design of sonar transducers*. Peninsula, Los Altos, CA, 1988.
27. K. K. Shung, M. B. Smith, and B. Tsui. *Principles of medical imaging*. Academic, San Diego, 1992.
28. R. E. Newnham, Q. C. Xu, and S. Yoshikawa. Transformed stress direction acoustic transducer. US Patent 4,999,819, March 12, 1991.
29. R. E. Newnham, Q. C. Xu, and S. Yoshikawa. Metal-electroactive ceramic composite actuators. US Patent 5,276,657, January 4, 1994.
30. E. Maione, K. K. Shung, R. J. Meyer, J. W. Hughes, R. E. Newnham, and N. B. Smith. Transducer design for a portable ultrasound enhanced transdermal drug delivery system. *IEEE Trans. Ultrason. Ferroelectr. Freq. Contr.* **49**:1430–1436 (2002).
31. N. B. Smith, S. Lee, and K. K. Shung. Ultrasound-mediated transdermal *in vivo* transport of insulin with low-profile cymbal arrays. *Ultrasound Med. Biol.* **29**:1205–1210 (2003).
32. S. Lee, R. E. Newnham, and N. B. Smith. Short ultrasound exposure times for noninvasive insulin delivery in rats using the light weight cymbal array. *IEEE Trans. Ultrason. Ferroelectr. Freq. Contr.* **51**:176–180 (2004).
33. S. Lee, B. Snyder, R. E. Newnham, and N. B. Smith. Noninvasive ultrasonic transdermal insulin delivery in rabbits

- using the light-weight cymbal array. *Diabetes Technol. Ther.* **6**:808–815 (2004).
34. B. Snyder, S. Lee, R. E. Newnham, and N. B. Smith. Ferroelectric transducer arrays for transdermal insulin delivery. *J. Mater. Sci.* **41**:211–216 (2006).
 35. S. Lee, V. Nayak, J. Dodds, M. Pishko, N. B. Smith. Ultrasonic mediated glucose measurements *in vivo* using the cymbal array. *Ultrasound Med. Biol.* **31**:971–977 (2005).
 36. R. J. Meyer, A. Dogan, C. Yoon, S. M. Pilgrim, and R. E. Newnham. Displacement amplification of electroactive materials using the cymbal flextensional transducer. *Sens. Actuators* **87**:157–162 (2001).
 37. IEEE. *IEEE guide for medical ultrasound field parameter measurements*. Institute of Electrical and Electronics Engineers, Inc., New York, 1990.
 38. AIUM. *Acoustic output labeling standard for diagnostic ultrasound equipment*. American Institute of Ultrasound in Medicine, Laurel, MD, 1998.
 39. W. G. Pond and K. A. Houpt. *The biology of the pig*. Cornell University Press, Ithaca, NY, 1978.
 40. D. Danfaer. *A quantitative biology of the pig*. CABI, New York, NY, 1998.
 41. J. F. Tressler, W. Cao, K. Uchino, and R. E. Newnham. Finite element analysis of the cymbal-type flextensional transducer. *IEEE Trans. Ultrason., Ferroelect. Freq. Contr.* **45**:1363–1369 (1998).
 42. J. E. Harkness and D. J. Wagner. *The biology and medicine of rabbits and rodents*. Williams and Wilkins, Baltimore MD, 1995.
 43. M. Pavlovic, K. Wroblewski, Y. Manevich, S. Kim, and J. E. Biaglow. The importance of choice of anaesthetics in studying radiation effects in the 9L rat glioma. *Br. J. Cancer., Suppl.* **27**:S222–S225 (1996).
 44. E. Hillyer and K. E. Quesenberry. *Ferrets, rabbits, and rodents: clinical medicine and surgery*. Saunders, Philadelphia PA, 1997.
 45. N. Kawai, R. F. Keep, and A. L. Betz. Hyperglycemia and the vascular effects of cerebral ischemia. *Stroke.* **28**:149–154 (1997).
 46. K. E. Heim, J. S. Morrell, A. M. Ronan, and A. R. Tagliaferro. Effects of ketamine-xylazine and isoflurane on insulin sensitivity in dehydroepiandrosterone sulfate-treated minipigs (*Sus scrofa domestica*). *Comp. Med.* **52**:233–237 (2002).
 47. H. Rifkin and D. Porte. *Ellenberg and rifkin's diabetes*. Elsevier, New York, NY, 1990.
 48. J. E. Shaw, P. Z. Zimmet, de Court, G. K. Dowse, P. Chitson, H. Gareeboo, F. Hemraj, D. Fareed, J. Tuomilehto, and K. G. Alberti. Impaired fasting glucose or impaired glucose tolerance. What best predicts future diabetes in Mauritius? *Diabetes Care.* **22**:399–402 (1999).
 49. G. P. Carnevale Schianca, A. Rossi, P. P. Sainaghi, E. Maduli, and E. Bartoli. The significance of impaired fasting glucose versus impaired glucose tolerance: importance of insulin secretion and resistance. *Diabetes Care.* **26**:1333–1337 (2003).

Editorial

Theme Section: Transdermal Delivery of Proteins

Received April 16, 2007; accepted April 19, 2007; published online May 11, 2007

ABOUT THE GUEST EDITOR

Dr. Ajay K. Banga is Professor and Chair in the Department of Pharmaceutical Sciences at the College of Pharmacy and Health Sciences, Mercer University, Atlanta, GA. He has a Ph.D. in pharmaceuticals from Rutgers University, NJ. He has over 50 publications and serves as the Editor-in-Chief for the journal *Critical Reviews in Therapeutic Drug Carrier Systems*. He has investigated transdermal iontophoretic drug delivery for several years and is the author of a book, *Electrically Assisted Transdermal and Topical Drug Delivery*. He has also written a book on *Therapeutic Peptides and Proteins: Formulation, Processing, and Delivery Systems*, which is now in its Second Edition. One major area of his research at this time is transdermal delivery of proteins.

GUEST EDITOR'S VIEWS ON TRANSDERMAL DELIVERY OF PROTEINS

Where is the field of transdermal delivery of proteins going and how do the articles in the theme section fill the gap?

Transdermal delivery products currently on the market tend to contain small moderately lipophilic drug molecules, which can be delivered through the skin. Opportunities in transdermal delivery can be expanded to include small water soluble drugs as well as macromolecules, such as therapeutic proteins, by several enhancement technologies that are being actively investigated. One promising technique is iontophoresis, which involves the use of a small electric field to push charged drug molecules into the body. Iontophoresis has been used for localized delivery of drugs for many years but recently has seen some success for systemic drug delivery from a pre-filled wearable iontophoretic patch. This has been made possible by the advancement in the field of iontophoretic drug delivery. Several academic groups, especially Professor Richard Guy's group at University of Bath, have contributed significantly to an understanding of transdermal delivery of proteins by iontophoresis as well as by other enhancement technologies. Our laboratory, as well as Dr. Kalia's group, who is a contributor to this theme section, have contributed to this field in addition to excellent contributions from Alza and other companies. Iontophoresis is generally believed to have a size limitation of about 10 kDa for systemic drug delivery. However, one of the papers in this

Theme Section reports that delivery of a 12.4-kDa protein by iontophoresis is feasible. There is some clinical literature, which suggests that localized delivery of much larger molecules is possible by iontophoresis.

Iontophoresis cannot deliver all proteins through the skin and researchers are investigating several other enhancement technologies, including thermal microporation, microneedles, and phonophoresis. Recently, considerable excitement has been generated around skin microporation technology, which involves the creation of micron dimension transport pathways in the skin using a minimally invasive technique, such as microneedles, thermal microporation or radiofrequency ablation. This theme section has two articles on skin microporation, one on the development of coated microneedles and the other on the use of thermal microporation for delivery of interferon across skin. Phonophoresis or the use of ultrasound energy is another promising technology for transdermal delivery of macromolecules and is discussed in one of the papers in this theme section. However, the miniaturization of ultrasound systems has not yet advanced to the point of enabling wearable patches as is now possible for iontophoretic patches. The paper in this theme section demonstrates the use of lightweight cymbal arrays, which will help to move towards this goal of miniaturization.

What are the challenges for transdermal delivery of protein drugs and how can these be overcome?

Several protein-based drugs are currently in clinical trials for transdermal delivery. Although transdermal delivery of protein drugs is an exciting opportunity, there are still several challenges to overcome. One challenge is that bioavailability currently tends to be low for some of the enhancement methods and this would be of concern, especially considering the high cost of many protein drug molecules. High bioavailability is desired to meet dosing requirements with a reasonable patch size. Bioavailability can be increased by using coated microneedles, where feasible, or by optimized formulation or device design. Some challenges may be specific to the enhancement technology being used. For example, there is a limit to the size of the molecule that can be delivered by iontophoresis. For iontophoresis, a high isoelectric point is desirable so that the drug does not precipitate within the skin. Technologies involving the creation of physical openings in the skin for protein delivery, may present an increased risk of infection.

Appendix III

As with conventional transdermal patches, irritation, patch fall-off and the effect of heat application will have to be minimized for a product to be successful and achieve FDA approval. Since the skin is an attractive site for immunization, there may be a greater immune response, which will depend on the nature and purity of the protein being delivered. The extent of immune response and how it affects treatment efficacy, needs further investigation. Also, the skin has proteolytic enzymes (though proteolytic activity is less compared to other mucosal routes) that may degrade the protein drug as it travels through the skin. We generally focus on how much of the protein has been delivered intact through the skin. More studies are needed to better understand the proteolytic barrier in the skin and its potential effect on protein drug delivery.

EDITORIAL FOR THEME SECTION/DR. AJAY K. BANGA

Significant strides have been made in drug delivery research in recent years, and several products have been commercialized, especially for oral and parenteral delivery. Of the various other routes investigated, transdermal drug delivery has achieved commercial success, with several drugs now in the market, including clonidine, estradiol, fentanyl, methylphenidate, nicotine, nitroglycerin, oxybutynin, scopolamine, selegiline, and testosterone. In addition, the estrogen/progestin combination patch for birth control is available. These drugs tend to be small moderately lipophilic drug molecules. Many of the new drugs are now protein-based, and these hydrophilic macromolecules do not diffuse through the skin. Some other routes such as pulmonary have shown promise for delivery of proteins and inhaled insulin has been recently commercialized. However, skin is an appealing site for drug delivery and in recent years, nontraditional enhancement technologies are being explored to enable the delivery of these molecules through the skin. These enhancement techniques include the use of electric energy (iontophoresis and electroporation), ultrasound (phonophoresis, also known as sonophoresis) or minimally invasive techniques such as skin microporation (microneedles, thermal microporation, and radiofrequency ablation).

Iontophoresis has been used for localized delivery of steroids or lidocaine using external palm sized power sources for several years. More recently, research has enabled the development of wearable self contained patches for systemic delivery of drugs. One systemically acting drug that has been recently approved for iontophoretic delivery from a pre-filled patch is fentanyl hydrochloride. The compact self contained iontophoretic patch (IONSYS™; Alza) is used in hospitalized patients for short-term management of acute postoperative pain as an alternative to a morphine PCA pump. The patch delivers a 40 µg dose of fentanyl over the course of 10 min when the patient activates dosing by pressing a button on the patch. A partial listing of companies pursuing iontophoresis include Alza, Iomed, Vyteris, Travanti Pharma, and Transport Pharmaceuticals. Other companies may work in collaboration with one of these companies to pursue development of an iontophoretic patch for a specific drug molecule of interest. Hydrophilic charged macromolecules such as polypeptides fit all the criteria needed for iontophoretic delivery.

Factors affecting transdermal iontophoretic delivery include size, charge, structure and lipophilicity. Polypeptides, which have a high isoelectric point are ideal candidates as they retain their charge during transport into and across the skin. Iontophoresis is generally believed to deliver polypeptides up to a MW of about 10 kDa. The research paper by Dr. Kalia's group in this theme section documents the delivery of a 12.4-kDa protein by iontophoresis and proposes that polypeptide charge can compensate for molecular weight and that electric mobility is the key parameter in governing peptide electrotransport. The paper also suggests that the three dimensional structure of proteins may also be important in determining transport across the skin. Most of the other skin enhancement technologies rely on permeabilization of skin by use of physical energy, which acts on the outer layers of the skin. However, the electrical current applied during iontophoresis primarily acts on the drug itself.

Skin microporation is an exciting technology that is actively being investigated for transdermal delivery of water soluble small drugs and macromolecules such as proteins and vaccines. It involves the creation of micron dimension transport pathways in the skin using a minimally invasive technique, such as microneedles, thermal microporation or radiofrequency ablation. These micron sized pathways are much smaller than the holes made by hypodermic needles but they are much larger than the size of macromolecules and can allow the delivery of dissolved drug molecules of any size, even DNA or monoclonal antibodies (in limited amounts). This theme section has two articles utilizing this technology, one on the development of coated microneedles and the other on use of thermal microporation for delivery of interferon across skin. Mechanical microneedles are typically made of silicon, metal or polymers and combine the effectiveness of needle-based delivery with the patient-acceptance of patch technology. These microneedles are typically 500 µ long, with a radius of curvature at the tip of about 1 µ, allowing easy penetration into the skin. A partial listing of companies pursuing microneedle technology includes Alza/Macroflux, Becton Dickinson, Corium, 3M, Norwood Abbey, Silex Microsystems, and Texmac. These companies may work in collaboration with pharmaceutical company partners to pursue development of a microneedle patch for specific drug molecules. An applicator can be used to apply the microneedles on the skin to create the micropores followed by patch application. Alternatively, the drug can be coated directly on the microneedles. The latter approach has been used for vaccine delivery since the amount of protein antigen needed to generate immune response is very little and the dose can be accommodated by coating on the microneedles. The paper from Dr. Prausnitz's group in this theme section investigates the coating of model proteins on microneedles using various formulations.

Thermal microporation involves thermal ablation of the stratum corneum to create microchannels in the skin. It is accomplished by the application of a short pulse of electrical current to an array of metallic filaments, which convert electricity to thermal energy. The rapid creation and conduction of thermal energy into the surface of the skin, in an area about the width of a human hair, painlessly ablates the stratum corneum under each filament to create an array of aqueous microchannels. After the microchannels are formed, the protein patch is applied using a simple fold-over

design that aligns it with the newly formed microchannels. This technology is being developed by Altea Therapeutics. This theme section has one paper, which demonstrates delivery of interferon alpha-2b, a 19.3-kDa protein, across the skin using thermal microporation.

Phonophoresis or sonophoresis is another transdermal enhancement technology that can enable delivery of macromolecules across the skin. This technology uses sound waves with a frequency beyond 20 kHz to drive molecules into the skin. A coupling medium is needed and several mechanisms have been proposed for delivery, including cavitation, acoustic microstreaming, heating or radiation pressure. Recently, it has been suggested that phonophoresis also creates micropores in the skin. Companies active in this area

include Dermasonics and Sontra Medical. Miniaturization of these ultrasound applicators has not advanced to the point of enabling wearable devices as is now possible for iontophoretic patches. **The paper from Dr. Smith's group in this theme section demonstrates the use of lightweight cymbal arrays, which will help to move towards this goal of miniaturization.**

Several other enhancement technologies can also be utilized to enable transdermal protein delivery. These are not discussed in this theme section but a partial list includes laser assisted thermal ablation (Norwood Abbey), RF-microchannels (TransPharma), controlled heat assisted delivery (Zars), particle-mediated immunization (PowderMed) or the possible use of dermabrasion, chemical enhancers or carrier molecules like liposomes or cyclodextrins.

Ajay K. Banga
College of Pharmacy and Health Sciences,
Mercer University,
Atlanta GA 30341, USA
e-mail: banga_ak@mercer.edu

Targeting Cutaneous Melanoma Using Ultrasound and Liposomes Containing siRNA Against Mutant (V600E) B-Raf

Melissa A. Tran¹, Raghavendra Gowda¹, E.J. Park⁶, James Adair^{4,7}, Nadine Barrie Smith^{4,6},
Mark Kester^{1,4} and Gavin P. Robertson^{1,2,3,4,5}

Departments of Pharmacology¹, Pathology² and Dermatology³, The Pennsylvania State University College of Medicine, Hershey, PA 17033; The Penn State Melanoma Therapeutics Program⁴, The Foreman Foundation for Melanoma Research⁵, Hershey, PA 17033. Departments of Bioengineering⁶, and Material Science and Engineering⁷, Pennsylvania State University, University Park, PA, USA.

Grant support: NIH/NCI 1-RO3-CA128033-01, The American Cancer Society (RSG-04-053-01-GMC), The Foreman Foundation for Melanoma Research, State of Pennsylvania Non-formulary Tobacco Settlement Funds. Department of Defense Technologies for Metabolic Monitoring Award No. W81XWH-05-1-0617.

Request for reprints: Gavin P. Robertson, Department of Pharmacology – R130, The Pennsylvania State University College of Medicine, 500 University Drive, Hershey, PA 17033. Phone: (717) 531-8098; Fax: (717) 531-5013; E-mail: gprobertson@psu.edu.

Running title: Topical treatment for melanoma

Key words: melanoma, ultrasound, B-Raf, liposomes, siRNA

Abstract

Melanoma is the most deadly form of skin cancer. Currently early surgical removal is the best treatment option for melanoma patients with little hope of successful treatment of late stage melanoma. Clearly new treatment options must be explored. Topical administration of drugs provides the advantage of being able to apply large quantities of drug in close proximity to the tumor without the issue of systemic side effects. However, the natural barrier formed by the skin must first be overcome for topical treatment to become a viable option. With this in mind we have sought to use low-frequency ultrasound to transiently permeabilize the stratum corneum and successfully deliver liposomal siRNA to melanoma cells residing at the basement membrane. B-Raf is one of the most frequently activated genes in melanoma, making it an ideal candidate for targeting via siRNA. By targeting directly the most common activating mutation, V600E, off target effects associated with inhibiting B-Raf in normal cells can be avoided. The novel liposomes used in this study load siRNA, protect it from the outside environment and lead to knockdown of target message. Combining ultrasound with liposomal siRNA we show that siRNA can be delivered into melanoma cells in artificial reconstructed skin. Additionally, we show that siRNA to mutant B-Raf can effectively inhibit melanoma growth in reconstructs and in mice by 60% and 30% respectively. Therefore, ultrasound with liposomal siMutB-Raf is a potentially valuable treatment option for melanoma patients.

INTRODUCTION

Melanoma is a cancer of melanocytes, which are pigmented skin cells residing at the epidermal-dermal junction (1). While early stage melanomas can be treated effectively by surgical removal, there are no effective topical agents that prevent the development and spread of melanocytic lesions (2). This is due in part to the architecture of the skin consisting of an outer epidermal and inner dermal region, which are protected by a surface keratinized layer called the stratum corneum (3, 4). The keratinized layer prevents most topically applied agents from reaching early melanocytic lesions developing at the epidermal-dermal junction or from reaching cutaneous metastases, which are locally invasive lesions in the skin dermis (5). Therefore, topical agents targeting early lesions, or cutaneous metastases hold significant potential to decrease melanoma incidence and mortality rates. Furthermore, localized application of topical therapies could enable high concentrations of agents to be administered directly to skin lesions, limiting toxicity caused by systemic administration (3, 6, 7). Thus, effective topical inhibitory agents need to be developed as well as delivery approaches established for skin penetration.

Melanomas can develop from preexisting nevi (moles) or arise directly from epidermal melanocytes (1). Most genetic alterations promoting development of early melanomas are yet to be identified. However, one frequent change is a T1799A mutation of B-Raf in the MAP kinase pathway (8-11). B-Raf in a normal cell is an intermediate protein in the MAP kinase pathway, which relays an ordered series of consecutive phosphorylation events from cell surface, via Ras, Raf, Mek and Erk, to nucleus (12, 13). However, in ~60% of advanced stage metastatic melanomas and ~90% of normal moles the activating V600E mutation leads to 10.7 times higher activity than occurs in normal cells (8-11). Thus, targeting ^{V600E}B-Raf in early melanocytic lesion or in cutaneous metastases could have significant potential to cause regression of moles, early melanocytic lesions or skin metastases containing the mutation.

Inhibition of ^{V600E}B-Raf using siRNA or pharmacological agents can effectively decrease tumor development in mice, validating this protein as a therapeutic target in melanoma (14, 15). Furthermore, siRNA can be designed that specifically reduces production of mutant V600E but not wild-type B-Raf protein, which effectively inhibits melanoma development (14,

15). The advantage of siRNA targeting ^{V600E}B-Raf is its specificity leading to negligible changes in normal B-Raf protein expression and hence potentially fewer side effects than occurs using agents inhibiting both mutant and wild-type protein (16). It is quite effective in cultured cells where it can be introduced using standard transfection methods (17-19). Unfortunately, widespread use of siRNA as therapeutic agent is limited due to rapid degradation and delivery related constraints in animal systems (16, 20-22). Therefore, strategies are needed to package and protect the siRNA, as well as, deliver it into cancer cells (20).

Encapsulating siRNA into liposomes is one approach enabling siRNA protection and systemic delivery following intravenous administration that can lead to tumor inhibition (23-25). In contrast, topical administration of most liposomal formulations leads to uptake confined to the upper epidermal layers without penetration of melanocytic lesions in epidermis and dermis (3). In order for topical delivery of siRNA to effectively treat melanocytic lesions, this boundary must be penetrated. A number of strategies including use of hydration agents, polar solvents, vesicles or particles, physical manipulation of the stratum corneum, and electrically-mediated approaches have been used to permeabilize the skin with varying success (5). One especially promising strategy utilizes low-frequency ultrasound which permeabilizes skin enabling passage of macromolecules including antisense oligonucleotides without significant skin damage (5, 7, 26-30). Combining the protective qualities of liposomes with the permeabilizing activities of low-frequency ultrasound is a novel unexplored strategy to deliver siRNA into melanoma cells present in skin.

In this study, we present data showing development of a unique liposomal-ultrasound mediated approach for delivering siRNA into melanocytic lesions present in skin, which inhibits early melanocytic lesion development, as well as, that of cutaneous metastases. The novel cationic liposome effectively encapsulates siRNA that specifically targets mutant ^{V600E}B-Raf present in melanocytic lesions. The liposomal formulation protects the siRNA from degradation and facilitates its entry into cultured cells to decrease expression of mutant V600E but not wild-type B-Raf protein. Furthermore, non-damaging low-frequency ultrasound of reconstructed or animal skin using a lightweight 4-cymbal transducer array enables siRNA penetration throughout epidermal and dermal layers leading to a 1-2 fold decrease in early

lesions or cutaneous metastasis development. Mechanistically, siRNA-targeting ^{V600E}B-Raf leads to 4-5 fold decrease in the proliferative potential of melanoma cells, which in turn reduces cells tumorigenic potential. Thus, topical delivery of novel siRNA containing cationic liposomes following low-frequency ultrasound can decrease early melanocytic lesion development or spread of metastases in skin.

DRAFT

MATERIALS AND METHODS:

Cell lines and culture conditions. The human melanoma cell lines UACC 903, UACC 903 GFP, 1205 Lu, C8161.C19, and human fibroblasts, FF2441, were maintained in DMEM (Invitrogen, Carlsbad, CA) supplemented with 10% fetal bovine serum (FBS, Hyclone, Logan, UT). WM35 and WM35-GFP cells were grown as described previously (31). Human keratinocytes, HFK, were grown in Epilife Medium (Cascade Biologics, Portland, OR) with Human Keratinocyte Growth Supplement (Cascade Biologics, Portland, OR). Mouse melanocytes, melan-a, were grown in RPMI 1640 (Mediatech, Herndon, VA) supplemented with 10% FBS, 2 mM L-glutamine, and 200 nM TPA (Sigma-Aldrich, St. Louis, MO).

Liposome composition, characterization and siRNA loading. Liposomes were created by combining DOTAP (1,2-Dioleoyl-3-Trimethylammonium-Propane), DOPE (1,2-Dioleoyl-sn-Glycero-3-Phosphoethanolamine) and DSPE-PEG(2000) (1,2-Distearoyl-sn-Glycero-3-Phosphoethanolamine-N-[Amino(Polyethylene Glycol)2000]) (Avanti Polar Lipids, Alabaster, AL) in chloroform at a 4.75:4.75:0.5 molar ratio and dried under nitrogen gas. The lipids were then resuspended in isotonic saline at 55°C. Resulting solution was sonicated for 5 minutes and extruded through a 100 nm polycarbonate filter using an Avanti Mini Extruder (Avanti Polar Lipids, Alabaster, AL). Complexing scrambled siRNA and liposomes (Invitrogen, Carlsbad, CA) occurred at specific weight ratios of 1:5, 1:10, and 1:15 for 30 minutes to 24 hours in order to generate liposomes containing siRNA. A quasielastic light scattering system (Malvern Nanosizer, Malvern Instruments, UK) was used to measure the particle size distribution of liposomes containing or lacking siRNA. Measurements were taken one day after preparation. Liposomal loading of siRNA was determined by mixing fluorescent, Alexa Fluor 546, siRNA (Qiagen, Valencia, CA) and liposomes at specific weight ratios (1:5, 1:10, 1:15) and complexing at room temperature for 0.5, 3, or 6 hours. Complexes were separated on a 2% agarose gel at 100 V for 20 minutes and visualized using UV light. Loading was considered complete when no free siRNA was evident and the entire complex was retained in the well. To measure liposome-mediated protection of siRNA, liposomes complexed with siRNA overnight were treated with 50% FBS for 10, 30, 60, 180, or 360 minutes. Following FBS treatment, half of the complex for each time point was treated with 0.5% SDS for 10 minutes at 37°C to disrupt the complexes and release free siRNA. Both disrupted and undisrupted

samples were run on a 2% agarose gel at 100 V for 20 minutes and visualized using UV fluorescence. siRNA alone was also digested with 50% FBS at each of the time points to serve as a control.

Liposomal toxicity. To assess cytotoxicity of liposomes in both normal and cancer cells; 5×10^3 fibroblasts (FF2441), keratinocytes (HFK), melanocytes (melan-a), and melanoma (1205 Lu) cells were plated into 96 well plates. Following 48 hours of growth, cells were treated with ghost liposomes for 24 hours at liposomal concentrations of 12.5, 25, and 50 μM and compared to untreated control cells. To assess cytotoxicity of liposomes containing siRNA, 5×10^3 1205 Lu cells were plated into 96 well plates. Following 48 hours of growth, cells were then treated with liposomes containing scrambled siRNA for 24 hours at 125, 250, 500, 1000, or 2000 nM of siRNA. Cytotoxicity was analyzed using the Cell Titer 96 aqueous nonradioactive cell proliferation assay (Promega, Madison, WI) according to manufacturer's instructions.

Uptake of liposomal siRNA into cells. Uptake and internalization of liposomal siRNA into cells was determined using fluorescently tagged Alexa Fluor 546, or fluorescein siRNAs (Invitrogen, Carlsbad, CA). 1×10^5 1205 Lu cells were plated and following overnight growth liposomal-siRNA complex (100 nM) was added. Three hours later cells were trypsinized and plated onto coverslips followed by overnight incubation. Coverslips were then rinsed with phosphate buffered saline (PBS) (Invitrogen, Carlsbad, CA), and fixed in 4% paraformaldehyde (Fisher Scientific, Waltham, MA) for 30 minutes, washed and mounted using a DAPI containing mountant (Vector Laboratories Inc., Burlingame, CA). Treatment of cells with ghost liposomes lacking siRNA served as a control. Uptake into cells was determined using fluorescence microscopy. Uptake of two different siRNAs into WM35 cells was determined by plating 2×10^4 cells onto coverslips allowing 24 hour growth, followed by addition of liposomal siRNA (10 or 20 nM) for three hours. Cells were then washed, fixed in 4% paraformaldehyde, mounted and analyzed using fluorescence microscopy. Uptake of siRNA-liposomal complex by normal cells was determined using Alexa Fluor 546 tagged siRNA. For these studies, 5×10^3 fibroblasts (FF2441), keratinocytes (HFK), or 1×10^4 melanocytes (melan-a) were plated onto coverslips and two days later, liposomal siRNA (50, 100, or 200 nM) added to cells for 3 hours. Cells

were then washed, fixed in 4% paraformaldehyde, mounted and analyzed using fluorescence microscopy.

Nucleofection of siRNA into cells. Duplexed Stealth siRNA (100 pmoles) (Invitrogen, Carlsbad, CA) was introduced into 1×10^6 UACC 903-GFP or WM35-GFP cells via nucleofection using an Amaxa Nucleofector (Koeln, Germany), Solution R/Program K-17 (UACC 903-GFP) or NHEM-NEO Solution/Program U-20 (WM 35-GFP) as described previously (14), with a transfection efficiency of ~99%. Following nucleofection, cells were replated for 48 hours after which cells were used to create skin reconstructs or lysates harvested for Western blot analysis. To measure the duration of siRNA knockdown, cells were harvested at 0, 2, 4, 6, and 8 days following nucleofection with siRNA to B-Raf or C-Raf and subjected to Western blot analysis. Cells used in skin reconstructs were nucleofected with buffer or siRNA to MutB-Raf (100, 50, or 12.5 pmoles), or C-Raf (100 pmoles), scrambled (100 pmoles) siRNA and allowed to recover for two days before mixing with keratinocytes and adding into the dermal equivalent as described below. 1×10^5 cells were used for 6-well plates and 5×10^4 cells were used for 12-well plates.

Western Blot Analysis. For Western blot analysis, cell lysates were harvested in petri dishes by the addition of lysis buffer containing 50 mmol/L HEPES (pH 7.5), 150 mmol/L NaCl, 10 mmol/L EDTA, 10% glycerol, 1% Triton X-100, 1 mmol/L sodium orthovanadate, 0.1 mmol/L sodium molybdate, 1 mmol/L phenylmethylsulfonyl fluoride, 20 μ g/mL aprotinin, and 5 μ g/mL leupeptin. Whole cell lysates were centrifuged ($\geq 10,000 \times g$) for 10 minutes at 4°C to remove cell debris. Protein concentration was measured using the bicinchoninic acid assay from Pierce (Rockford, IL), and 30 μ g of lysate per lane were loaded onto a NuPAGE Gel (Invitrogen, Carlsbad, CA). Following electrophoresis, samples were transferred to polyvinylidene difluoride membrane (Pall Co., Pensacola, FL). The blots were probed with antibodies according to the supplier's recommendations: primary antibodies to B-Raf, Erk2, and C-Raf and secondary antibodies conjugated with horseradish peroxidase were obtained from Santa Cruz Biotechnology (Santa Cruz, CA). The immunoblots were developed using the enhanced chemiluminescence detection system (Amersham Pharmacia Biotech, Piscataway, NJ). Blots were normalized to Erk2 and quantified using ImageJ software (32).

Liposomal-siRNA complex mediated protein knockdown. 5×10^5 1205 Lu cells were plated in six well plates followed by two days growth in a cell culture incubator. Liposomal-siMutB-Raf or liposomal-siScrambled complex ($1 \mu\text{M}$) was added to cell culture media and protein lysates collected 18 and 32 hours later for Western blot analysis. Blots were probed to measure B-Raf and Erk2. Protein levels were quantified using ImageJ software and normalized to Erk2 from three blots and average levels of B-Raf calculated (32).

Generation of laboratory reconstructed skin containing melanocytic lesions. To create human skin in a culture dish containing a dermis and epidermis, human fibroblasts, FF2441 were trypsinized and resuspended in 10% reconstitution buffer ($22 \mu\text{g}/\mu\text{l}$ sodium bicarbonate (Cambrex Bio Science Walkersville, Inc., Walkersville, MD), $47.7 \mu\text{g}/\mu\text{l}$ HEPES (Fisher Scientific, Waltham, MA) in 0.062 N sodium hydroxide (Fisher Scientific, Waltham, MA), 10% 10X DMEM (Mediatech, Herndon, VA), $2.4 \mu\text{l}/\text{ml}$ of 10 M NaOH, and 80% collagen I (BD Discovery Labware Inc., Bedford, MA) at a concentration of 2.5×10^5 cells/ml on ice (33). Mixture was then aliquoted into 6 or 12 well plates and incubated at 37°C for 3 hours to enable polymerization of the collagen matrix. E-media was then added to each well to equilibrate the dermal matrix (34). After two days of growth, human keratinocytes and human melanoma cells (WM35-GFP or UACC 903-GFP) were trypsinized and resuspended at a 1:10 ratio of melanoma cells (nucleofected or untreated) to keratinocytes in E-media. One milliliter of cell suspension added to each well on top of the dermal layer. Following two days growth, reconstructed skin was transferred onto wire grids and fed via diffusion from E-media below the platforms.

Ultrasound treatment and analysis of damage, liposomal siRNA uptake and tumor inhibition in reconstructed skin. Skin reconstructs were treated with ultrasound for 20 minutes by removing media and submerging skin reconstructs in PBS. Ultrasound was administered for 20 minutes at a frequency of 20 kHz and a duty cycle of 20% (30). Liposomal-siRNA complex was then topically applied at a concentration of $1 \mu\text{M}$ and allowed to soak into the skin. For damage studies ghost liposome was applied after ultrasound treatment and skin was harvested one hour after treatment and fixed in 4% paraformaldehyde at 4°C overnight. H&E stained paraffin embedded cross sections were examined for skin damage using microscopy. For uptake studies skin reconstructs were treated with Alexa Fluor 546

containing liposomes (1 μ M) or ghost liposomes and harvested one hour after treatment. Uptake was analyzed using stereo fluorescence microscopy. Laboratory generated skin reconstructs were treated on alternate days starting on day 10 up to day 20. On day 21 skin was harvested. Skin reconstructs from all experiments were fixed in 4% paraformaldehyde at 4°C overnight. After fixation skin was stored in 0.5 M EDTA pH 8.0 (Fisher Scientific, Waltham, MA). To quantify differences between treatment groups following nucleofection or ultrasound treatment + siRNA-liposomal complex, 4-6 images of each reconstruct were taken. Total area occupied by GFP-tagged tumor nodules in each image was analyzed using IP Lab software. Average area was then calculated for each piece of skin and for each treatment group.

Cell doubling time. The *in vitro* doubling time of UACC 903 cells nucleofected with control or experimental siRNA was estimated by plating 3×10^3 per well for UACC 903 in 200 μ L of DMEM supplemented with 10% FBS in multiple rows of wells in five 96-well plates. Growth was measured colorimetrically using the sulforhodamine B binding assay (Sigma Chemical Co., St. Louis, MO) every 24 hours over a period of 5 days on one plate each day. Absorbance was measured at 570 nm using a Perkin-Elmer HTS 700+ Bioassay Plate Reader (Foster City, CA). Doubling times were calculated using the exponential equation of a best-fit line ($y = y_0 e^{ax}$) for each condition (14). Values are averages \pm SE obtained from three independent experiments by calculating the amount of time (x) it took the absorbance (y) to double.

In vivo cell proliferation. For mechanistic studies, 5×10^6 UACC 903 cells nucleofected with siRNA were injected into mice and tumors harvested 4 days post-injection of cells to measure changes in cell proliferation (14). Cell Proliferation rates in formalin-fixed tumor sections were measured using the RPN 20 cell proliferation kit (Amersham Pharmacia Biotech) that uses bromodeoxyuridine incorporation and immunocytochemistry. Two hours before sacrificing, 0.2 ml of bromodeoxyuridine was injected i.p. into mice and tumors processed according to the proliferation kit's instructions. The number of bromodeoxyuridine-stained cells was scored as the percentage of total cells in tumors treated with siC-Raf or siMutB-Raf.

Ultrasound followed by siRNA-liposomal complex treatment of tumors in mice. 1×10^6 UACC 903-GFP cells were injected subcutaneously into the right flank of nude mice. After 24

hours, mice were treated by ultrasound for 15 minutes followed by topical addition of liposomal-siRNA (siMutB-Raf or siScrambled) complex (25 μ g) on alternate days up to day 23. Prior to ultrasound treatment mice were anesthetized using ketamine/xylazine (2:1), and area sterilized using alcohol pads. Aquaflex Gel Pads (Parker Laboratories, Inc., Fairfield, NJ) were used as an ultrasound standoff. Ultrasound was administered for 15 minutes at a frequency of 20 kHz and a duty cycle of 20% (30). Liposomal siRNA was administered to the ultrasound treated area overlying the tumor and allowed to soak into the skin.

Toxicity analysis in mice. To establish toxicity associated with ultrasound plus siRNA-liposomal complex, nude mice were treated with ultrasound for 15 minutes followed by topical addition of liposomal-siRNA (siMutB-Raf or siScrambled) complex on alternate days up to day 23. Mice were weighed before treatments and on euthanization at day 23, blood was collected and serum separated to measure Serum glutamic oxaloacetic transaminase (SGOT), Serum glutamic pyruvic transaminase (SGPT), glucose, and alkaline phosphatase. Values represent the average of three samples \pm SE. Livers were harvested, fixed in formalin, sectioned and stained with hematoxylin and eosin (H&E) to assess changes in liver morphology.

Statistical analysis. One-Way or Two-Way ANOVA followed by the appropriate post hoc test (Tukey's or Bonferroni) or t-test was used to ascertain whether significant differences occurred between groups. Differences were considered significant at $P < 0.05$.

RESULTS

Development of stable cationic liposomes effective at loading siRNA. Since liposomes have been reported as potential delivery vehicles into which siRNA can be loaded, we evaluated a number of possible formulations and found that a novel DOTAP, DOPE and DSPE-PEG(2000) ratio of 4.75:4.75:0.5 efficiently loaded siRNA. Loading efficiency was measured by adding Alexa Fluor 546 fluorescently tagged siRNA to liposomes at ratios of 1:5, 1:10, or 1:15 (siRNA: liposome by weight) and allowing complexing for 0.5, 3, or 6 hours. Loading efficiency was observed by running samples on an agarose gel and using UV fluorescence to determine whether free siRNA was seen in the gel or as a siRNA-liposome complex retained in the gel well. The 1:5 ratio following 0.5 hours incubation showed both loaded and unloaded siRNA, which was in stark contrast to the 1:10 and 1:15 ratios since fluorescently tagged siRNA was only present in wells of the gel indicating it was completely complexed with liposomes (Fig. 1A; left panel). Since maximal loading occurred following 30 minutes incubation at the 1:10 ratio, this siRNA-liposomal complex formulation was used for subsequent experiments. Size of the siRNA-liposome complexes one day after preparation was measured using dynamic light scattering, which showed an average size of 50.9 nm and a size range of 34.5 - 67.3 nm (Fig 1A; right panel). Ghost liposomes were of a similar size with an average of 48.1 nm and a size range of 32.2 – 64 nm. Thus, liposomes were generated that can effectively load siRNA and are stable.

siRNA in liposomes is protected from serum degradation. Since the function of liposomes was to protect siRNA from degradation, fluorescently tagged free siRNA or siRNA-liposome complexes were exposed to 50% FBS for 10, 30, 60, 180, or 360 minutes since it is rich in RNA degrading factors. Partial degradation of free siRNA was observed by 10 minutes and complete degradation occurred after one hour of incubation (Fig. 1B; left panel). In contrast, siRNA complexed with liposomes remained in the well at all time points, indicating siRNA was protected from degradation (Fig. 1B; middle panel). To verify that the siRNA-liposome complex incubated with FBS contained intact siRNA, half of the original sample was treated with 0.5% SDS for 10 minutes to disrupt the liposomes in order to release the complexed siRNA, which was then run on an agarose gel. Similar levels of free siRNA were released at all time points from disrupted liposomes indicating siRNA was protected by the liposomal

components of the complex (Fig. 1B; right panel). Thus, siRNA in liposomes is protected from degradation by external factors.

Liposomal-siRNA complex is non-toxic and taken up by normal as well as cancer cells.

To determine whether liposomes mediated cellular uptake of siRNA and measure possible toxicity of the siRNA-liposomal complex, normal fibroblast (FF2441), keratinocyte (HFK), and melanocyte (melan-a) cell lines were treated with ghost liposomes or liposomes containing fluorescent Alexa 546 tagged siRNA (50, 100, or 200 nM) for three hours followed by fixation. Fluorescence microscopy was used to measure uptake of fluorescent Alexa Fluor 546 tagged siRNA into cells. Red fluorescence indicating uptake of liposomal siRNA was observed in ~100% of all three-cell lines treated with siRNA-liposomal complex but not in those exposed to control ghost liposomes (Fig. 1C and data not shown). Next, toxicity mediated by ghost liposomes was examined in fibroblast (FF2441), keratinocyte (HFK), melanocyte (melan-a), or melanoma cells (1205 Lu). Cells were plated in 96-well plates and treated with increasing concentrations of ghost cationic liposomes (12.5, 25, and 50 μ M) for 24 hours. Effect of the liposomes on cell viability was quantified using the MTS assay, which measures the dehydrogenase activity found in metabolically active cells (35). When compared to untreated cells, no decrease in cellular viability was observed in any of the cells, indicating ghost liposomes were not toxic at concentrations examined (Fig. 1D; left panel). Toxicity of the siRNA-liposomal complex was examined next in 1205 Lu melanoma cells by comparing untreated cells to those treated with increasing concentrations of agent (Fig. 1D; right panel). No alterations were observed in cell viability indicating negligible toxicity. Thus, the siRNA-liposome complex is non-toxic and taken up equally by normal and cancer cells.

Liposomes deliver single or multiple siRNAs into the cytoplasm of cells. The possibility of loading multiple siRNAs into a single liposome for delivery was examined using Alexa Fluor 546 (red) and fluorescein (green) fluorescently tagged siRNA (10 or 20 nM). Liposomes were prepared using equal concentrations of each fluorescently tagged siRNA, which was then added to WM35 melanoma cells for three hours followed by fixation. Compared to cells treated with control ghost liposomes, fluorescence microscopy showed that cells treated with liposome complex containing two differentially tagged siRNA had Alexa Fluor 546 (red) and fluorescein (green) fluorescence indicating uptake of both (Fig. 2A and data not shown). Then

to verify that liposomes were taken into the cytoplasm of cells to deliver siRNA and not merely adhering to the cell surface, 1205 Lu melanoma cells were treated with fluorescein tagged siRNA-liposomal complex (100 nM) or ghost liposomes for three hours. Cells were then trypsinized, which served to remove any cell surface bound liposomes and replated overnight followed by fixation (36). Fluorescence microscopy showed presence of fluorescein (green) tagged siRNA in cytoplasm of cells surrounding a nuclear shadow indicating that liposomal siRNA was internalized into the melanoma cells (Fig. 2B). In contrast, no fluorescein fluorescence was observed in cells treated with empty ghost liposomes. Thus, liposomes can be loaded with multiple different siRNA, which are taken up into the cytoplasm of cells.

siRNA targeting ^{V600E}B-Raf specifically decreases mutant but not wild-type protein expression in cells. siRNA can be designed overlapping the T1799A mutation site of B-Raf, which has the potential of selectively decreasing expression of mutant but not wild-type protein (14, 15, 37). To verify specificity of the siRNA targeting mutant but not wild-type B-Raf for this study, 100 pmoles (1 μ M) of siRNA specific to mutant ^{V600E}B-Raf were transferred via nucleofection into melanoma cells containing mutant (UACC 903) or wild-type protein (C8161.CI9). After 48 hours, protein lysates were harvested for Western blot analysis and knockdown by siRNA specific to ^{V600E}B-Raf (siMutB-Raf) compared to siRNA knocking down both wild-type and mutant protein (siWTB-Raf). Densitometric analysis of B-Raf protein levels normalized against Erk2 loading are shown beneath Western blots in Fig. 2C. Compared to control cells nucleofected with buffer, scrambled siRNA or siRNA to C-Raf, siRNA designed to sequences present in both mutant and wild-type B-Raf decreased protein expression by 50-75% in both cell lines (Fig. 2C). In contrast, siRNA designed specifically against ^{V600E}B-Raf reduced B-Raf protein levels ~70% in UACC 903 cells containing the mutation but not in C8161.CI9 lacking the mutation (Fig. 2C). Thus, siRNA can be designed that specifically decreases expression of mutant ^{V600E}B-Raf but not wild-type B-Raf protein.

siRNA targeting ^{V600E}B-Raf can be loaded into liposomes, delivered into cells and decrease expression of mutant protein. Having validated the specificity of siMutB-Raf siRNA for preferentially decreasing ^{V600E}B-Raf protein expression in cells, siMutB-Raf was loaded into liposomes and efficacy of complex for decreasing protein expression in cells examined. 1205 Lu melanoma cells containing mutant ^{V600E}B-Raf were treated with siMutB-

Raf-liposomal complex (1 μ M) for 18, or 32 hours and protein lysates harvested for Western blot analysis. Three blots were densitometrically analyzed and averages plotted. At both 18 and 32 hours following exposure, a 50-60% knockdown of ^{V600E}B-Raf protein was observed compared to the control group treated with liposomes containing scrambled siRNA (Fig 2D). A representative Western blot at 32 hours, in the inset of Fig. 2D, shows an example of decreased ^{V600E}B-Raf protein expression. Thus, siRNA specific to mutant ^{V600E}B-Raf can be loaded into cationic liposomes, delivered into cells and decrease protein expression by up to 60%.

siRNA-based therapeutics can be evaluated on reconstructed skin containing melanocytic lesions. Initially, feasibility of the skin-melanocytic lesion model for examining the efficacy of siRNA-based therapeutics on reconstructed skin containing melanocytic lesions was established. Duration of siRNA-mediated protein knockdown in melanoma cells following a single siRNA treatment was measured and inhibitory effectiveness on melanocytic lesions growing in laboratory generated skin established. Approach involved nucleofecting siRNA into cells and using Western blotting to establish duration of protein knockdown following a single treatment. UACC 903 cells were nucleofected with siMutB-Raf, cells replated into culture dishes and protein lysates collected on days 2, 4, 6, and 8. Blots were densitometrically scanned and knockdown of B-Raf protein compared to control cells nucleofected with siRNA targeting C-Raf (Fig. 3A). A consistent 60-70% decrease in protein expression was observed through day 8 (Fig. 3A). Next, efficacy of siMutB-Raf for inhibiting early melanocytic lesion development was evaluated by nucleofecting siRNA into GFP-expressing WM35 cells, and seeding them into the epidermis of reconstructed skin. Ten days later, skin was fixed and fluorescence microscopy used to quantify average area occupied by GFP expressing nodules formed from the cancer cells at the epidermal-dermal junction. Compared to skin containing WM35-GFP cells nucleofected with buffer, scrambled siRNA or siRNA targeting C-Raf, an ~10-fold smaller area was occupied by cells treated with siMutB-Raf siRNA (Fig. 3B; left and upper right panels, One-Way ANOVA p<0.05). Knockdown of ^{V600E}B-Raf protein expression in these cells was confirmed by Western blotting of protein lysates collected from cells at time of seeding to create the reconstructed skin. Knockdown of B-Raf was only observed for siMut-B-Raf treated cells and not cells exposed to buffer, scrambled siRNA or siRNA targeting C-Raf (Fig. 3B; lower right panel). This approach was then validated using a second more

aggressive melanoma cell line UACC 903-GFP, which is invasive in the reconstructed skin model and represents a cutaneous metastasis model. GFP-expressing UACC 903 cells were seeded into the epidermis of the skin following nucleofection with 12.5 or 50 pmoles of siRNA and area occupied by skin tumors quantified 10-days later. A dose dependent decrease in area occupied was observed compared to scrambled siRNA treated cells (Fig. 3C).

Mechanism leading to decreased cutaneous tumor development was established by calculating *in vitro* doubling times and comparing size and time matched tumors for differences in proliferation. The *in vitro* doubling time of cells nucleofected with siMutB-Raf was found to be approximately 1.3 times that of buffer or siScrambled treated cells (Fig. 3D left panel). A statistically significant 4-5 fold decrease in proliferating cells was observed in siMutB-Raf treated tumor cells compared to siC-Raf treated cells (Fig. 3D middle and right panels). This growth inhibitory mechanism of action is consistent with prior reports (14, 37). Thus, it is feasible to measure inhibitory effects of siMutB-Raf on early melanocytic lesion development or of invasive cutaneous melanoma cells if siRNA can be introduced into these cells in the skin environment.

Ultrasound treatment of skin reconstructs delivers the siMutB-Raf-liposomal complex to melanocytic lesions at the epidermal-dermal junction. Initially, liposomal-siRNA complex was topically applied to the skin; however, the complex only penetrated the upper layers of the stratum corneum (data not shown). This occurs because skin forms a natural barrier preventing uptake of agents, including lipids (3, 5). Therefore, a strategy was developed to permeabilize the skin to enable topically administered liposomes containing siRNA to reach skin melanocytic lesions. This involved a combination approach using ultrasound followed by topical administration of siMutB-Raf-liposomal complex to skin. A lightweight four-cymbal array that delivers insulin through skin and into the blood stream was used to ultrasound the skin prior to administration of the siRNA-liposomal complex (Fig. 4A). To evaluate whether ultrasound damaged the skin, untreated was compared to treated skin to which ghost liposomes had been added after ultrasound treatment (Fig. 4B). Reconstructed skin was treated with ultrasound for 20 minutes, ghost liposome topically added and let recover for 1 hour followed by fixation in 4% paraformaldehyde, afterwards skin were sectioned and stained with H&E (Fig. 4B). This array configuration did not cause significant damage to the skin at the settings used for this study since no detectable damage was observed when comparing

untreated control to with ultrasound and ghost liposome treated skin (Fig. 4B). Next, penetration of skin by the siRNA-liposomal complex following ultrasound treatment was measured. Skin was treated with ultrasound for 20 minutes followed by topical addition of liposome loaded with Alexa Fluor 546-tagged siRNA (1 μ M). One hour after topical application of liposomal-siRNA complex, skin was fixed in 4% paraformaldehyde and presence of Alexa Fluor 546 tagged siRNA (red) in GFP-tagged skin cells examined using stereo fluorescence microscopy. Top down views of the skin reconstructs show uptake of liposomal siRNA by both keratinocytes and GFP tagged UACC 903-GFP melanoma cells (Fig. 4C and not shown). Compared to treatment with control ghost liposomes, cross sections of skin treated with liposomes containing Alexa Fluor 546 tagged siRNA (red) showed presence of the complex in melanoma cells located in both the epidermis and at the epidermal-dermal junction (Fig. 4D). Similar results were seen with skin reconstructs containing WM35-GFP (data not shown). Thus, ultrasound treatment of skin prior to topical application with a siRNA-liposomal complex enables delivery of siRNA to melanocytic lesion cells located within skin.

Following ultrasound treatment, siMutB-Raf-liposomal complex inhibits melanocytic lesion development in laboratory-generated skin. To evaluate the effectiveness of the siMutB-Raf liposomal complex for inhibiting early melanocytic skin or cutaneous metastasis development, skin reconstructs were created into which GFP-tagged WM35 or UACC 903 melanoma cells were seeded. Skin reconstructs differentiated up until day 10 at which point treatment was begun and administered on alternate days (Fig 5A). Treatment regimen consisted of 20 minutes ultrasound treatment followed by addition of liposomal siMutB-Raf or ghost liposome. On day 21, stereo fluorescence microscopy was used to quantify average area occupied by GFP fluorescent skin lesions. Average area occupied was calculated for each treatment group and compared to ultrasound + ghost liposome treated skin, a statistically significant 50-60% reduction in area occupied was observed for WM35-GFP (Fig. 5B) and UACC 903-GFP (Fig. 5C) tumor nodules ($p < 0.05$; One-Way ANOVA). Thus, siRNA mediated inhibition of mutant B-Raf decreased the proliferative capacity of tumor cells decreasing skin nodule development.

Following ultrasound treatment, siMutB-Raf-liposomal complex decreases melanocytic lesion development in animal skin. To determine whether ultrasound followed by topical

treatment of liposomal-siRNA complex could decrease skin lesion development in animals, 1×10^6 GFP-tagged UACC 903 were subcutaneously injected into the flanks of nude mice. Twenty-four hours later and on every alternate day thereafter, mice under anesthesia, were treated with ultrasound for 15 minutes at the tumor site followed by topical application of either liposomal-siMutB-Raf (25 μ g) or control siScrambled-liposomal complex (Fig. 6A). Along with measurement of developing tumors (Fig. 6B), mice were also weighed (Fig. 6C) on alternate days. A statistically significant ~30-40% reduction in tumor size compared to mice treated with the control ultrasound + siScrambled-liposomal complex was observed starting at day 13 and on days 17, 19, 21 and 23 (Fig. 6B, $p < 0.05$; Two-Way ANOVA). Furthermore, no significant weight loss between control and experimental animal groups was observed suggesting negligible weight related toxicity (Fig. 6C, $p > 0.05$; Two Way ANOVA). Lack of systemic toxicity between groups was confirmed by analyzing blood for SGPT, SGOT, alkaline phosphatase, and glucose levels (data not shown), which showed no significant differences between animal groups ($p > 0.05$; t-test). Additionally, no changes in liver morphology were detected in H&E stained liver sections (Fig. 6D). Thus, ultrasound followed by topical treatment of liposomal-siRNA complex targeting ^{V600E}B-Raf in melanocytic lesions significantly decreased cutaneous tumor development in animals.

DISCUSSION:

Novel therapeutic regimens must be developed for treating early melanocytic lesions and cutaneous metastases since aside from surgical excision few treatment options are available (2). Current therapeutic approaches are frequently limited by toxicities associated with systemic administration and various off target effects (3). These issues would be decreased for topical and localized treatment regimes, which could permit high concentrations of agents to be used with less associated systemic toxicity (3, 6). The end result could be dramatic improvement in therapeutic treatments for patients with early melanocytic lesions and cutaneous metastases leading to significantly decreased mortality rates. These agents could be especially useful for cutaneous lesions not amenable to surgical removal, which has been demonstrated through studies utilizing interlesional injections of IL-2, and electroporation for improved topical delivery of bleomycin (6, 38). In the search for potent topical drugs and technologies to deliver agents into skin to target early melanocytic lesions and cutaneous metastases, this study details development of a novel approach to deliver therapeutic siRNA targeting mutant ^{V600E}B-Raf into early and invasive cutaneous melanocytic lesions. Ultrasound treatment of skin followed by topical application of liposomes containing siRNA targeting ^{V600E}B-Raf, caused reduction in protein expression leading to a significant decrease in early and invasive cutaneous lesion development.

The novelty of this approach stems from its use of siRNA as a therapeutic. RNAi based therapeutics is a rapidly evolving field with potential to specifically target genes mutated in cancer cells without inhibiting activity of normal protein (39). Specifically, siRNA can be designed to target proteins such as mutant ^{V600E}B-Raf in melanoma cells, which would affect only cells containing the mutation but not normal non-cancerous cells (14, 15, 37). Unfortunately, systemic administration of free unmodified siRNA by intravenous injection is not clinically feasible due to limitations of the siRNA itself (39, 40). In serum, siRNA has a short half life and is rapidly degraded, therefore, clinically useful concentrations are not achievable (40). To circumvent these limitations, a number of laboratories are developing novel agents into which siRNA can be loaded for delivery to distant sites around the body (22-25, 41-43). A case in point is this study, where the utility of using cationic liposomes to load, protect and deliver therapeutic siRNA into cancer cells is demonstrated. By creating a liposomal

formulation to load and protect siRNA, degradation is avoided increasing the half-life of the siRNA. Also, use of pegylated lipids in generation of the liposomes increases the half-life as well as avoidance of the reticulo-endothelial system, which degrade these structures (44). This protection is valuable both for long-term storage and increased bioavailability (44). Creation of a liposome containing siRNA targeting mutant ^{V600E}B-Raf selectively could be taken up by all cells but would only have an effect in cells containing the mutation. Therefore, it would decrease the need to link an antibody to the liposome's surface to promote preferential uptake by cancer cells, which could have the drawbacks of increasing immunogenicity, size and clearance rates (45). A further advantage of this liposomal formulation is that it can simultaneously deliver multiple siRNA targeting expression of different proteins as demonstrated by the uptake of two differently tagged siRNAs by melanoma cells. It also has potential to be used to load siRNA in combination with other drugs that could lead to cooperative tumor inhibition. This liposomal-siRNA complex is readily taken up into cells without detectable toxicity due in part because the liposomes are nanosized at ~50 nm with a tight size distribution ranging from 32-64 nm irrespective of whether siRNA is loaded. This factor is important since small size is important for decreasing immunological or inflammatory responses because particles of this size range bypass the reticulo-endothelial system (45).

Application of liposomes topically to skin, including those containing tretinoin, have been shown to deliver drugs primarily to cells in the upper layers of the epidermis (5). This requires development of strategies for delivery to melanocytic lesions in epidermis, at the epidermal-dermal junction or in the dermis (3, 5). The novelty of this study is that it details use of ultrasound as a skin permeabilizing strategy that has previously been shown to be effective at delivering various macromolecules into and through the various layers of skin (7, 27-30). Specifically, the light-weight transducer used for these studies delivers insulin successfully through the skin and into the bloodstream resulting in decreased glucose levels in blood (27-30). Additionally, antisense oligonucleotides have been introduced into pig skin using low-frequency ultrasound devices similar to this one (46). However, while siRNA was delivered into cells in skin, no demonstration of functionality was shown (46). In this study, low-frequency ultrasound was used to successfully permeabilize the skin enabling delivery of the siRNA-liposomal complex into melanoma cells residing at the dermal-epidermal junction of skin reconstructs validating this method as a feasible way to deliver siRNA.

This report demonstrates that inhibition of mutant $V600E$ B-Raf using liposome-mediated delivery of therapeutic siRNA inhibits early as well as invasive melanoma growth in the cutaneous skin environment. Mechanistically, inhibition occurs by decreasing $V600E$ B-Raf activity, which reduces MAP kinase signaling (14, 15, 37). Since ~90% of moles and premalignant lesions have mutant $V600E$ B-Raf, use of this strategy could be a feasible non-surgical approach to decrease benign or early stage melanocytic skin lesions (8-11). Purchase of an “over-the counter” miniaturized ultrasound device and siRNA-liposomal complex solution could enable rapid removal of normal or abnormal moles by patients, which could have the consequence of decreasing melanoma incidence rates with a corresponding decrease in mortality rates. For patients with more advanced disease, these agents could also provide a therapeutic benefit. Cutaneous and subcutaneous metastases are the most common form of metastases and are often the first sign of disease spread (47). Ultrasound in conjunction with topical siMut-Braf-liposomal complex would allow for treatment of areas not amenable to surgical removal or limb perfusion. Additionally this therapy could be combined with more traditional methods of therapy to increase response rates. Sentinel lymph node biopsy is generally performed on melanoma patients having primary melanomas of a thickness of more than 1mm in order determine degree of invasion and long-term prognosis (48-50). Approach involves injecting isosulfan blue dye at the tumor sites, tracking the lymphatic drainage and removing lymph nodes to which the tumor drains (48, 49). Lymph nodes are then examined for the presence of metastatic melanoma cells. Positive nodes generally imply a worse patient prognosis (51). Since >60% of these metastatic cells would contain mutant $V600E$ B-Raf, treating the area with siRNA-liposomal complex in addition to surgical removal could be used to therapeutically target in transit metastatic cancer cells thereby inhibiting early metastatic disease (8-11). End result could be reduction of metastatic progression thereby increasing disease free survival for patients. Thus, ultrasound followed by treatment with the siRNA-liposomal complex has potential to inhibit early and invasive lesions, which could decrease melanoma incidence and mortality rates.

In conclusion, a unique liposomal-ultrasound mediated approach for delivering siRNA into melanocytic lesions present in skin has been developed. The novel cationic liposome effectively encapsulates siRNA that specifically targets mutant $V600E$ B-Raf present in

melanocytic lesions, protects the siRNA from degradation and facilitates its entry into cells. Following non-damaging low-frequency ultrasound of skin the siRNA-liposomal formulation penetrates epidermal and dermal layers leading to a 1-2 fold decrease in early lesion or cutaneous metastasis development by causing a 4-5 fold decrease in cellular proliferative potential. Thus, topical delivery of novel siRNA containing cationic liposomes following low-frequency ultrasound can decrease early melanocytic lesion development or spread of metastases in skin.

DRAFT

ACKNOWLEDGEMENTS:

We would like to thank James Kaiser, Julie Anderson, and Nishit Trivedi for technical assistance. We would also like to thank Shantu Amin for reading this manuscript.

DRAFT

REFERENCES:

1. Satyamoorthy K, Herlyn M. Cellular and molecular biology of human melanoma. *Cancer Biol Ther* 2002;1:14-7.
2. Garbe C, Eigentler TK. Diagnosis and treatment of cutaneous melanoma: state of the art 2006. *Melanoma Res* 2007;17:117-27.
3. El Maghraby GM, Williams AC, Barry BW. Can drug-bearing liposomes penetrate intact skin? *J Pharm Pharmacol* 2006;58:415-29.
4. Lee SH, Jeong SK, Ahn SK. An update of the defensive barrier function of skin. *Yonsei Med J* 2006;47:293-306.
5. Ting WW, Vest CD, Sontheimer RD. Review of traditional and novel modalities that enhance the permeability of local therapeutics across the stratum corneum. *Int J Dermatol* 2004;43:538-47.
6. Radny P, Caroli UM, Bauer J, et al. Phase II trial of intralesional therapy with interleukin-2 in soft-tissue melanoma metastases. *Br J Cancer* 2003;89:1620-6.
7. Lavon I, Kost J. Ultrasound and transdermal drug delivery. *Drug Discov Today* 2004;9:670-6.
8. Brose MS, Volpe P, Feldman M, et al. BRAF and RAS mutations in human lung cancer and melanoma. *Cancer Res* 2002;62:6997-7000.
9. Davies H, Bignell GR, Cox C, et al. Mutations of the BRAF gene in human cancer. *Nature* 2002;417:949-54.
10. Yazdi AS, Palmedo G, Flaig MJ, et al. Mutations of the BRAF gene in benign and malignant melanocytic lesions. *J Invest Dermatol* 2003;121:1160-2.
11. Miller CJ, Cheung M, Sharma A, et al. Method of mutation analysis may contribute to discrepancies in reports of (V599E)BRAF mutation frequencies in melanocytic neoplasms. *J Invest Dermatol* 2004;123:990-2.
12. Smalley KS. A pivotal role for ERK in the oncogenic behaviour of malignant melanoma? *Int J Cancer* 2003;104:527-32.
13. Mercer KE, Pritchard CA. Raf proteins and cancer: B-Raf is identified as a mutational target. *Biochim Biophys Acta* 2003;1653:25-40.
14. Sharma A, Trivedi NR, Zimmerman MA, Tuveson DA, Smith CD, Robertson GP. Mutant V599EB-Raf regulates growth and vascular development of malignant melanoma tumors. *Cancer Res* 2005;65:2412-21.
15. Hingorani SR, Jacobetz MA, Robertson GP, Herlyn M, Tuveson DA. Suppression of BRAF(V599E) in human melanoma abrogates transformation. *Cancer Res* 2003;63:5198-202.
16. Kim DH, Rossi JJ. Strategies for silencing human disease using RNA interference. *Nat Rev Genet* 2007;8:173-84.
17. Brazas RM, Hagstrom JE. Delivery of small interfering RNA to mammalian cells in culture by using cationic lipid/polymer-based transfection reagents. *Methods Enzymol* 2005;392:112-24.
18. Gresch O, Engel FB, Nestic D, et al. New non-viral method for gene transfer into primary cells. *Methods* 2004;33:151-63.
19. Muratovska A, Eccles MR. Conjugate for efficient delivery of short interfering RNA (siRNA) into mammalian cells. *FEBS Lett* 2004;558:63-8.
20. Leung RK, Whittaker PA. RNA interference: from gene silencing to gene-specific therapeutics. *Pharmacol Ther* 2005;107:222-39.

21. Shankar P, Manjunath N, Lieberman J. The prospect of silencing disease using RNA interference. *Jama* 2005;293:1367-73.
22. Sioud M, Sorensen DR. Systemic delivery of synthetic siRNAs. *Methods Mol Biol* 2004;252:515-22.
23. Zhang C, Tang N, Liu X, Liang W, Xu W, Torchilin VP. siRNA-containing liposomes modified with polyarginine effectively silence the targeted gene. *J Control Release* 2006;112:229-39.
24. Halder J, Kamat AA, Landen CN, Jr., et al. Focal adhesion kinase targeting using in vivo short interfering RNA delivery in neutral liposomes for ovarian carcinoma therapy. *Clin Cancer Res* 2006;12:4916-24.
25. Pal A, Ahmad A, Khan S, et al. Systemic delivery of RafsiRNA using cationic cardiolipin liposomes silences Raf-1 expression and inhibits tumor growth in xenograft model of human prostate cancer. *Int J Oncol* 2005;26:1087-91.
26. Mitragotri S, Kost J. Low-frequency sonophoresis: a review. *Adv Drug Deliv Rev* 2004;56:589-601.
27. Lee S, Newnham RE, Smith NB. Short ultrasound exposure times for noninvasive insulin delivery in rats using the lightweight cymbal array. *IEEE Trans Ultrason Ferroelectr Freq Control* 2004;51:176-80.
28. Park EJ, Werner J, Smith NB. Ultrasound mediated transdermal insulin delivery in pigs using a lightweight transducer. *Pharm Res* 2007;24:1396-401.
29. Smith NB, Lee S, Maione E, Roy RB, McElligott S, Shung KK. Ultrasound-mediated transdermal transport of insulin in vitro through human skin using novel transducer designs. *Ultrasound Med Biol* 2003;29:311-7.
30. Smith NB, Lee S, Shung KK. Ultrasound-mediated transdermal in vivo transport of insulin with low-profile cymbal arrays. *Ultrasound Med Biol* 2003;29:1205-10.
31. Satyamoorthy K, DeJesus E, Linnenbach AJ, et al. Melanoma cell lines from different stages of progression and their biological and molecular analyses. *Melanoma Res* 1997;7 Suppl 2:S35-42.
32. Rasband WS. ImageJ. In: Health USNIo, editor. Bethesda, Maryland, USA; 1997-2007.
33. Ozbun MA, Meyers C. Transforming growth factor beta1 induces differentiation in human papillomavirus-positive keratinocytes. *J Virol* 1996;70:5437-46.
34. Wu YJ, Parker LM, Binder NE, et al. The mesothelial keratins: a new family of cytoskeletal proteins identified in cultured mesothelial cells and nonkeratinizing epithelia. *Cell* 1982;31:693-703.
35. Cory AH, Owen TC, Barltrop JA, Cory JG. Use of an aqueous soluble tetrazolium/formazan assay for cell growth assays in culture. *Cancer Commun* 1991;3:207-12.
36. RNA Interference - Technical Reference & Application Guide. Lafayette, CO: Dharmacon, Inc.; 2004.
37. Sharma A, Tran MA, Liang S, et al. Targeting Mitogen-Activated Protein Kinase/Extracellular Signal-Regulated Kinase Kinase in the Mutant (V600E) B-Raf Signaling Cascade Effectively Inhibits Melanoma Lung Metastases. *Cancer Res* 2006;66:8200-9.

38. Mir LM, Glass LF, Sersa G, et al. Effective treatment of cutaneous and subcutaneous malignant tumours by electrochemotherapy. *Br J Cancer* 1998;77:2336-42.
39. Aagaard L, Rossi JJ. RNAi therapeutics: principles, prospects and challenges. *Adv Drug Deliv Rev* 2007;59:75-86.
40. Behlke MA. Progress towards in vivo use of siRNAs. *Mol Ther* 2006;13:644-70.
41. Sorensen DR, Leirdal M, Sioud M. Gene silencing by systemic delivery of synthetic siRNAs in adult mice. *J Mol Biol* 2003;327:761-6.
42. Baigude H, McCarroll J, Yang CS, Swain PM, Rana TM. Design and creation of new nanomaterials for therapeutic RNAi. *ACS Chem Biol* 2007;2:237-41.
43. Derfus AM, Chen AA, Min DH, Ruoslahti E, Bhatia SN. Targeted Quantum Dot Conjugates for siRNA Delivery. *Bioconjug Chem* 2007.
44. Gabizon A, Catane R, Uziely B, et al. Prolonged circulation time and enhanced accumulation in malignant exudates of doxorubicin encapsulated in polyethylene-glycol coated liposomes. *Cancer Res* 1994;54:987-92.
45. Treat J, Damjanov N, Huang C, Zrada S, Rahman A. Liposomal-encapsulated chemotherapy: preliminary results of a phase I study of a novel liposomal paclitaxel. *Oncology (Williston Park)* 2001;15:44-8.
46. Tezel A, Dokka S, Kelly S, Hardee GE, Mitragotri S. Topical delivery of anti-sense oligonucleotides using low-frequency sonophoresis. *Pharm Res* 2004;21:2219-25.
47. Balch CM. Cutaneous melanoma. 3rd ed. St. Louis, Mo.: Quality Medical Pub.; 1998.
48. Morton DL, Wen DR, Wong JH, et al. Technical details of intraoperative lymphatic mapping for early stage melanoma. *Arch Surg* 1992;127:392-9.
49. Ruiter DJ, Spatz A, van den Oord JJ, Cook MG. Pathologic staging of melanoma. *Semin Oncol* 2002;29:370-81.
50. Thompson JF, McCarthy WH, Bosch CM, et al. Sentinel lymph node status as an indicator of the presence of metastatic melanoma in regional lymph nodes. *Melanoma Res* 1995;5:255-60.
51. Balch CM, Soong SJ, Gershenwald JE, et al. Prognostic factors analysis of 17,600 melanoma patients: validation of the American Joint Committee on Cancer melanoma staging system. *J Clin Oncol* 2001;19:3622-34.

FIGURE LEGENDS:

Figure 1: Characterization of cationic siRNA-liposome complexes. **A.** Loading of fluorescently tagged siRNA into liposomes. Fluorescently tagged siRNA was complexed with cationic liposomes at ratios of 1:5, 1:10, or 1:15, for 0.5, 3, or 6 hours and run on a 2% agarose gel to determine loading efficiency. Maximal loading was reached at a 1:10 ratio following a 0.5-hour incubation (left panel). siRNA at a 1:10 ratio with liposomes were sized using dynamic light scattering and similar size ranges observed for ghost or liposomes loaded with siRNA (right panel). **B.** Protection of siRNA from degradation in liposomes. siRNA protection by cationic liposomes was measured by complexing fluorescent siRNA with liposomes overnight followed by exposure to serum for 10, 30, 60, 180, or 360 minutes. Release of siRNA in liposomes was accomplished by collapsing serum treated siRNA-liposomal complexes with SDS to release free siRNA, which was then run on an agarose gel. Free fluorescent siRNA alone was used as a control. **C.** siRNA-liposomal complex is taken up into normal cells. Uptake of siRNA-liposomal complex into normal cells was measured by adding fluorescently tagged siRNA-liposomal complex (200 nM) to fibroblasts, keratinocytes, and melanocytes for 3 hours followed by fixation and imaging using fluorescence microscopy (magnification; 400X). Ghost liposomes lacking fluorescent siRNA were used as a control. **D.** Ghost liposome or siRNA-liposomal complex exhibited not significant toxicity in normal or cancer cells. Cellular toxicity of ghost liposome and siRNA-liposomal complex was measured by adding liposomes (12.5, 25, and 50 μ M) to fibroblasts, keratinocytes, melanocytes, or melanoma cells for 24 hours followed by MTS assay analysis. Untreated cells (-) were used for comparison.

Figure 2: siRNA in siRNA-liposomal complexes is taken up into the cytoplasm of cells and decreases protein expression. **A.** Liposomes can load and deliver siRNA targeting different proteins into cells. WM35 cells were treated for 3 hours with liposomes containing both Alexa Fluor 546 and fluorescein labeled siRNAs (20 nM) or ghost liposomes, fixed and imaged using fluorescence microscopy (magnification; 400X). **B.** siRNA-liposomal complex is taken up into the cytoplasm of cells and is not merely surface bound. siRNA-liposomal complex localization in cells following treatment with siRNA-liposomal complexes (100 nM) was ascertained by exposing 1205 Lu melanoma cells for 3 hours after which cells were trypsinized to remove surface bound complex and replated overnight onto coverslips. Cells

were fixed and imaged using fluorescent microscopy (magnification; 400X). **C.** siRNA can be designed to decrease expression of mutant ^{V600E}B-Raf but not normal protein expression. To verify specificity of siMutB-Raf for decreasing expression of mutant but not wild-type protein, melanoma cells containing normal (C8161.C19) or mutant (UACC 903) protein were nucleofected with buffer, siScrambled, siC-Raf, siWTB-Raf, or siMutB-Raf siRNA, protein lysates harvested 48 hours later, and analyzed by Western blot analysis for B-Raf and C-Raf knockdown. Erk2 served as a loading control. **D.** siMutB-Raf siRNA-liposomal complex decreases expression of mutant ^{V600E}B-Raf protein in cells. 1205 Lu cells were exposed to siMutB-Raf or siScrambled-liposomal complex, protein lysates harvested at 18 and 32 hours and analyzed by Western blot analysis. Erk2 served as a control for protein loading.

Figure 3: siMutB-Raf inhibits melanocytic lesion growth in reconstructed skin. A. Duration of ^{V600E}B-Raf protein knockdown following exposure to siRNA targeting mutant protein is beyond 8-days. Cells were nucleofected with C-Raf or ^{V600E}B-Raf siRNA, replated in culture dishes and protein harvested 2, 4, 6 and 8 days later to measure duration of protein knockdown. Untreated cells or cells nucleofected with siRNA targeting C-Raf served as controls. **B.** Targeting melanocytic lesions using siRNA against ^{V600E}B-Raf decreases melanocytic lesion development in laboratory-generated skin. Effectiveness of siRNA targeting ^{V600E}B-Raf for decreasing cutaneous tumor development was established by nucleofecting GFP-tagged WM35 cells with buffer, scrambled siRNA or siRNA targeting C-Raf, or ^{V600E}B-Raf (100 pmoles). Cells were then seeded into laboratory-generated skin at time of creation and 10 days later, average area occupied by green melanocytic lesions quantified (left panel). A statistically significant reduction in green fluorescent lesions was observed following siMutB-Raf treatment ($p < 0.05$; One-Way ANOVA) (upper right panel). Protein lysates harvested from cells were analyzed by Western blot for B-Raf or C-Raf protein expression. Erk2 served as a control for protein loading (lower right panel). **C.** siRNA-mediated inhibition of ^{V600E}B-Raf protein expression in GFP-tagged UACC 903 cells decreases lesion formation in skin reconstructs. UACC 903-GFP cells were nucleofected with siScrambled or siB-Raf (12.5 or 50 pmoles) and cells seeded into laboratory generated skin at time of creation. Reconstructed skin was analyzed using fluorescence microscopy 10 days later and area occupied by developing GFP lesions quantified. **D.** Mechanistically, siRNA-mediated targeting of ^{V600E}B-Raf protein decreases the proliferative capacity of cells. Cultured UACC 903

melanoma cells treated with siMutB-Raf had an increased doubling time indicating cells were proliferating at a slower rate (left panel). Quantifying proliferating cells showed a 2-3 fold decrease following siMutB-Raf treatment of tumor cells in size and time matched tumor controls treated with siRNA to C-Raf (middle and right panels).

Figure 4: Ultrasound treatment permeabilizes skin enabling melanocytic lesions to take up siRNA-liposomal complexes.

A. Ultrasound assembly. A lightweight, low-profile ultrasound array was constructed using four cymbal transducers, which were connected in parallel and encased in polymer. **B.** Ultrasound treatment does not damage skin. Laboratory generated skin was ultrasound treated followed by addition of ghost liposome, skin sectioned and H&E stained. No changes cellular structure or in skin morphology was observed compared to untreated control skin (magnification; 200X). **C., D.** Following ultrasound treatment of skin, siRNA-liposomal complex is taken up by melanocytic lesions in the epidermis and at the epidermal-dermal junction. Following 20 minutes of ultrasound treatment, fluorescent siRNA-liposomal complex or ghost liposomes were applied topically onto reconstructed skin. One hour later, skin was fixed and analyzed using fluorescent microscopy looking down at the skin (Magnification; 4X) (**B.**), or by cross sections (magnification; 400X) (**C.**). Fluorescence (red) indicating presence of siRNA-liposomal complex was evident in melanocytic lesions in both the epidermis and at the epidermal-dermal junction (arrows).

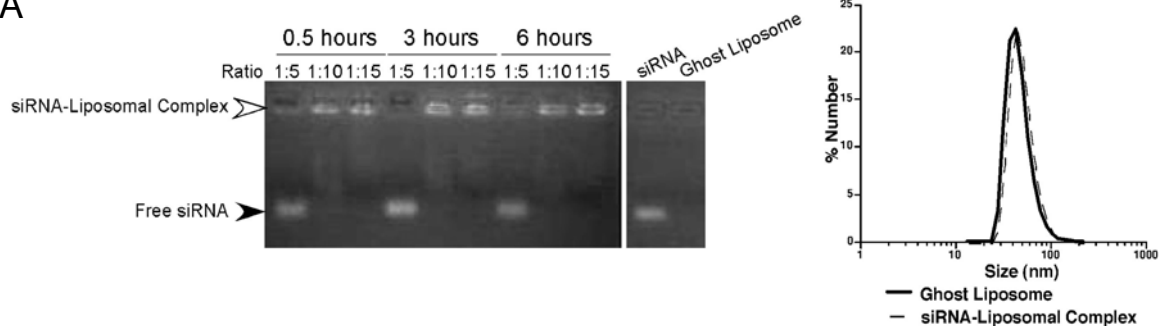
Figure 5: Ultrasound treatment followed by topical application of siMutB-Raf-liposomal complex inhibits melanocytic lesion development in reconstructed skin.

A. Schematic showing treatment regime. Beginning on day 10 and on alternate days thereafter up to day 20, reconstructed skin was treated with ultrasound for 20 minutes followed by topical administration of siMutB-Raf-liposomal complex (100 pmoles) or ghost liposomes. **B., C.** Ultrasound followed by addition of siMutB-Raf-liposomal complex decreases melanocytic lesion development in skin. Reconstructed skin containing UACC 903-GFP or WM35-GFP cells were treated with ultrasound for 20 minutes followed by topical administration of siMutB-Raf-liposomal complex on alternated days from day 10 to 20. Skin was harvested on day 21, and average area occupied by GFP-tagged tumors calculated for each group. Ultrasound treatments followed by exposure to ghost liposomes served as a control.

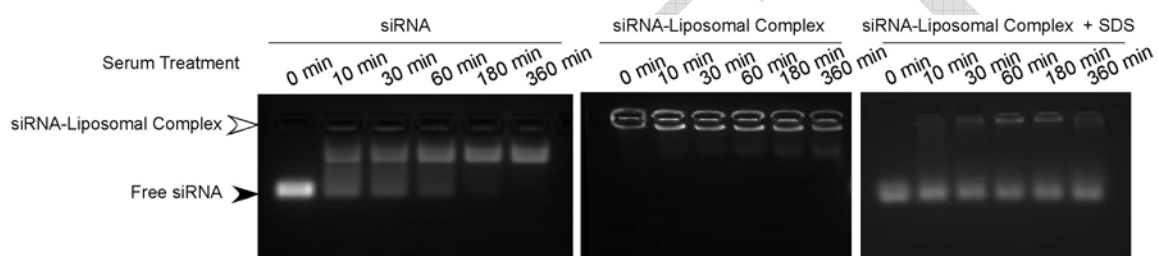
Figure 6: Ultrasound treatment followed by topical application of siMutB-Raf-liposomal complex inhibits melanocytic lesion development in animal skin.

A. Schematic showing treatment regime. Ultrasound treatment followed by topical application of siMutB-Raf-liposomal complexes started the day after injection of melanoma cells and continued on alternate days up until day 23. During the procedure, anesthetized mice were treated with ultrasound at the injection site for 15 minutes followed by topical application of siMutB-Raf-liposomal complex. **B.** Ultrasound treatment followed by topical application of siMutB-Raf-liposomal complexes decreases melanocytic tumor development in animal skin. UACC 903-GFP cells (1×10^6), were injected subcutaneously into nude mice and after 24 hours, tumor forming at injection sites treated on alternate days with ultrasound for 15 minutes followed by topical administration of siMutB-Raf-liposomal complex. Tumors were measured on alternate days beginning on day 3. Control mice were ultrasound treated followed by addition of siScrambled-liposomal complex. Statistically significant differences between control and siMutB-Raf-liposomal complex treated tumors were observed beginning on day 13 and on days 17, 19, 21 and 23 (Two-Way ANOVA; $p < 0.05$). **C.** Ultrasound treatment followed by topical application of siMutB-Raf-liposomal complex does not cause significant change in animal body weight. Animal weights were measured on alternate days beginning on day 1 to determine whether any weight related toxicity occurred. No significant weight loss was observed between control and experimental groups (Two-Way ANOVA; $p > 0.05$). **D.** Ultrasound treatment followed by topical application of siMutB-Raf-liposomal complex does not cause significant changes in liver morphology. Livers were collected from animals at day 23 to assess morphological changes (magnification; 400X).

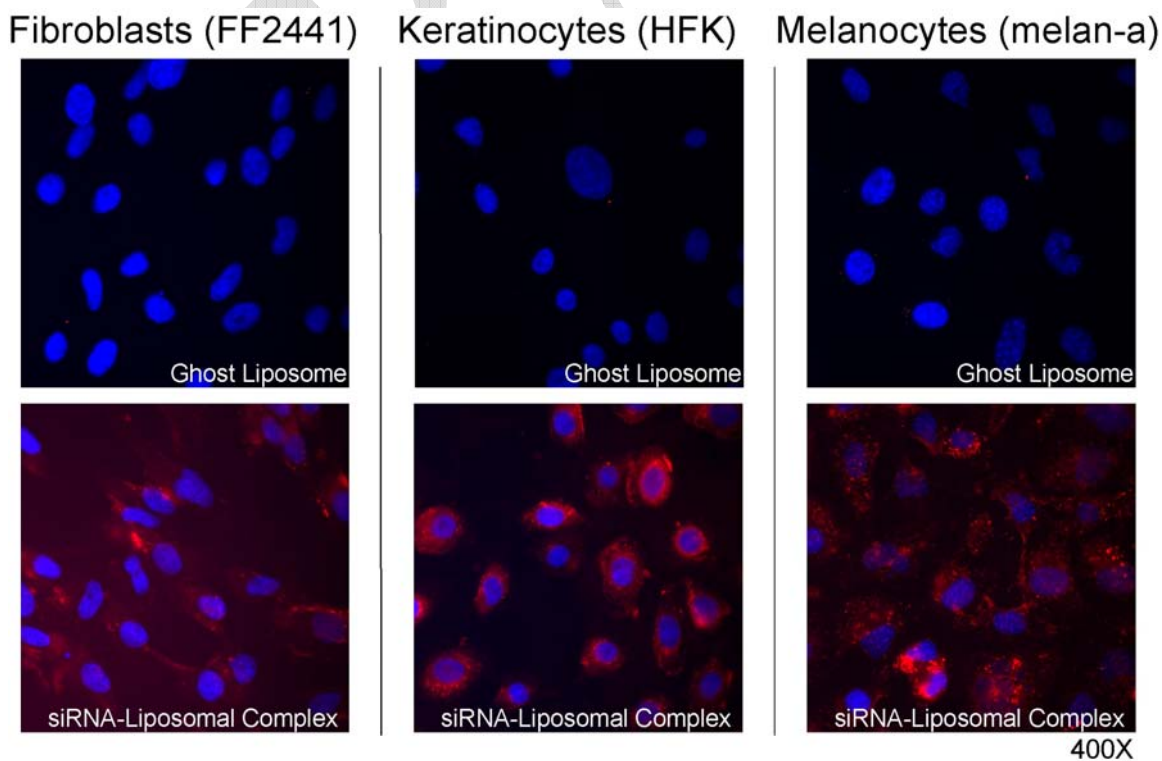
1A



1B

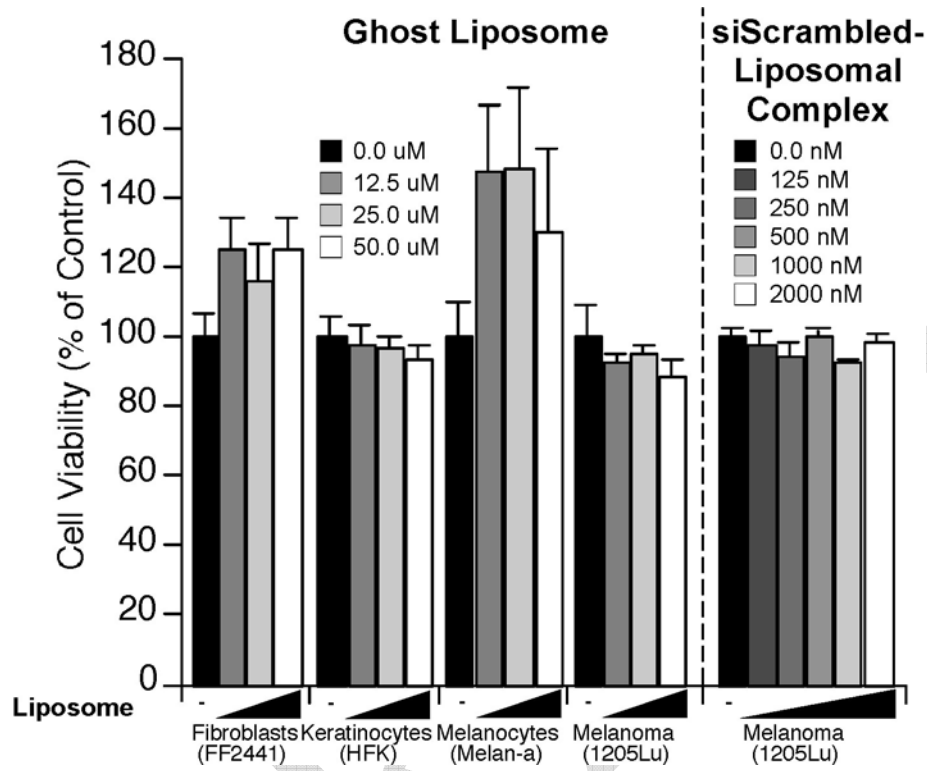


1C



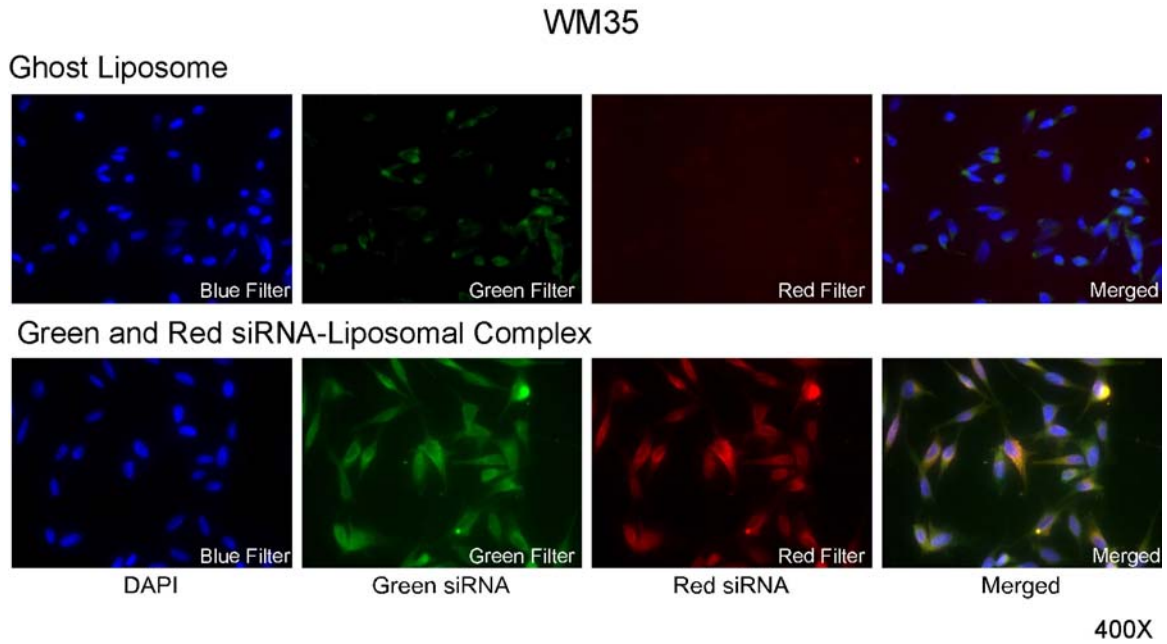
Tran, M.A. et al
Fig. 1D

1D

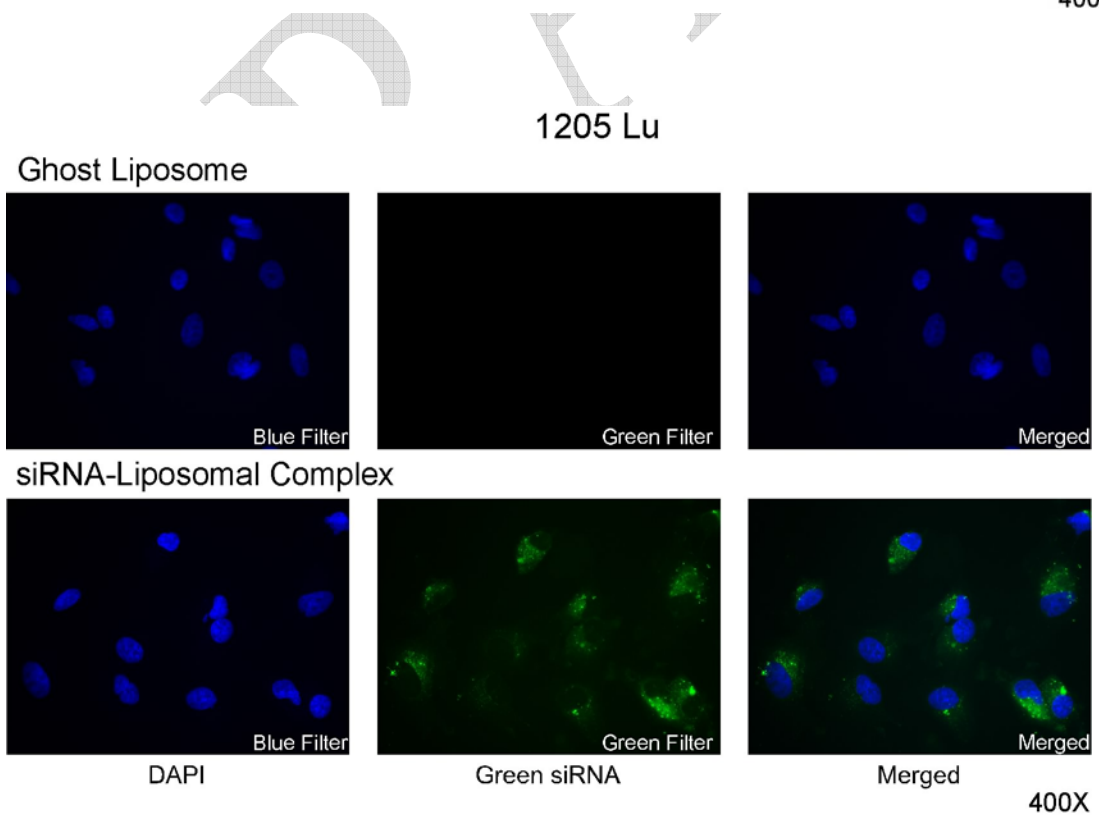


Tran, M.A. et al
Fig. 2A, 2B

2A

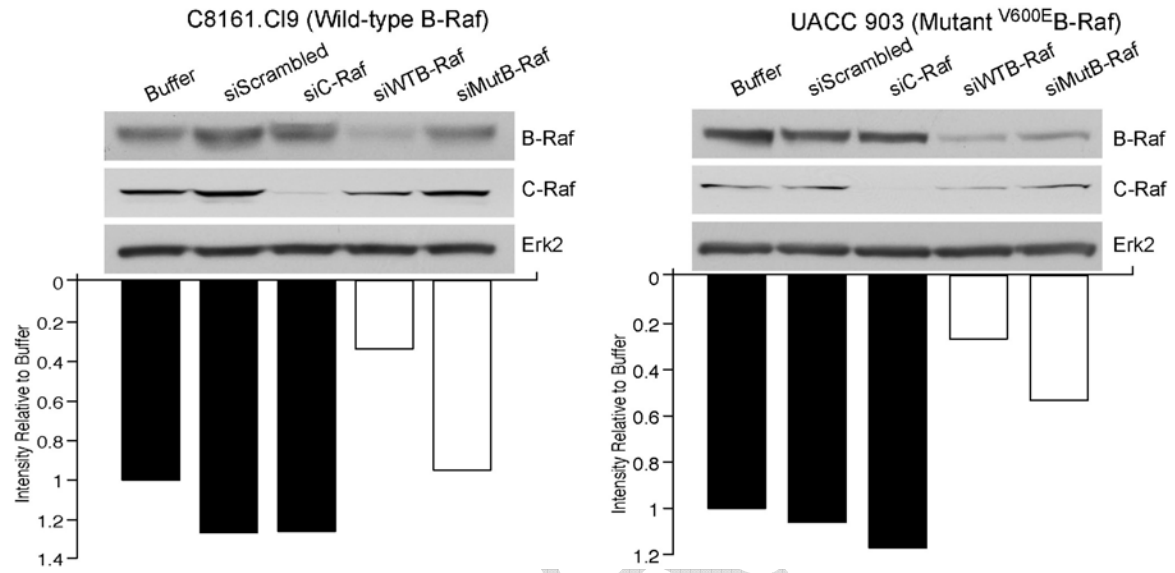


2B

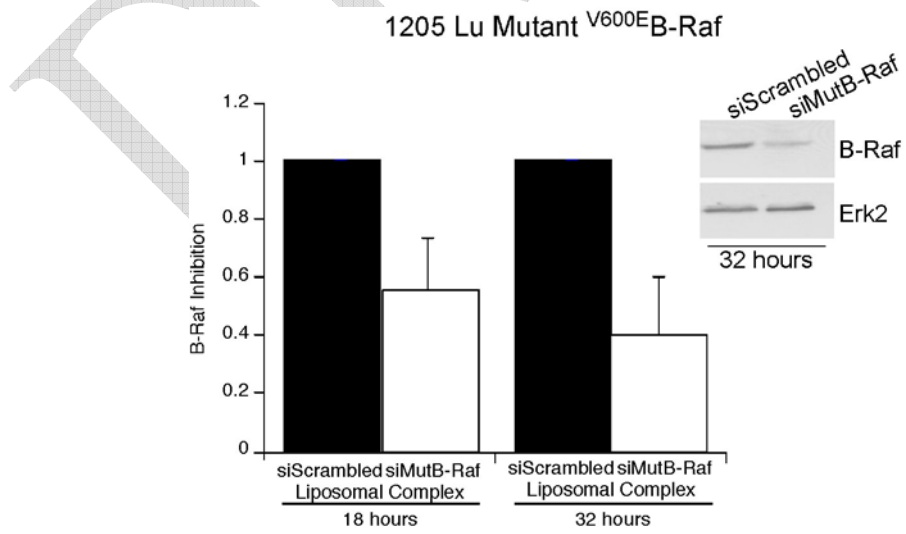


Tran, M.A. et al
Fig. 2C, 2D

2C

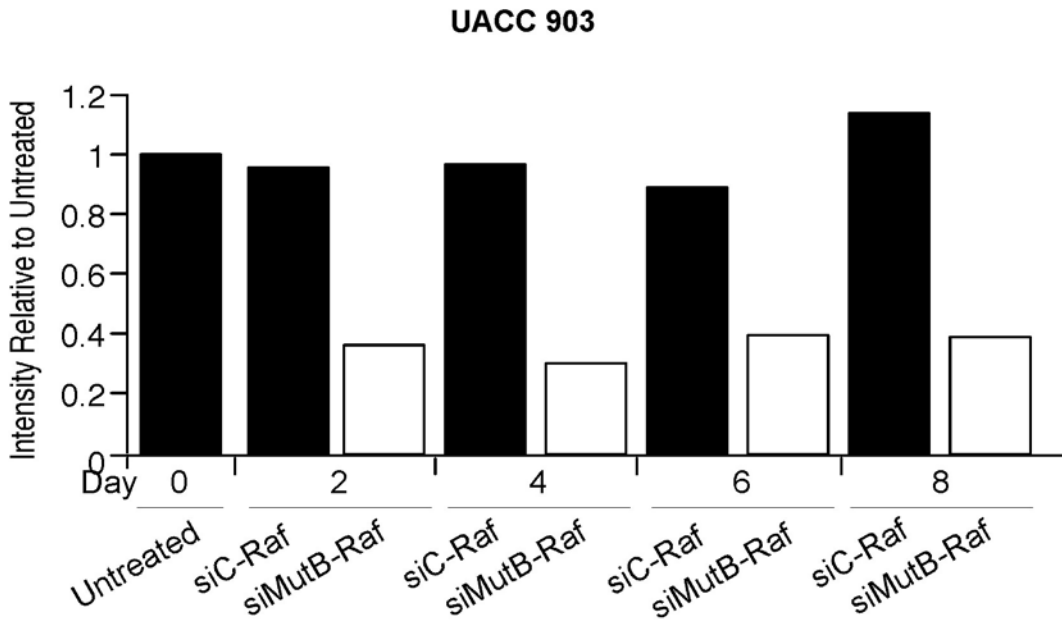


2D

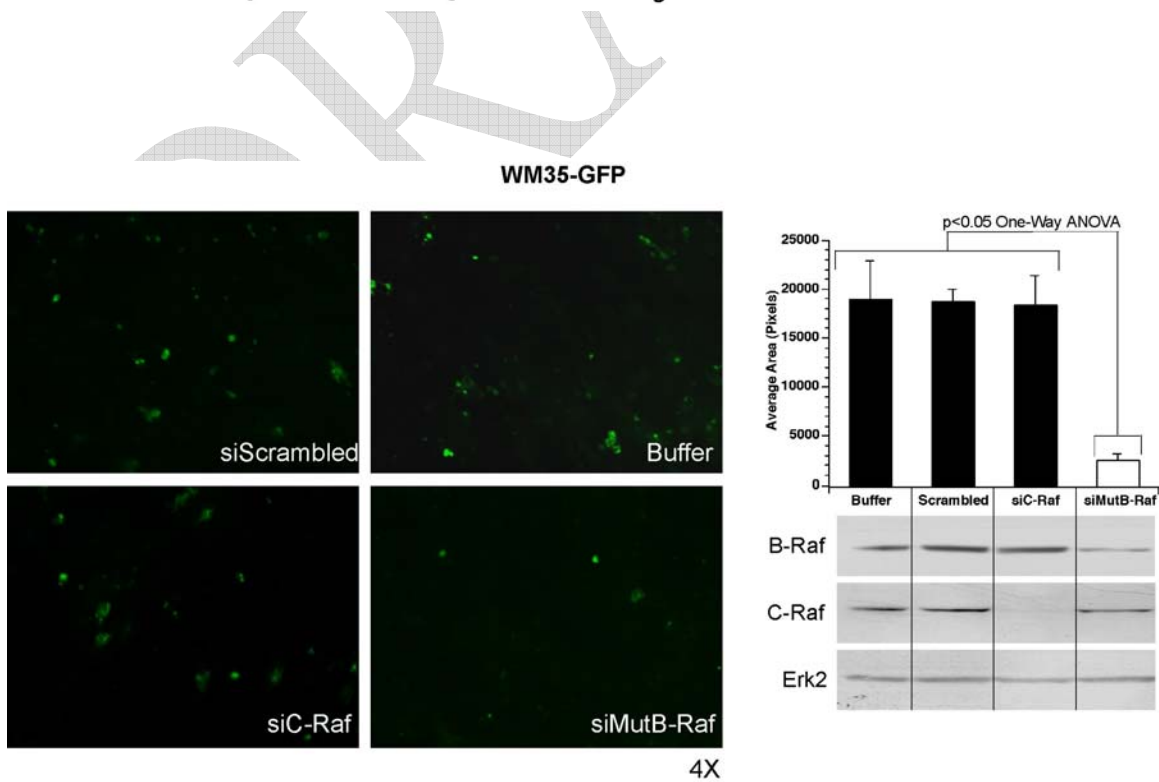


Tran, M.A. et al
 Fig. 3A, 3B

3A

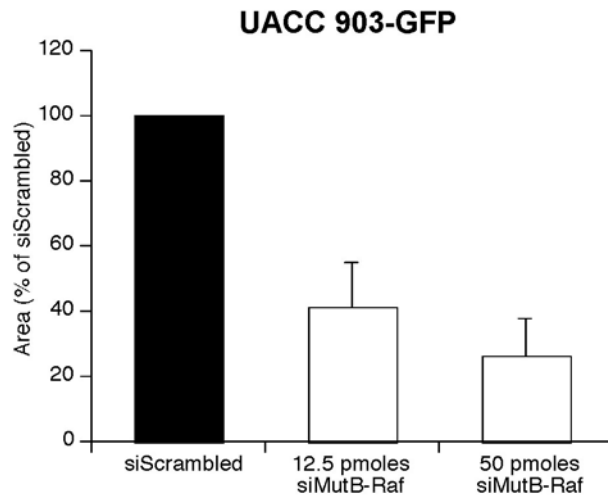


3B

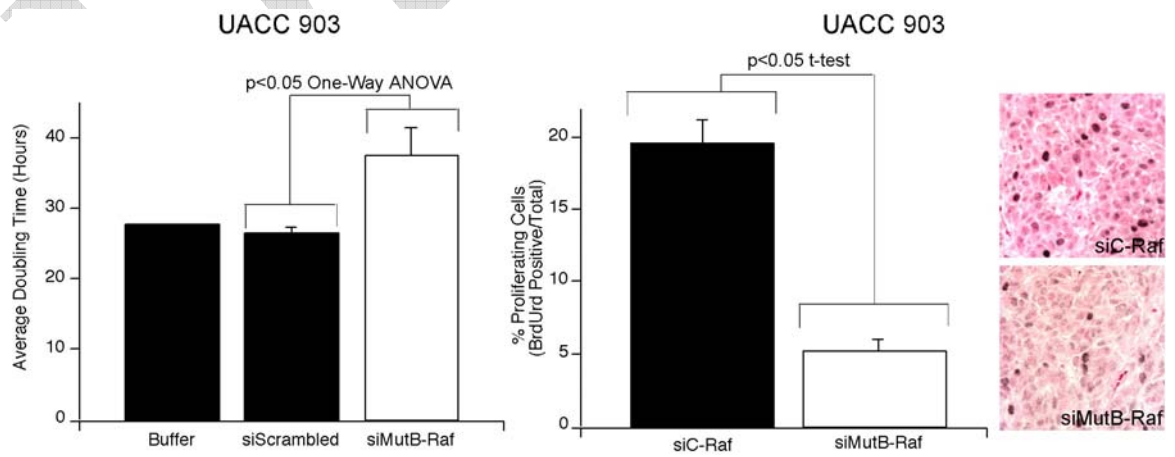


Tran, M.A. et al
Fig. 3C, 3D

3C

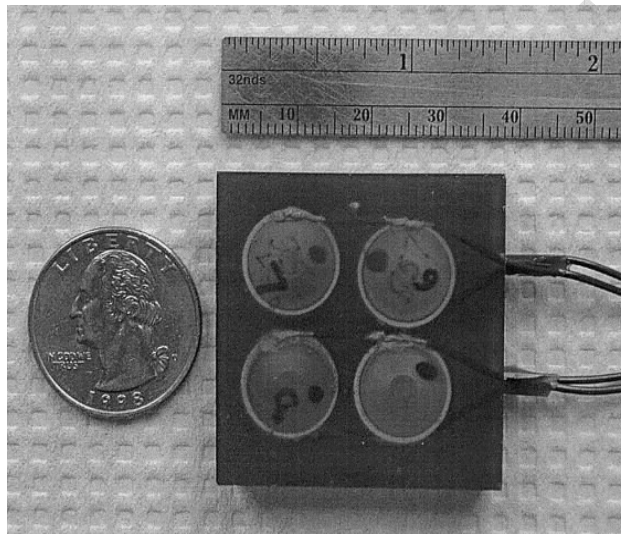


3D

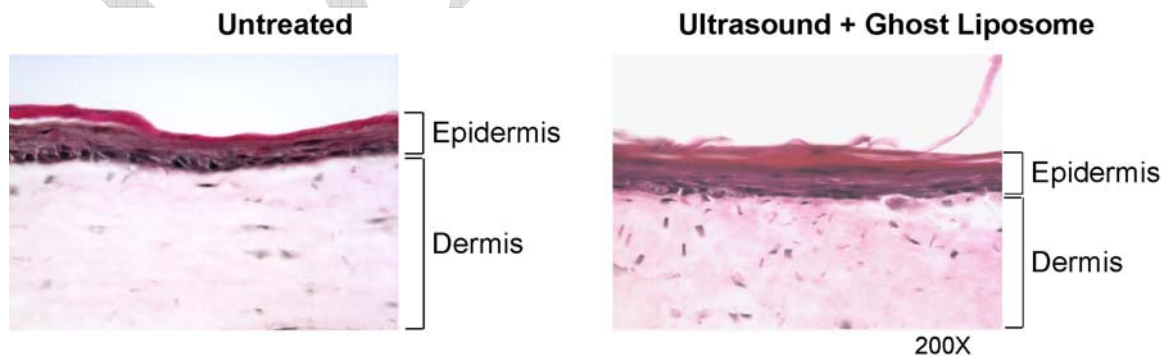


Tran, M.A. et al
Fig. 4A, 4B

4A

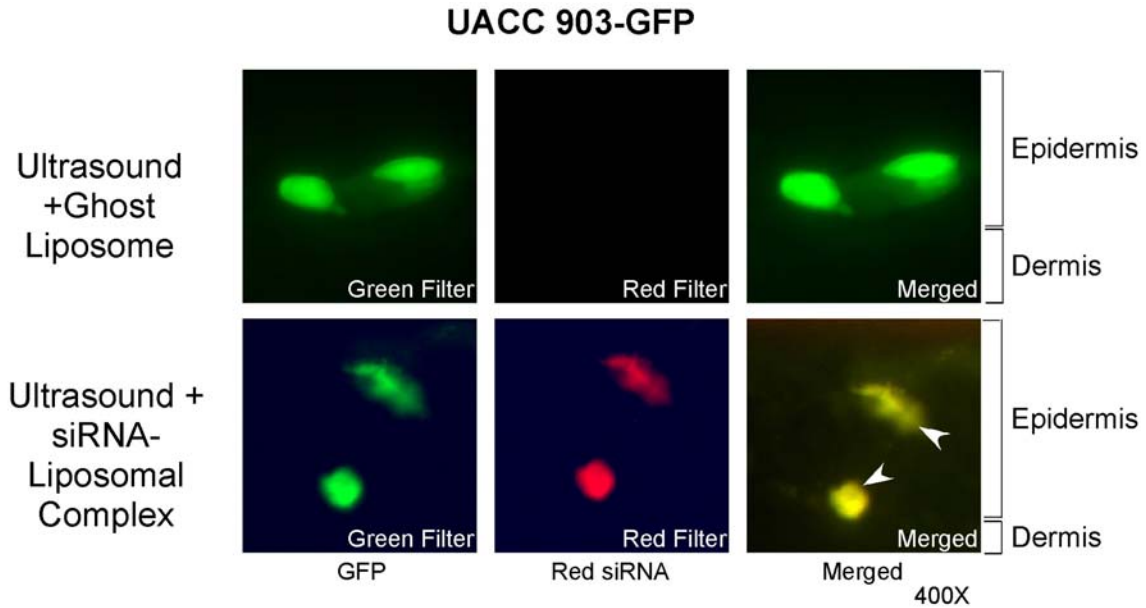


4B

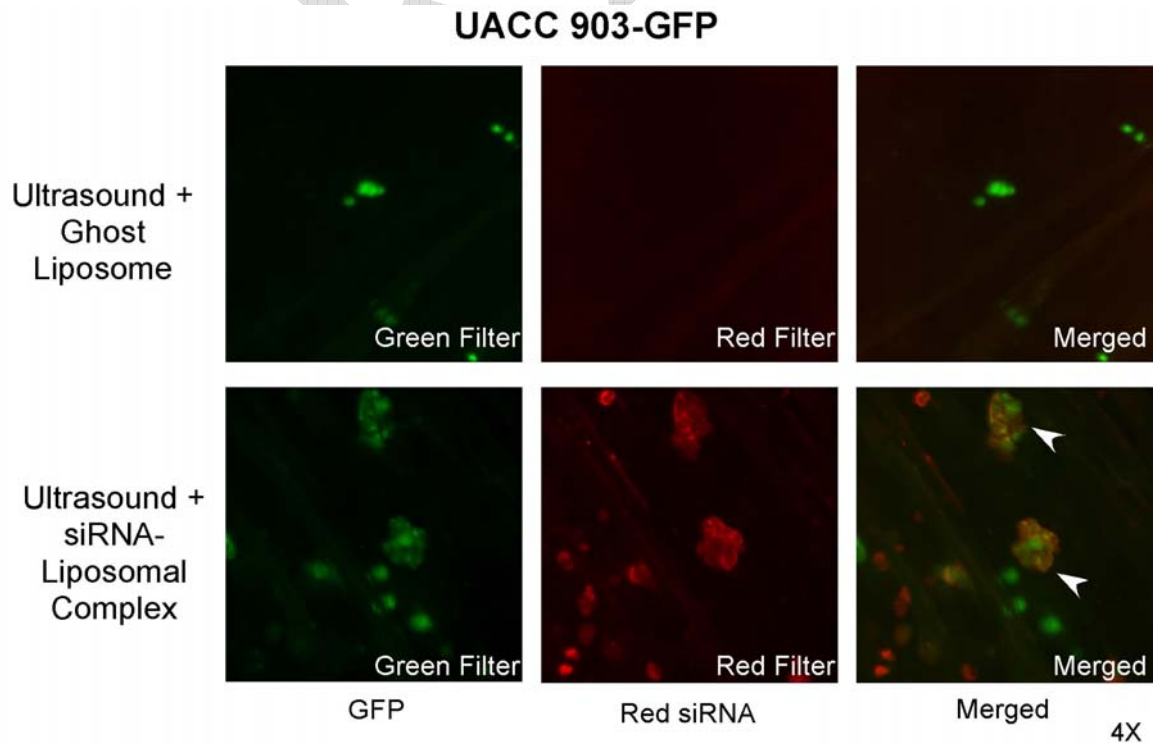


Tran, M.A. et al
Fig. 4C, 4D

4C

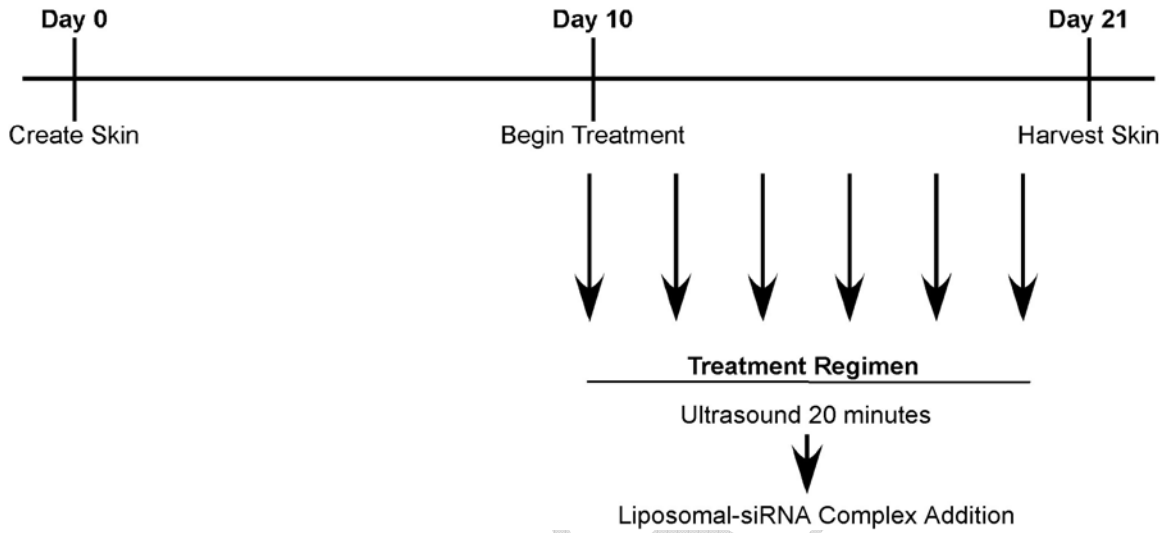


4D

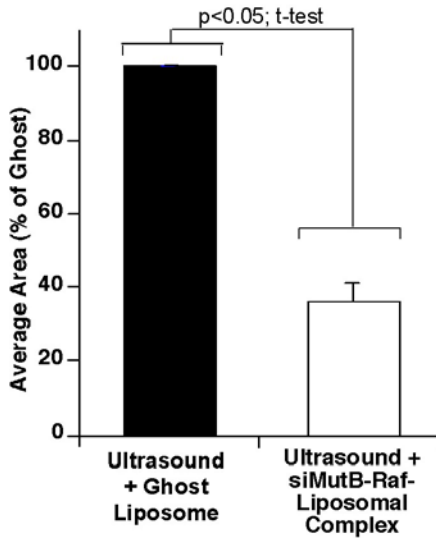


Tran, M.A. et al
Fig. 5A, 5B, 5C

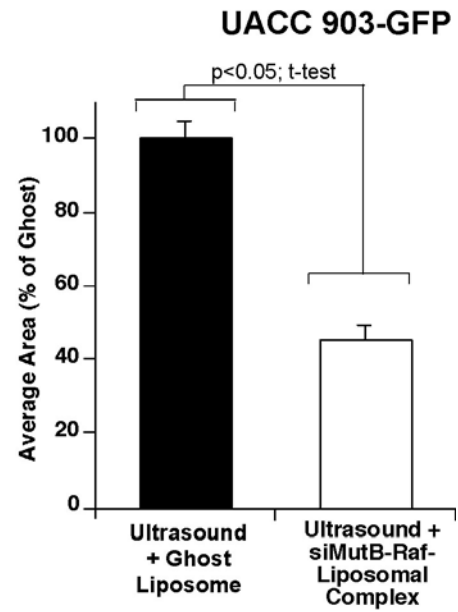
5A



5B

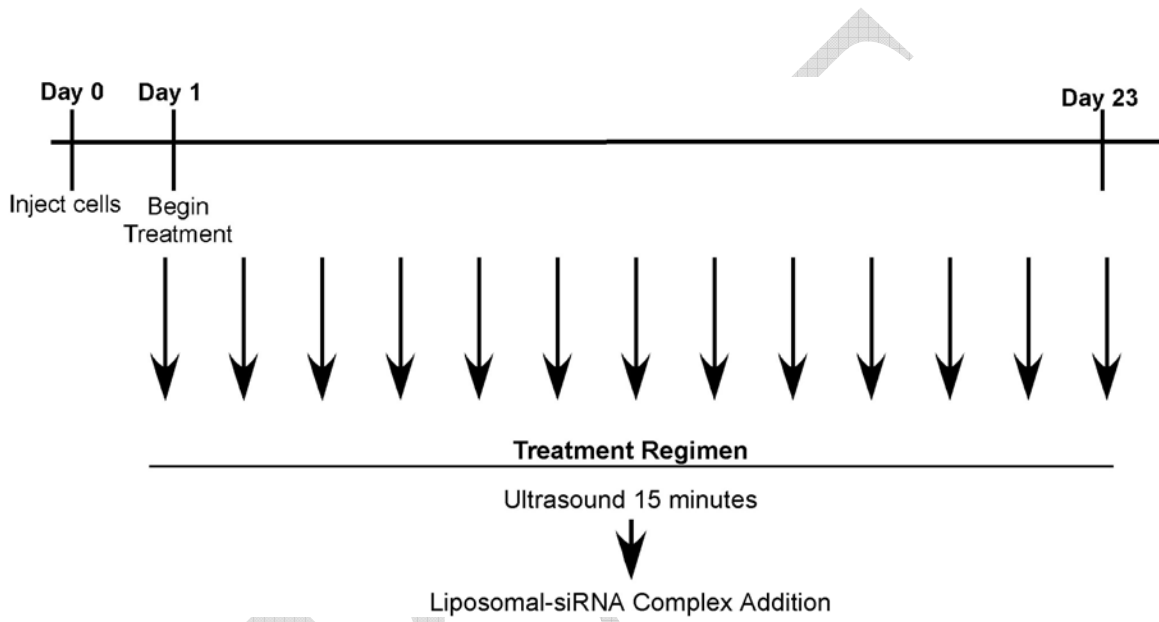


5C

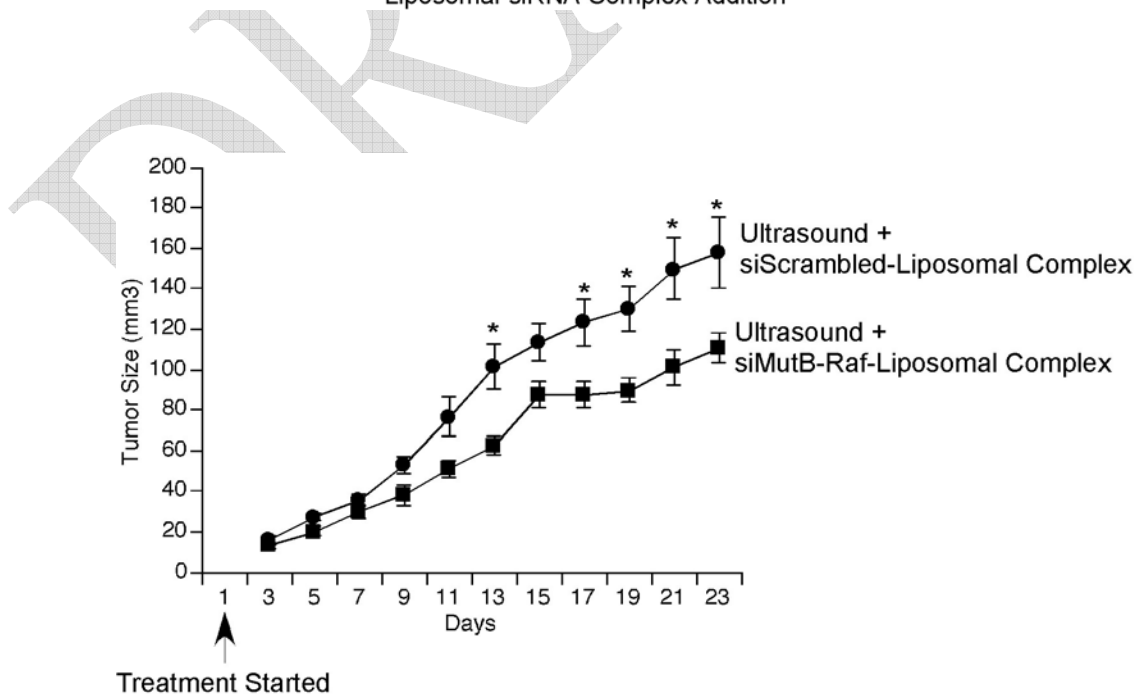


Tran, M.A. et al
Fig. 6A

6A

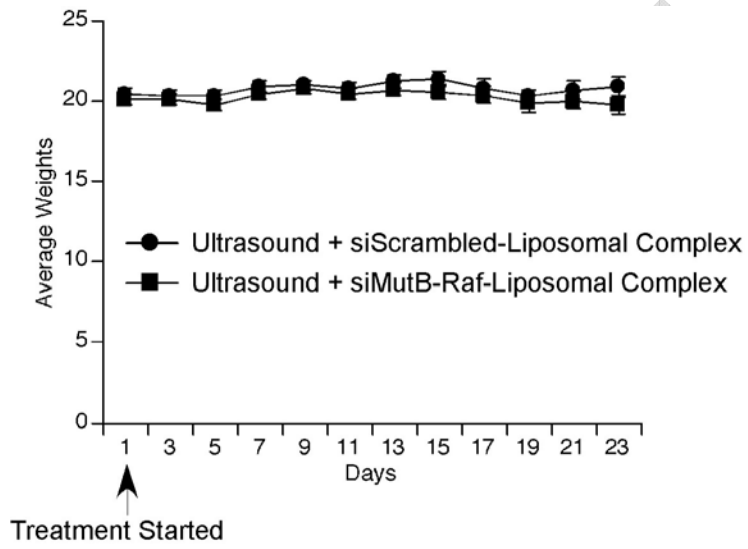


6B



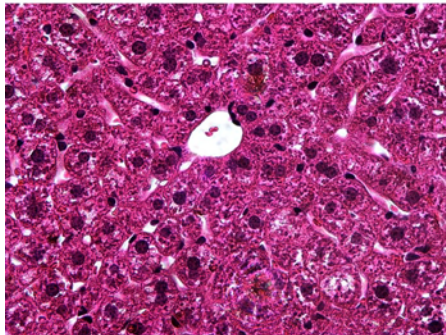
Tran, M.A. et al
Fig. 6C, 6D

6C

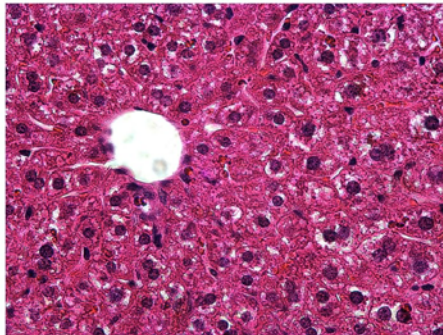


6D

Ultrasound + Liposomal Scrambled



Ultrasound + Liposomal siMutB-Raf



400X